AD_____

Award Number: DAMD17-00-1-0352

TITLE: Regulation of Tumor Progression by Mgat5-Dependent Glycosylation

PRINCIPAL INVESTIGATOR: James W. Dennis, Ph.D.

CONTRACTING ORGANIZATION: Samuel Lunenfeld Research Institute of Mount Sinai Hospital
Toronto, Ontario M5G 1X5 Canada

REPORT DATE: July 2002

TYPE OF REPORT: Annual

PREPARED FOR: U.S. Army Medical Research and Materiel Command
Fort Detrick, Maryland 21702-5012

DISTRIBUTION STATEMENT: Approved for Public Release;
Distribution Unlimited

The views, opinions and/or findings contained in this report are those of the author(s) and should not be construed as an official Department of the Army position, policy or decision unless so designated by other documentation.

REPORT DOCUMENTATION PAGE

Form Approved
OMB No. 074-0188

1. AGENCY USE ONLY (Leave blank)	2. REPORT DATE	3. REPORT TYPE AND DATES COVERED
	July 2002	Annual (1 Jun 01 -1 Jun 02)

4. TITLE AND SUBTITLE
Regulation of Tumor Progression by Mgat5-Dependent Glycosylation

5. FUNDING NUMBERS
DAMD17-00-1-0352

6. AUTHOR(S)
James W. Dennis, Ph.D.

7. PERFORMING ORGANIZATION NAME(S) AND ADDRESS(ES)
Samuel Lunenfeld Research Institute of
Mount Sinai Hospital
Toronto, Ontario M5G 1X5 Canada
E-Mail: Dennis @MSHRI.on.ca

8. PERFORMING ORGANIZATION REPORT NUMBER

9. SPONSORING / MONITORING AGENCY NAME(S) AND ADDRESS(ES)
U.S. Army Medical Research and Materiel Command
Fort Detrick, Maryland 21702-5012

10. SPONSORING / MONITORING AGENCY REPORT NUMBER

11. SUPPLEMENTARY NOTES
Original contains color plates: All DTIC reproductions will be in black and white.

12a. DISTRIBUTION / AVAILABILITY STATEMENT
Approved for Public Release; Distribution Unlimited

12b. DISTRIBUTION CODE

13. Abstract *(Maximum 200 Words) (abstract should contain no proprietary or confidential information)*

Task 1 was to further define the phenotype of *Mgat5*$^{-/-}$ cells regarding adhesion, signal transduction, and growth factor responsiveness. We have established immortalized embryonic fibroblast cell lines form Mgat5-/- mice, made Mgat5 retrovial vector for rescue of the mutant phenotypes, and established new technology (the Cellomics scan array system) to measure these parameters with precision. **Task 2** was to use genetic methods to analysis *Mgat5* dependent tumor progression *in vivo*. We have interbred Mgat5 mice with Pten mutant mice and preliminary results suggest the genes interaction, in the immune system and cancer. **Task 3&4** was to location β1,6GlcNAc-branched N-glycans that mediate phenotype. We identified T cell receptor and a new mechanism of N-glycan action, and more will identified this year.

14. SUBJECT TERMS	15. NUMBER OF PAGES
protein glycosylation, glycosyltransferase, cell adhesion, cadherins, integrins, cytokine receptors, signal transduction	53
	16. PRICE CODE

17. SECURITY CLASSIFICATION OF REPORT	18. SECURITY CLASSIFICATION OF THIS PAGE	19. SECURITY CLASSIFICATION OF ABSTRACT	20. LIMITATION OF ABSTRACT
Unclassified	Unclassified	Unclassified	Unlimited

Table of Contents

INTRODUCTION:

Genes devoted to oligosaccharide biosynthesis comprise approximately 1% of the translated genome in vertebrates, on the same order as genes encoding protein kinases, suggesting functional complexity and a fundamental role in metazoan biology [1]. Cancer-associated changes in glycoprotein glycosylation are well-documented [2], but the molecular functions of these carbohydrates in normal tissues and disease progression are poorly understood. Golgi UDP-N-acetylglucosamine:α-6-D-mannoside β1,6 N-acetylglucosaminyltransferase V (GlcNAc-TV) is highly expressed in proliferating and migrating cells, and the *Mgat5* gene is transcribed in response to activation of the RAS pathway. The enzyme initiates β1-6GlcNAc-branching of asparagine-linked oligosaccharides (N-glycans), which are generally extended with polylactosamine in cancer cells (Fig 1A). Mgat5 activity increases with malignant transformation is associated with poor survival in colon cancer [3,4]. Over-expression of Mgat5 in epithelial cells causes morphologically transformed, indicating a cell autonomous effect on the malignant phenotype [5].

To study Magt5 further, we generated Mgat5-deficient mice, and although apparently normal at birth, the mice display a complex phenotype that might be described as abnormal responses to extrinsic stimuli or stresses [6]{3929}. The mutation causes T cell hypersensitivity, impaired leukocyte motility, reduced cancer progression, a behavioral defect of failure to nurture, premature aging with osteoporosis, decreased fat mass, intestinal prolapse and increased mortality at 12-18 mon.

We demonstrated that T cell receptor (TCR) mobilization and clustering in response to agonist is greatly enhanced in *Mgat5*$^{-/-}$ cells and this results in enhanced signaling, notably TCR-dependent tyrosine phosphorylation, actin microfilament reorganization, and Ca^{++} mobilization [6] (Fig 1B). The α,β,γ,δ chains of TCR are N-glycosylated and a fraction these N-glycans are Mgat5 modified. We demonstrated that Mgat5-modified N-glycans on the TCR complex bind to galectin-3 (Gal-3), which impedes receptor clustering in response to antigen [6]. Mgat5 glycans display greater affinity for Gal-3 than less branched N-glycans, which appears to that inhibits TCR recruitment into the immune synapse (Fig 1B,C). Based on these studies, our working hypothesis is that Mgat5-modified N-glycans on multiple receptors bind galectins, which may regulate cell motility, tumor growth and metastasis.

There are 10 mammalian galectins, a family of β-galactoside-binding lectins containing either one or two carbohydrate-recognition domains (CDR), a 12 β-stranded fold [7]. Gal-3 monomers equilibrate with higher order oligomers bound to glycoproteins at the cell surface and extracellular matrix. Gal-3 cross-links cell surface glycoproteins forming a dynamic multivalent lattice, which impedes agonist-dependent TCR clustering. Gal-3 has an extended binding site that accommodates polylactosamine, a sequence preferentially added to Mgat5-modified N-glycans. Complex-type N-glycan can extend at least 30Å from the protein surface [8], and Gal-3 homodimers with the carbohydrate-recognition domains (CDR) spaced by ~50Å can bridge glycoproteins by >120 Å [9] (Fig 1B). The monomeric affinity of galectins for lactosamine and lactose are very low at ~10^{-3}M [10], but comparable to the affinity of peptide-MHC-induced oligermerization of TCR measured in solution [11], and therefore compatible with exchange between TCR clustering and TCR-galectin binding. At the contact site with MHC-peptides of sufficient

affinity for T cell activation, TCR is removed from a galectin-glycoprotein multivalent lattice and reorganize into macromolecular immune synapse.

The extracellular domains of most cytokine receptors are N-glycosylated, and variation in glycan structures may impart a range of affinities for galectins. EGFR is a transmembrane 70 KDa protein core with 10-11 N-glycan chains for a mature size of 170KDa. NMR and mass spectrometry analysis of EGFR from A431 cells revealed 55 different structures including the β1,6GlcNAc-branched N-glycans extended with polylactosamine [12]. Multiple N-glycans should increase the binding avidity of EGFR in the galectin-glycoprotein lattice, ligand binding and receptor dimerization occurs with affinities (>10^{-9} M), greatly exceeding that of the galectin-glycan interaction (10^{-3}-10^{-4} M). Therefore, it is unlikely that ligand-dependent trafficking of cytokine receptors is impeded by galectins. However, galectin binding to Mgat5 glycans on cytokine receptors and integrins may block spontaneous receptor clustering, while enhancing retention of non-ligand bound receptors at the cell surface, particularly in cells with high endocytic activity. In this regard, Mgat5 is expressed in cell layers known to be active in endocytic and secretory activity [13].

BODY:

Our studies are the first to demonstrate that N-glycans, through their interactions with galectins, can regulate ligand-dependent receptor signaling [6]. Our recent progress in the second year of this grant has greatly refined the working model for Mgat5 functions (Fig 1)

Task 1 was to define the phenotype of *Mgat5*$^{-/-}$ mice, tumor progression and tumor cells phenotypes. We have used the Cellomics Scan Array automated fluorescence microscope to measure and quantify motility as well as Erk and Smad-2 activation. The instrument is designed for high through put analysis in 96 well plates and has been extremely useful completing task 1.

To determine whether Mgat5 could regulate cytokine receptors, we measured EGF and TGF-β dependent Erk-2 and Smad-2 phosphorylation by Western-blotting and nuclear translocalization by Scan Array immunoflourecence microscopy (Fig 2,3). With suitable antibodies, the scan array cyto-nuclear translocation method quantifies nuclear translocation of signaling proteins for individual cells, and making it possible to study single cells or averaged over populations. Signal transduction was deficient for both cytokines. EGFR and TβRII were distributed in punctate patterns in Mgat5$^{-/-}$ cells, coincident in greater measure with endocytic compartments marked by EEA-1 and Cav-1 compared to that of Mgat5$^{+/+}$ cells (Fig 4). K+ depletion and nystatin were used to disrupt coated-pits and caveolae, respectively. The combined treatments inhibited receptor co-localization with endosomal marker EEA-1 and Cav-1, and more importantly, restored EGF and TGF-β signaling (Fig 2,4). Receptor levels were reduced on Mgat5$^{-/-}$ cells, and restored by inhibiting endocytosis. Lactose treatment of wild type cells to disrupts galectin binding reduced levels of cell surface receptors (Fig 5) while enhancing their resideny in endosomes (Fig 7). The Mgat5 retroviral vector normalized the EGF and TGF-β responses in Mgat5$^{-/-}$ cells, while retrovirus encoding the mutant Mgat5 (Lec 4a L188R) failed to rescue. Experiments are in progress to reveal the direct physical interaction between receptors and galectins. However, our results indicate that Mgat5-

modified N-glycans on TβR and EGFR bind to galectins at the cells surface, which inhibits their removal into endosomes (model in Fig 1D).

Although the major effect of the Mgat5 deficiency is loss of receptors, an increase in spontaneous receptor aggregation was also observed. EGFR and TβR appeared more punctate in Mgat5$^{-/-}$ cells by immunofluorescence microscopy and lactose treatment of Mgat5-expressing cells for 1hr mimiced this punctate receptor distribution. Furthermore, disruption of coated-pits caused ligand-independent Erk activation, which was much greater in Mgat5$^{-/-}$ cells than Mgat5$^{+/+}$ cells (Fig 2). Disruption of both compartments restored ligand dependent signaling and the receptors displayed the more dispersed pattern. Ligand-independent aggregation of EGFR can activated signaling but not simply by inhibiting caoted-pits. Based on our results, Mgat5 may prevent spontaneous clustering and activation of EGFR which can take place in cholesterol-rich lipid rafts. TGF-β1 induces epithelial-mesenchymal transition (EMT) in premalignant epithelial cells, which requires PI3K/Akt and Ras pathways [14]. EMT refers to a morphological conversion where polarized epithelial cells acquire fibroblastic characteristics, including motility, loss of tight junctions and E-cadherin protein from adhesions. As an autocrine factor, TGF-β1 maintains EMT in some tumor. TGF-β induces the fibroblastic morphology in PyMT Mgat5$^{+/+}$ and in rescued Mgat5$^{-/-}$ cells, but in Mgat5$^{-/-}$ cells which retained a coble-stone epithelial morphology and E-cadherin in tight junctions. TGF-β enhances Mgat5 expression in B16 melanoma cells suggesting a positive feedback relationship. To determine whether a TGF-β autocrine loop is compromised in Mgat5$^{-/-}$ cells, we will suppress autocrine TGF-β activity with the antagonist Ahsg [15,16], and examine EMT as well as basal and TGF-β induced Smad-2 activity. We will attempt to rescue the failure of EMT in PyMT Mgat5$^{-/-}$ cells with a dominant active TβRI, and with dominant negative (dn-)dynamin (K44A) to block endocytosis. Rescue with these constructs would support a causal relationship between TGF-β signaling, the Mgat5$^{-/-}$ defect in EMT, and receptor residency at the cell surface, respectively. dn-dynamin (K44A) may enhance surface levels of other receptors and rescue additional Mgat5 cellular phenotypes as noted below.

Task 2: Genetic experiments are used to identify the critical pathways regulated by Mgat5 in cancer cells. In the first year our grant, we established that most PyMT-induced mammary tumors in *Mgat5*$^{-/-}$ mice grow slowly, and displayed impaired focal adhesion signaling and PI3K/PKB activation [17]. Steady-state phospho(473)-Akt was lower in PyMT *Mgat5*$^{-/-}$ tumor homogenates, while phospho-Erk was similar in both PyMT *Mgat5*$^{-/-}$ and PyMT *Mgat5*$^{+/+}$ tumors [17]. Importantly, the few (5%) PyMT *Mgat5*$^{-/-}$ tumors that escaped growth suppression, presumable due to additional mutations, had high levels of activated Akt similar to wild type tumors. These data suggested that Mgat5-modified glycans on cell surface receptors collaborate with intracellular PyMT to activate PI3K/Akt in the tumor cells. PI3K activation is required for cell motility and tumor cell invasion [18,19]. Indeed, PyMT Mgat5$^{-/-}$ tumor cells are deficient in membrane ruffling, actin filament turnover and cell motility (Fig 8). Cell motility is rescued by infecting mutant cells with an Mgat5 retroviral vector, while the Mgat5 ($L_{188}R$) mutation did not rescue the defects. The Mgat5 ($L_{188}R$) mutant enzyme fails to localize in the Golgi, and glycoproteins are not Mgat5-modified.

Curiously, constitutive PI3K/Akt activity but not that of Erk is impaired in PyMT transformed Mgat5$^{-/-}$ cells, while acute Erk activation in serum-arrested cells by EGF or

serum is severely impaired but that of Akt is only delayed. A deficiency in constitutive PI3K/Akt activity is likely to produce additional phenotypes affecting cell size, cell cycle checkpoint, sensitivity to stress, senescence and glucose homeostasis [20]. Indeed, $Mgat5^{-/-}$ PyMT tumor cells have reduced cell volume and defects in cell cycle checkpoints revealed as resistance to hydroxurea and colcemid (Fig 9). The Mgat5 retoviral vector rescued both of these phenotypes. In cycling cells, volume increases in G1 phase, preceding start at the G1/S transition.

$Pten^{+/-}$ cells are partially deficient in PIP3 phosphatase, and the resultant increase in PIP3,4 and PIP3,4,5 enhances Akt activation [21,22]. Pten is commonly mutated in human cancers and associated with progression [23]. To determine whether the $Mgat5^{-/-}$ mutation might suppress the hyper-activation of PI3K/Akt in $Pten^{+/-}$ mice, we have interbred Mgat5 and Pten mutant mice and preliminary results suggest these genes interaction, in the immune system and in other tissues. If a deficiency in PI3K/Akt down-stream of Mgat5 is causal in cell volume, checkpoints, and motility phenotypes, then increasing PIP3,4 and PIP3,4,5 levels may rescue some or all phenotypes. Pten deficiency increased phospho(473)-Akt, enhanced cell motility [24], enhances cell survival [25], and cell size[26], and over-expression of PTEN induces premature senescence. In preliminary experiment double mutant $Mgat5^{-/-}$ $Pten^{+/-}$ mice showed normalization of phospho(473)-Akt in kidney homogenates. As molecular evidence that rescue has occurred through this pathway, we plan to measure phospho- Akt and –Erk by Western blots, and kinase activities by ip of Akt, Pdk1, S6K and RSK in liver, spleen, intestine, kidney and lungs. Neutrophil migration is slower in $Mgat5^{-/-}$ mice (Fig 8). To determine whether the compensating effects of PTEN and Mgat5 normalize cell migration *in vivo* (a marker of metastatic cells), we will measure neutrophil migration into the peritoneal cavity 3hr post injection of thioglycolate. Migration rates might be expected to correlate with phospho(473)-Akt levels, producing the relationship; $Mgat5^{+/+}/PTEN^{+/-} > Mgat5^{+/+}/PTEN^{+/+} > Mgat5^{-/-}/PTEN^{+/-} > Mgat5^{-/-}/PTEN^{+/+}$. This result would indicate that opposition by PTEN and Mgat5 controls PI3K/Akt activity and cell motility. This would suggest Mgat5 antagonists should block malignant phenotypes associated loss of Pten or over-expression of PI3K, common events in human cancers.

Task 3: is to identify targets for Mgat5 glycosylation that are important in cancer growth. Since last year we identify EGF receptor and TGF-β receptor as two more targets in addition to T cell receptor and β1 integrins. In addition, we have determined the Mgat5-glycans interact with galectins at the cell surface. The interaction of receptors and galectins impedes receptor endocytosis and enhances signaling. This is a novel and exciting advance in our understanding of N-glycan function on signaling receptors. More work is required to identify additional receptors and quantify their interactions with specific galectins. We will determine whether Mgat5 glycans on integrins through galectins binding, destabilize adhesion plaques and accelerate turnover, thereby promote cell migration.

Task 4 was to location β1,6GlcNAc-branched N-glycans that mediate phenotype. Since last year, we have attached functional significance to Mgat5-modification of EGF receptor and TGF-β receptor. In preliminary experiments, both receptor show an Mgat5-dependent increase in binding to galectins-3 at the cell surface. We plan to compete this biochemical analysis of Mgat5-modified glycans on these receptors.

KEY RESEARCH ACCOMPLISHMENTS:

- We have rescued defects in PyMT Mgat5$^{-/-}$ tumor cells with an Mgat5 retoviral vector, proving cause and effect.
- We used the new scan array assay to measure signaling and cell motility which allowed us to completion of task 1. In these studies we have shown that Mgat5 regulates EGFR and TGF-β receptor cell surface residency.
- We have generated Mgat5 crosses with Pten mutant mice, and preliminary results suggest a gene interactions and therefore the possibility of targeting this pathway in cancer with anti-Mgat5 agents.

REPORTABLE OUTCOMES:

- Publications:

We published a key paper last year in the high-impact journal ***Nature*** and another equally important paper is being prepared. We published the first paper on C. elegans Mgat5 this year in ***J. Biol. Chem***. We have done several invited reviews on the wider implications of our findings, the most recent for ***Biochem. Biophys. Act.***

- Patent:

A US patent application was files last coving methods of drug discovery based on the concept of N-glycans as a modifier of receptor clustering.

- Invited Lectures:

Dr. Dennis has presented aspects of this work at NIH Glycobiology and Cancer Workshop, Bethesda, Jul 17; Lake Ontario Metastasis Society; Chicago Sep 20, 13th Annual CEA meeting, "key note speaker" Aug 11; Mizutani symposium, Tokyo, Dec 9; Japanese Immunology Society Meeting, Tokyo, Dec 4; Immunology Council Seminar, Johns Hopkins; Roswell Park, Molecular & Cellular Biophysics Department.

- Trainees:

Mike Demetriou MD, PhD has taken a tenure track position at U. of Irvine, CA
Pam Chueng, a Ph.D. student in the Molecular and Medical Genetics Department at University of Toronto has been working on project since early 2000.
Emily Partidge has joined the project early this year as a PhD student in the Department of laboratory Medicine, University of Toronto

CONCLUSIONS: We have used tumor cell lines derived from mutant mice effectively this year to show that Mgat5 regulates adhesion and cytokine receptors in cancer cells. The data identifies important targets and suggests a broader mechanism of action for Mgat5 in the regulation of tumor cell responses to trophic factors. Agents that deprive tumors of trophic growth stimulation are an important new approach to cancer therapy (eg Herceptin and Glevac). Our results suggest that these agents may work well with inhibitors of Mgat5, and target receptors to suppress cancer growth. We are testing this hypothesis further by comparing the sensitivity of Mgat5 mutant wild type tumors to a variety of chemotherapeutics and other anti-cancer agents.

REFERENCES:

1. Varki, A. and Marth, J. Oligosaccharides in vertebrate development. Dev.Biol., *6*: 127-138, 1995.

2. Hakomori, S.-I. Aberrant glycosylation in tumors and tumor-associated carbohydrate antigens. Adv.Cancer Res., *52*: 257-331, 1989.

3. Fernandes, B., Sagman, U., Auger, M., Demetriou, M., and Dennis, J. W. β1-6 branched oligosaccharides as a marker of tumor progression in human breast and colon neoplasia. Cancer Res., *51*: 718-723, 1991.

4. Seelentag, W. K., Li, W. P., Schmitz, S. F., Metzger, U., Aeberhard, P., Heitz, P. U., and Roth, J. Prognostic value of beta 1,6-branched oligosaccharides in human colorectal carcinoma. Cancer Res., *58*: 5559-5564, 1998.

5. Demetriou, M., Nabi, I. R., Coppolino, M., Dedhar, S., and Dennis, J. W. Reduced contact-inhibition and substratum adhesion in epithelial cells expressing GlcNAc-transferase V. J.Cell Biol., *130*: 383-392, 1995.

6. Demetriou, M., Granovsky, M., Quaggin, S., and Dennis, J. W. Negative regulation of T-cell activation and autoimmunity by Mgat5 N-glycosylation. Nature, *409*: 733-739, 2001.

7. Hughes, R. C. Secretion of the galectin family of mammalian carbohydrate-binding proteins. Biochim.Biophys.Acta, *1473*: 172-185, 1999.

8. Rudd, P. M., Wormald, M. R., Stanfield, R. L., Huang, M., Mattsson, N., Speir, J. A., DiGennaro, J. A., Fetrow, J. S., Dwek, R. A., and Wilson, I. A. Roles for glycosylation of cell surface receptors involved in cellular immune recognition. J Mol Biol, *293*: 351-366, 1999.

9. Mandal, D. K. and Brewer, C. F. Cross-linking activity of the 14-kilodalton beta-galactoside-specific vertebrate lectin with asialofetuin: comparison with several galactose-specific plant lectins. Biochemistry, *31*: 8465-8472, 1993.

10. Herman, T. and Horvitz, H. R. Three proteins involved in *Caenorhabditis elegans* vulval invagination are similar to components of a glycosylation pathway. Proc.Natl.Acad.Sci.USA, *96*: 974-979, 1999.

11. Yeh, J. C., Ong, E., and Fukuda, M. Molecular cloning and expression of a novel beta-1, 6-N-acetylglucosaminyltransferase that forms core 2, core 4, and I branches. J Biol Chem, *274*: 3215-3221, 1999.

12. Stroop, C. J. M., Weber, W., Gerwing, G. J., Nimtz, M., Kamerling, J. P., and Vliegenthart, J. F. G. Characterization of the carbohydrate chains of the secreted form of the human epidermal growth factor receptor. Glycobiology, *10*: 901-917, 2000.

13. Granovsky, M., Fode, C., Warren, C. E., Campbell, R. M., Marth, J. D., Pierce, M., Fregien, N., and Dennis, J. W. GlcNAc-transferase V and core 2 GlcNAc-transferase expression in the developing mouse embryo. Glycobiology, *5*: 797-806, 1995.

14. Bakin, A. V., Tomlinson, A. K., Bhowmick, N. A., Moses, H. L., and Arteaga, C. L. Phosphatidylinositol 3-kinase function is required for transforming growth factor beta-mediated epithelial to mesenchymal transition and cell migration. J Biol Chem, *275*: 36803-36810, 2000.

15. Szweras, M., Liu, D., Partridge, E. A., Pawling, J., Sukhu, B., Clokie, C., Jahnen-Dechent, W., Tenenbaum, H. C., Swallow, C. J., Grynpas, M., and Dennis, J. W. α2-HS Glycoprotein /Fetuin, a transforming growth factor-β/bone morphogenetic protein antagonist, Regulates Postnatal Bone Growth and Remodeling. J.Biol.Chem., *277*: 19991-19997, 2002.

16. Demetriou, M., Binkert, C., Sukhu, B., Tenenbaum, H. C., and Dennis, J. W. Fetuin/α2-HS glycoprotein is a transforming growth factor-β type II receptor mimic and cytokine antagonist. J.Biol.Chem., *271*: 12755-12761, 1996.

17. Granovsky, M., Fata, J., Pawling, J., Muller, W. J., Khokha, R., and Dennis, J. W. Suppression of tumor growth and metastasis in Mgat5-deficient mice. Nature Med., *6*: 306-312, 2000.

18. King, W. G., Mattaliano, M. D., ChanT.O., Tsichlis, P. N., and Brugge, J. S. Phosphatidylinositol 3-kinase is required for integrin-stimulated AKT and Raf-1/mitogen-activated protein kinase pathway activation. Mol.Biol.Cell, *17*: 4406-4418, 1997.

19. Keely, P. J., Westwick, J. K., Whitehead.I.P., Der, C. J., and Parise, L. V. Cdc42 and Rac1 induce integrin-mediated cell motility and invasiveness through PI(3)K. Nature, *390*: 632-636, 1997.

20. Lawlor, M. A., Mora, A., Ashby, P. R., Williams, M. R., Murray-Tait, V., Malone, L., Prescott, A. R., Lucocq, J. M., and Alessi, D. R. Essential role of PDK1 in regulating cell size and development in mice. EMBO J, *21*: 3728-3738, 2002.

21. Katso, R., Okkenhaug, K., Ahmadi, K., White, S., Timms, J., and Waterfield, M. D. Cellular function of phosphoinositide 3-kinases: implications for development, homeostasis, and cancer. Annu.Rev.Cell Dev.Biol., *17*: 615-675, 2001.

22. Moretta, A. Molecular mechanisms in cell-mediated cytotoxicity. Cell, *90*: 13-18, 1997.

23. Marsh, D. J., Dahia, P. L., Caron, S., Kum, J. B., Frayling, I. M., Tomlinson, I. P., Hughes, K. S., Eeles, R. A., Hodgson, S. V., Murday, V. A., Houlston, R., and Eng, C. Germline PTEN mutations in Cowden syndrome-like families. J.Med.Genet., *35*: 881-885, 1998.

24. Higuchi, M., Masuyama, N., Fukui, Y., Suzuki, A., and Gotoh, Y. Akt mediates Rac/Cdc42-regulated cell motility in growth factor-stimulated cells and in invasive PTEN knockout cells. Curr.Biol., *11*: 1958-1962, 2001.

25. Stambolic, V., Suzuki, A., de la Pompa, J. L., Brothers, G. M., Mirtsos, C., Sasaki, T., Ruland, J., Penninger, J. M., Siderovski, D. P., and Mak, T. W. Negative regulation of PKB/Akt-dependent cell survival by the tumor suppressor PTEN. Cell, *95*: 29-39, 1998.

26. Huang, H., Potter, C. J., Tao, W., Li, D.-M., Brogiolo, W., Hafen, E., Sun, H., and Xu, T. PTEN affects cell size, cell proliferation and apoptosis during *Drosophila* eye development. Development, *126*: 5365-5372, 1999.

APPENDICES:

Granovsky, M., Fata, J., Pawling, J., Muller, W.J., Khokha, R., and Dennis, J.W. Suppression of tumor growth and metastasis in Mgat5-deficient mice. Nature Med., *6*: 306-312, 2000.

M. Demetriou, M. Granovsky, S. Quaggin J. W. Dennis. Negative regulation of T cell receptor and autoimmunity by *Mgat5* N-glycosylation. **Nature** 409:733-739, (2001).

C. E. Warren, A. Krizus, P. J. Roy, Joseph G. Culotti and James W. Dennis (2001) The non-essential *C. elegans* gene, *gly-2*, can rescue the *N*-acetylglucosaminyltransferase V mutation of Lec4 cells. (2002) **J. Biol. Chem.** 277:22829-22838.

J.W. Dennis, C.E. Warren and M. Demetriou M. Granovsky. Genetic defects in *N*-glycosylation and cellular diversity in mammals. (2001) **Current Opinions in Structural Biol.** 11: 601-607, 2001.

Legends:

Figure 1:

N-glycosylation and Mgat5: (A) N-glycosylation pathway and galectin interaction with polylactosamine. **(B)** Ribbon structure of TCR with space filling model of N-glycans. The Gal-3 structure is depicted as bridging the distance between TCR and another glycoprotein. **(C)** The phosphoinositide pathway and localization in membrane compartment of the cell. **(D)** Scheme of receptor movement into endosomes either through clathrin-coated pits or through caveolae lipid rafts, followed by ubiquitination and destruction in lysosomes. In our working model, galectins binding to Mgat5 glycans on receptors forming a lattice that prevents the receptors from entering the endosomes and thereby enhancing cell surface expression.

Figure 2:

Erk phosphorylation and nuclear translocation in response to EGF is defective in Mgat5-/- tumor cells. **(A)** Staining with phospho-ERK antibodies. **(B)** Western blots for phospho-ERK antibodies at times course following addition of 100 ng/ml of EGF.

Figure 3:
Smad-2 phosphorylation and nuclear translocation in response to EGF is defective in Mgat5-/- tumor cells. **(A)** Staining with phospho-Smad-2 antibodies. **(B)** Western blots for phospho-Smad-2 antibodies at times course following addition of 100 ng/ml of TGF-β1

Figure 4:
Co-staining for EGFR (red) and endocytic compartments (green) coated-pits (EEA1) and caveolae (Cav-1) with and without drug treatments. Nystatin block cholesterol in caveolae lipid rafts and K+ depletion blocks clathrin coated-pit formation.

Figure 5:
Cell surface TGF-β receptor type II is depleted in Mgat5-/- cells. **(A)** cell surface biotinylation followed by incubation for various times then ip of receptor followed by SDS-PAGE and Western bloting with Step-HPA. **(B)** cell surface biotinylation following control or 1h treatment with nystatin and K+ depeletion to block endocytosis. Cells are cultured for various times following treatment in normal growth medium. Receptor are ip from lysates and Westerns probed with Step-HPA. **(C)** TGF-β1 cross-linking to cell surface receptor was performed as previously described. PyMT tumor cells were incubated for 30 minutes at 37°C in KRH plus 0.5% BSA. The plates were placed on ice and washed once with cold KRH plus 0.5% BSA and 125I-labeled TGF-β1 added for 30 min. The cells were then washed twice with cold KRH plus 0.5% BSA, once with cold KRH, then 0.5ml of DSS at 60 μg/ml was added and incubated for 15 minutes at 4°C with agitation. The cells were then incubated for various times at 37°C in medium. The cell lysates were centrifuged, and the supernatants from equal cell numbers were subjected to SDS-PAGE. **(D)** Cells were treated as in panel B, but pretreated with sucrose or lactose for 1 hr prior to biotinylation.

Figure 6:
EGFR co-localization with endocytotic compartments; coated-pits (EEA1) and caveolae (Cav-1) is enhance in Mgat5-/- cells and the mutant phenotype is mimicked treating wild type cells with lactose to disrupt the galectins interactions.

Figure 7:
(A-G) Kinetics for Erk and Samd-2 nuclear translocation in response t EGF and TGF-β respectively. **(H)** schematic characterizing the differences in time courses.

Figure 8:
Cell migration, spreading and growth: **(A)** PyMT tumor cell motility on fibronectin coated wells quantified by imaging the migration paths through a lawn of fluorescent beads using scan array **(A)** Mgat5+/+ and **(B)** Mgat5$^{-/-}$ PyMT tumor cells. **(C)** Path area made by cells after 18hr and quantified for 100 per well. Each bar is the mean ± SE of 6

replicate wells. From top to bottom, the cells are PyMT wild type, PyMT Mgat5-/-, rescue of the latter with Mgat5, and rescue with Lec4A Mgat5($L_{188}R$) mutant Mgat5. The Mgat5 enzyme activity in the cells is listed beside the bars **(D,E)** The scratch wound assay was used to compare cell motility. Wild type PyMT tumor cells were mixed 1:1 with either **(D)** $Mgat5^{-/-}$ cells rescued with the Mgat5 retroviral vector or **(E)** rescued with the Lec4A Mgat5($L_{188}R$) mutant Mgat5 gene. Confluent and serum starved monolayer of cells on glass slides are wounded by a lane scraped with a pipet tip and on examined 24h later. **(F)** L-PHA lectin blot showing rescue of cell surface β1,6GlcNAc-branched N-glycans in PyMT $Mgat5^{-/-}$ tumor cells infected with the Mgat5 retroviral vector. **(G)** PyMT tumor cell spreading for 4hrs as a function of fibronectin concentration on coated surfaces. Data from 3 $Mgat5^{-/-}$ and 1 wild type line is shown. **(H)** Ear inflammation induced by arachidonic acid and **(G)** neutrophil infiltration 3hr after thioglycolate injection.

Figure 9:
(Top) Cell volume measure on a Coulter counter. **(Bottom)** Cell cycle distribution of PYMT tumor cells growing in log phase cultures, and sensitivity to mitotic blockers

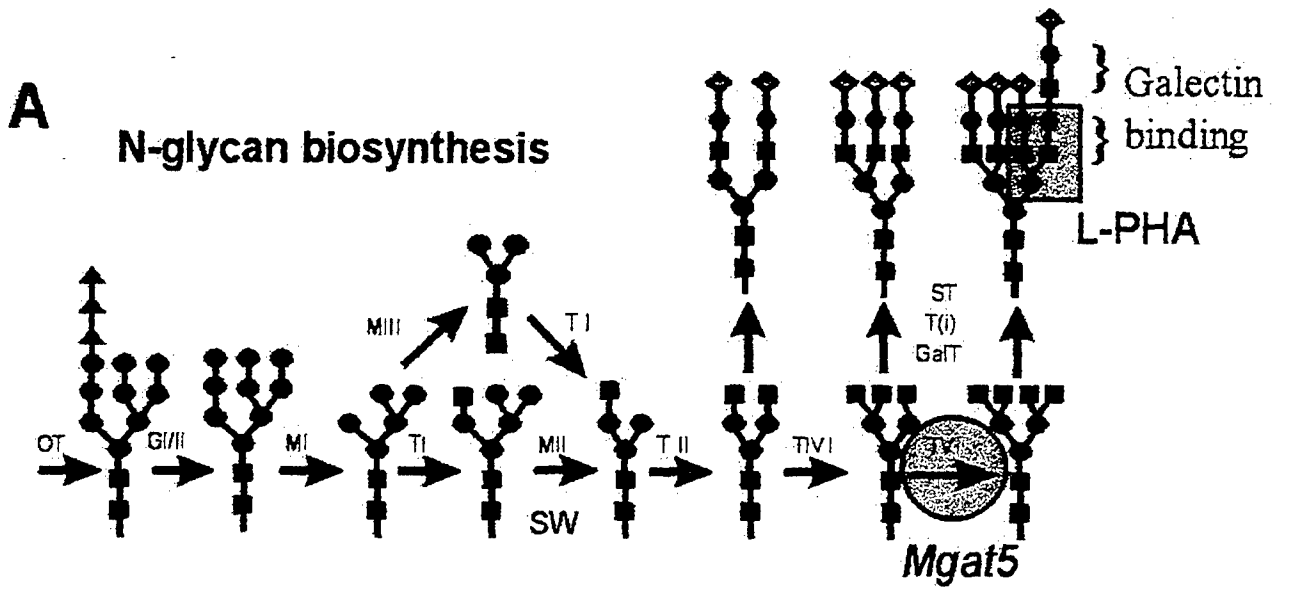

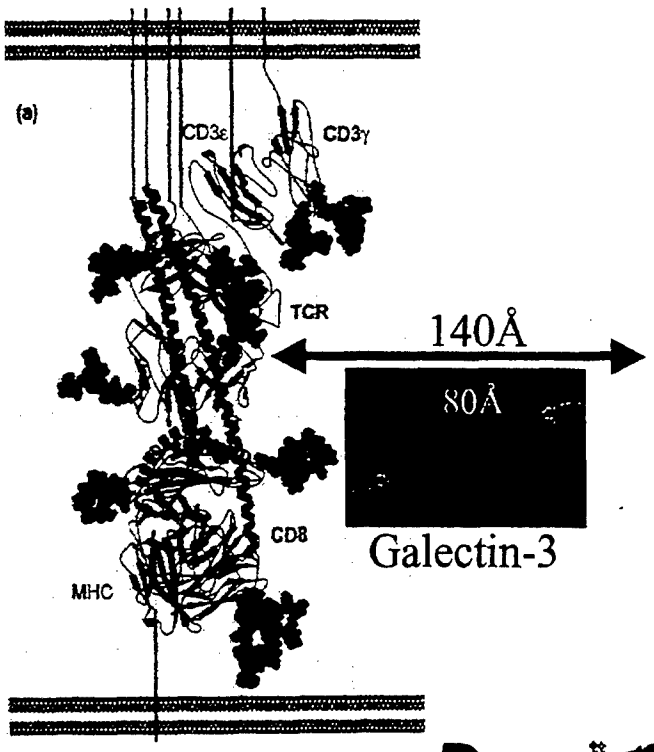

Rudd et al JMB
293:351, 1999

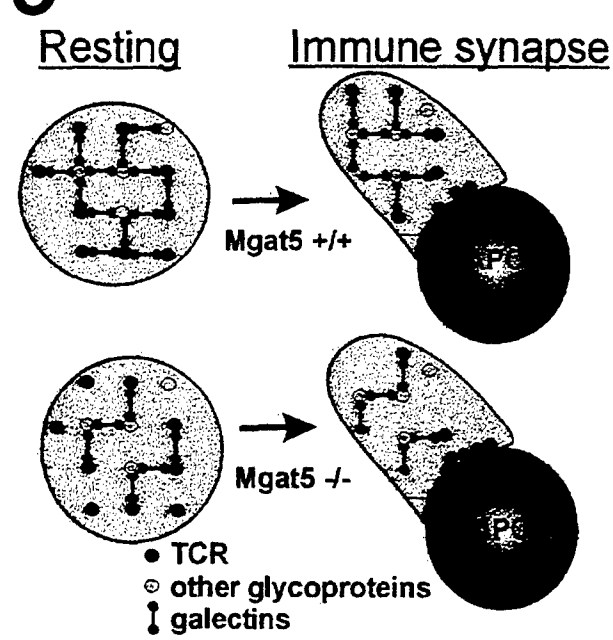

Demetriou et al Nature
409; 733,2001

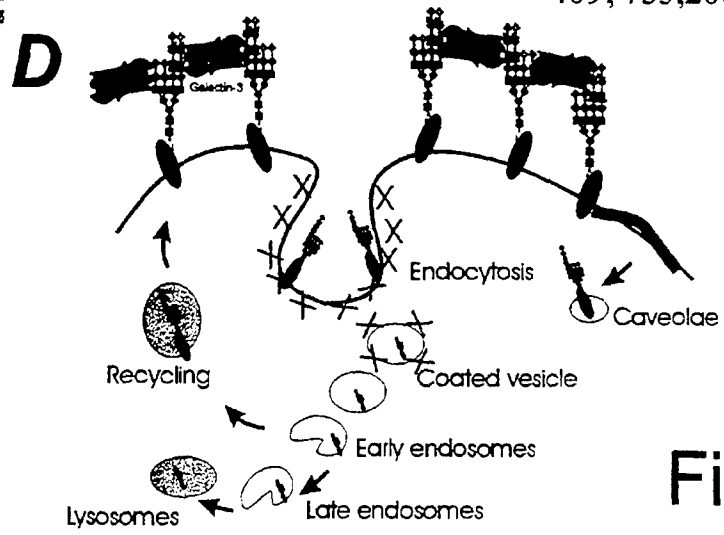

Figure 1

EGFR signaling is deficient in Mgat5-/- cells

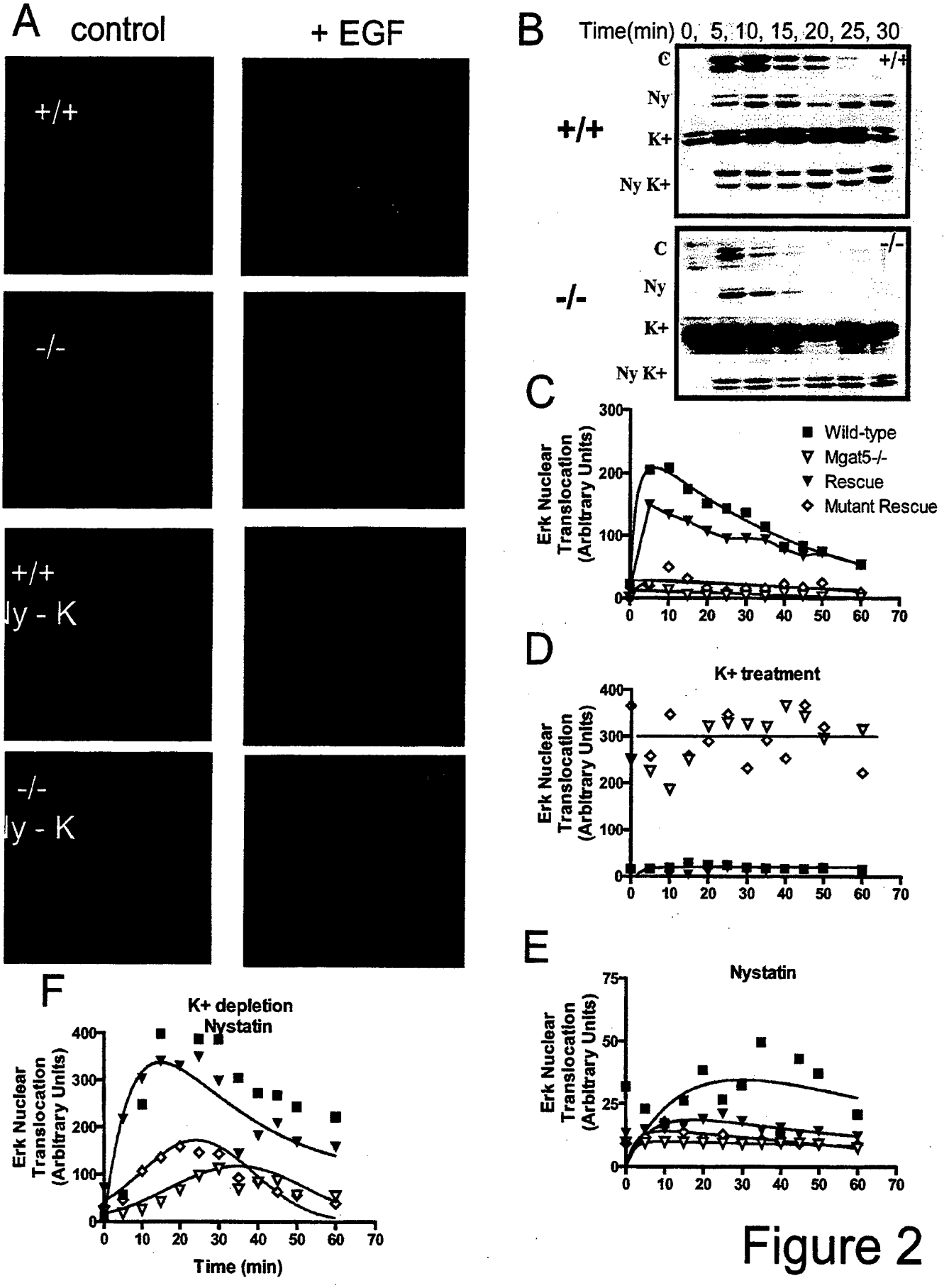

Figure 2

TβRII signaling is deficient in Mgat5-/- cells

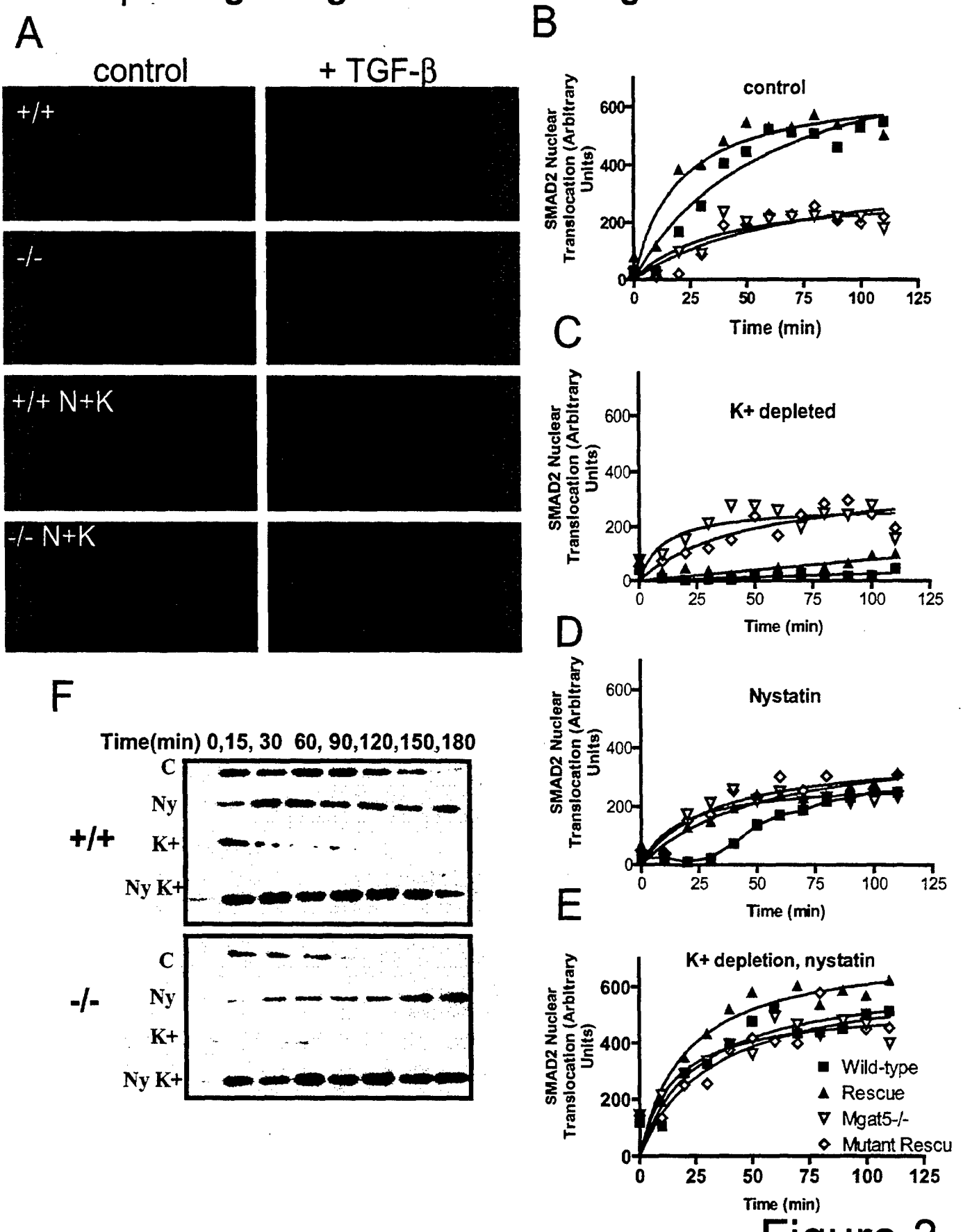

Figure 3

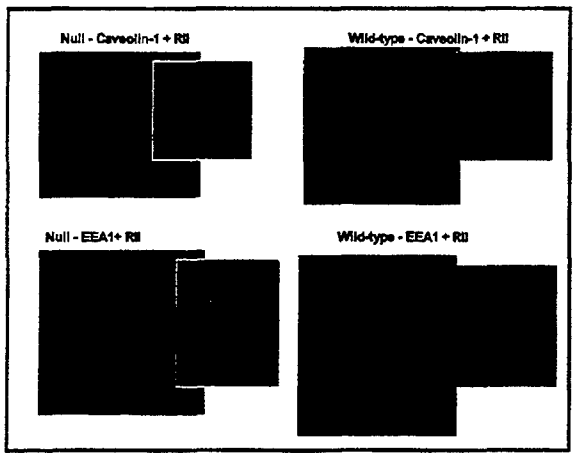
Null - Caveolin-1 + RII
Wild-type - Caveolin-1 + RII
Null - EEA1+ RII
Wild-type - EEA1 + RII

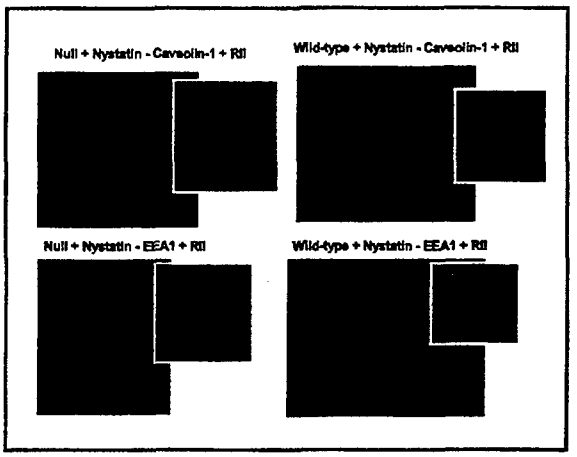
Null + Nystatin - Caveolin-1 + RII
Wild-type + Nystatin - Caveolin-1 + RII
Null + Nystatin - EEA1 + RII
Wild-type + Nystatin - EEA1 + RII

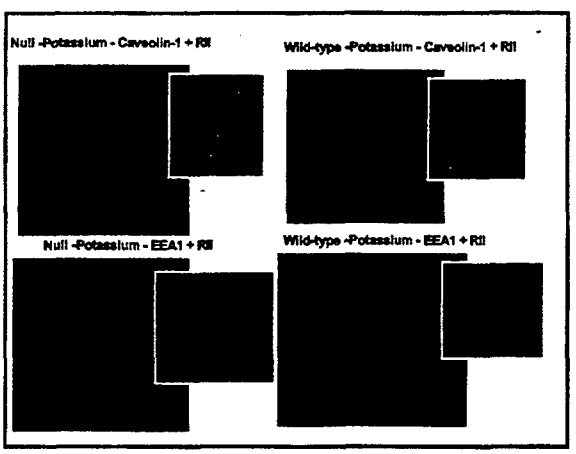
Null -Potassium - Caveolin-1 + RII
Wild-type -Potassium - Caveolin-1 + RII
Null -Potassium - EEA1 + RII
Wild-type -Potassium - EEA1 + RII

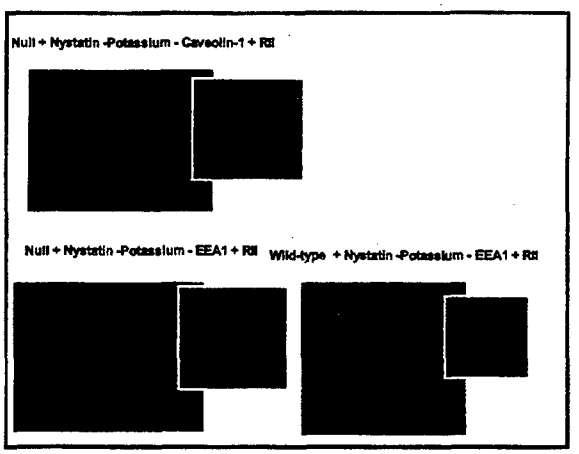
Null + Nystatin -Potassium - Caveolin-1 + RII
Null + Nystatin -Potassium - EEA1 + RII
Wild-type + Nystatin -Potassium - EEA1 + RII

Figure 4

Cell surface TβRII is depleted in Mgat5-/- cells

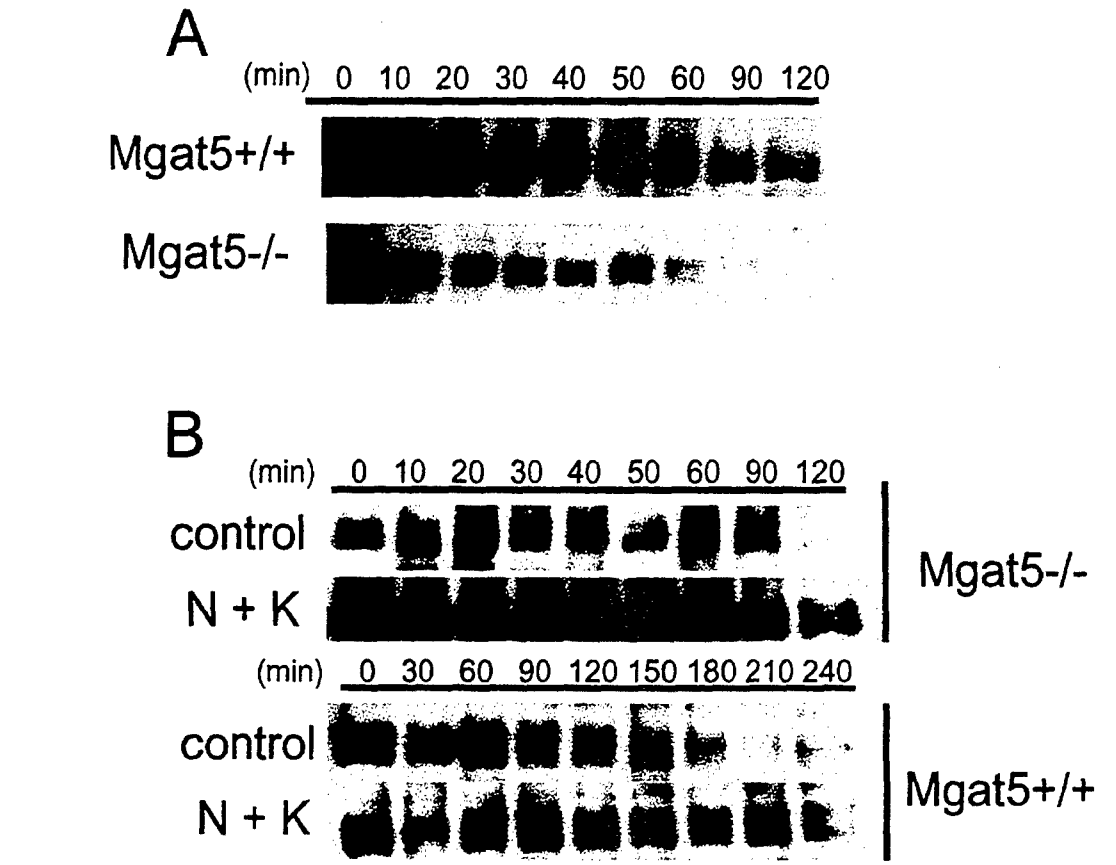

Figure 5

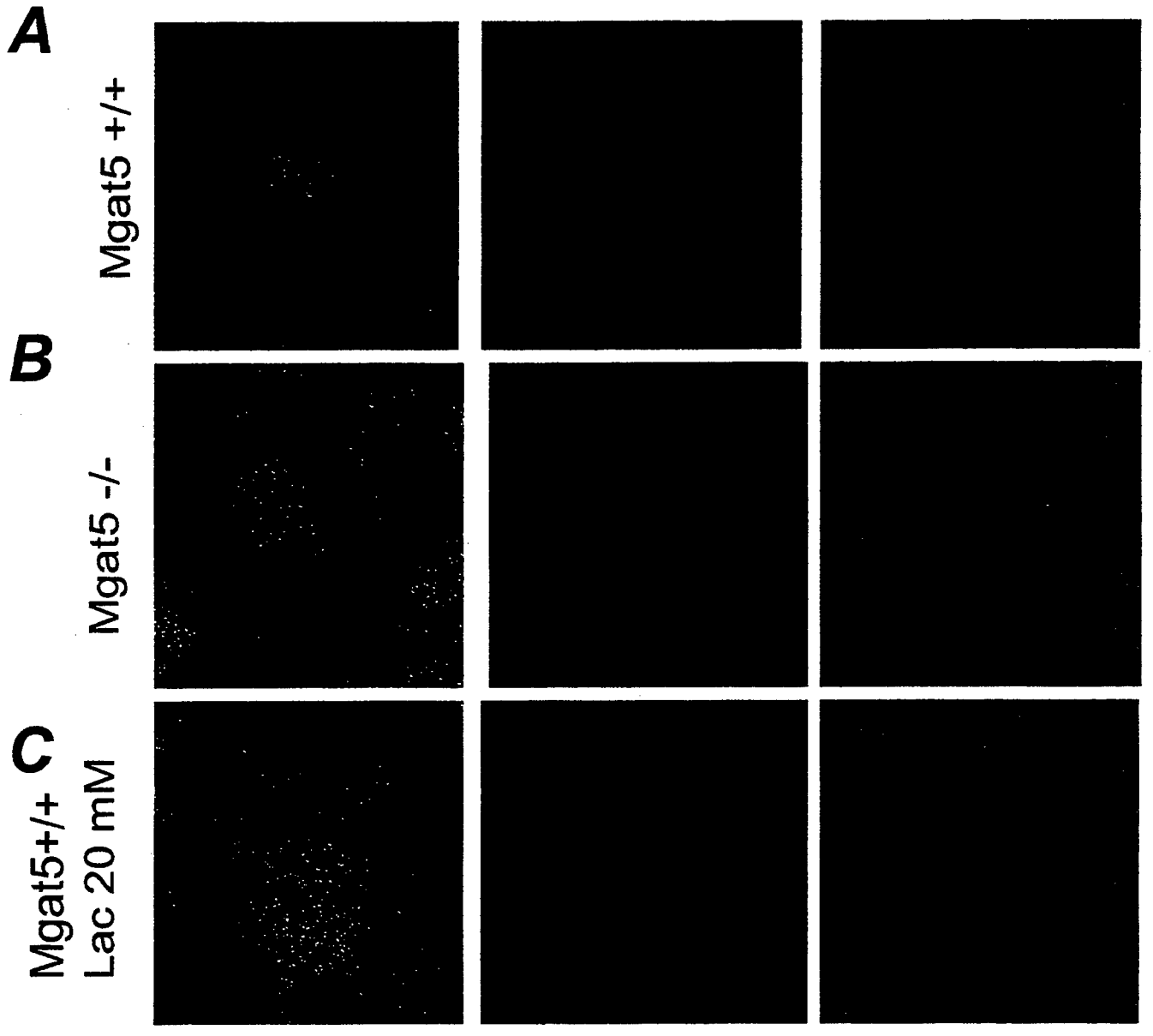
A
Mgat5 +/+
B
Mgat5 -/-
C
Mgat5+/+
Lac 20 mM

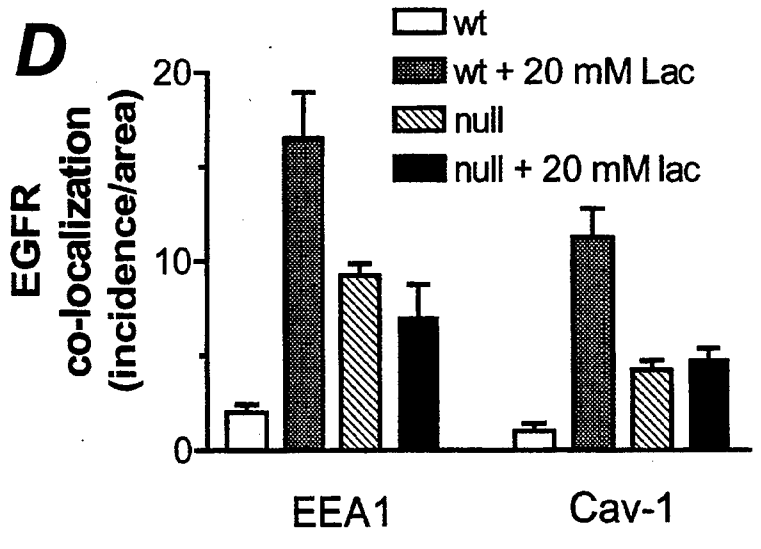
D
EGFR
co-localization
(incidence/area)
20
10
0
wt
wt + 20 mM Lac
null
null + 20 mM lac
EEA1
Cav-1

Figure 6

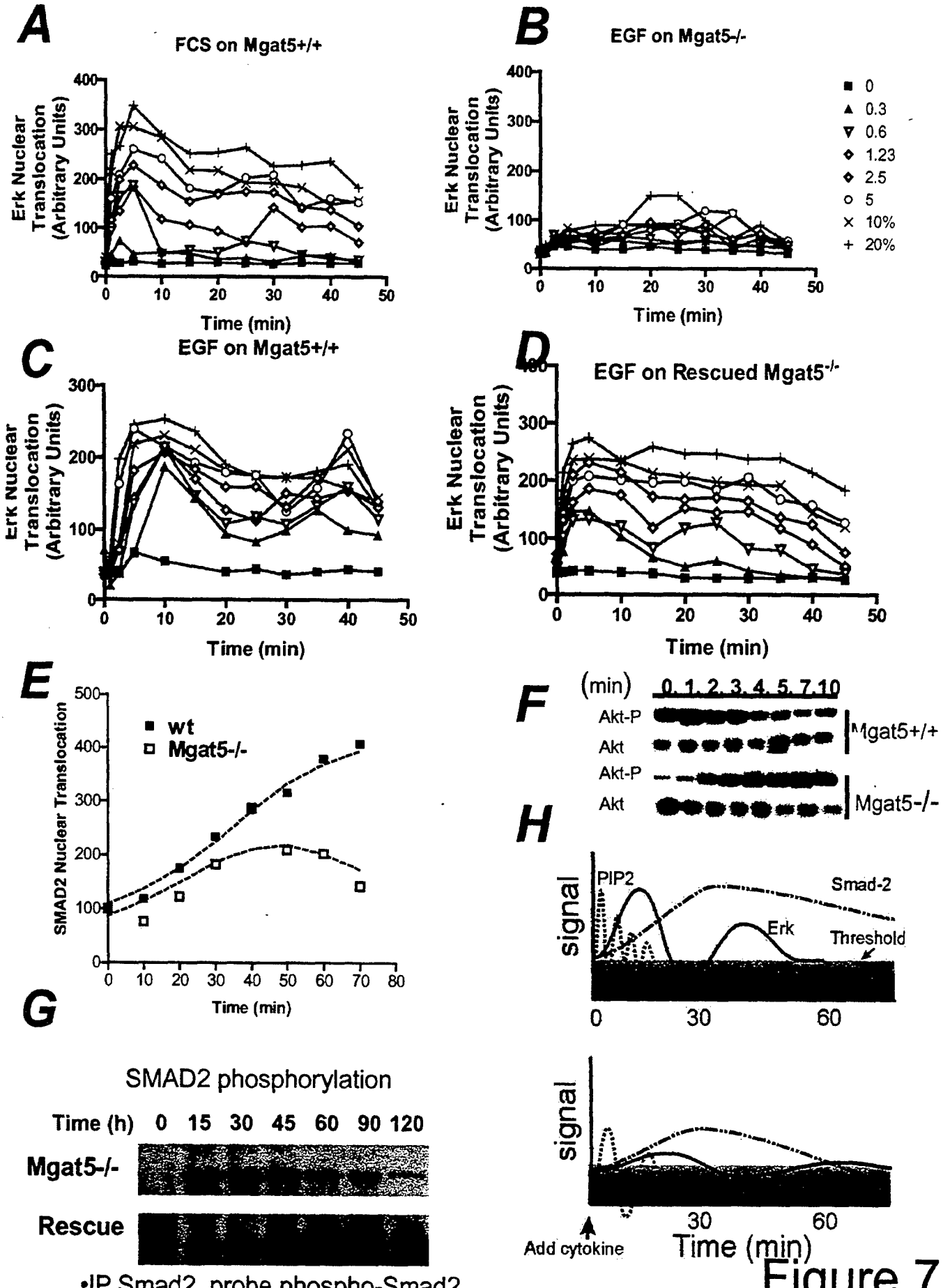
A
FCS on Mgat5+/+
Erk Nuclear Translocation (Arbitrary Units)
Time (min)
B
EGF on Mgat5-/-
Erk Nuclear Translocation (Arbitrary Units)
Time (min)
0
0.3
0.6
1.23
2.5
5
10%
20%
C
EGF on Mgat5+/+
Erk Nuclear Translocation (Arbitrary Units)
Time (min)
D
EGF on Rescued Mgat5-/-
Erk Nuclear Translocation (Arbitrary Units)
Time (min)
E
SMAD2 Nuclear Translocation
wt
Mgat5-/-
Time (min)
F
(min) 0 1 2 3 4 5 7 10
Akt-P
Akt
Mgat5+/+
Akt-P
Akt
Mgat5-/-
H
signal
PIP2
Smad-2
Erk
Threshold
0
30
60
G
SMAD2 phosphorylation
Time (h) 0 15 30 45 60 90 120
Mgat5-/-
Rescue
•IP Smad2, probe phospho-Smad2
signal
30
60
Add cytokine
Time (min)

Figure 7


A


B

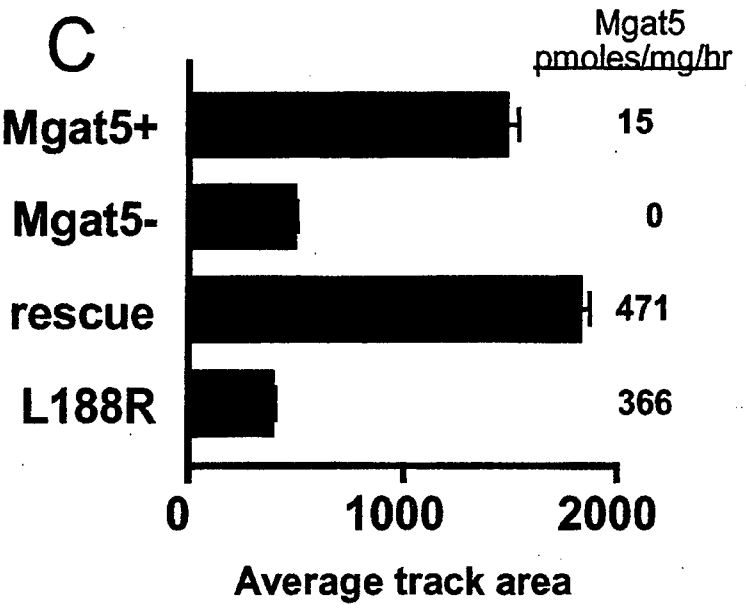
C
Mgat5
pmoles/mg/hr
Mgat5+
15
Mgat5-
0
rescue
471
L188R
366
0
1000
2000
Average track area

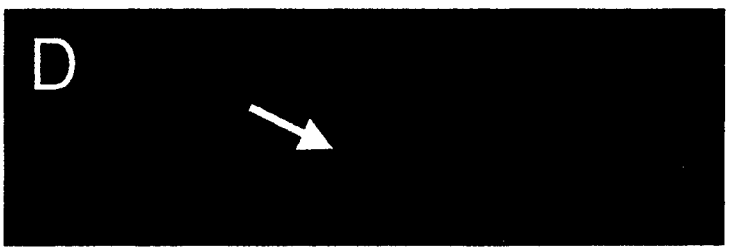
Mgat5
rescue
D

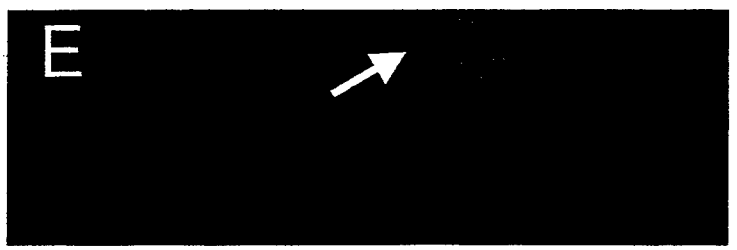
L188R
rescue
E

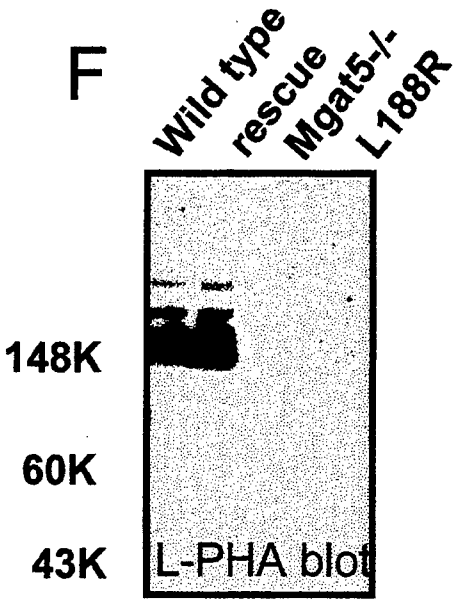
F
Wild type
rescue
Mgat5-/-
L188R
148K
60K
43K
L-PHA blot

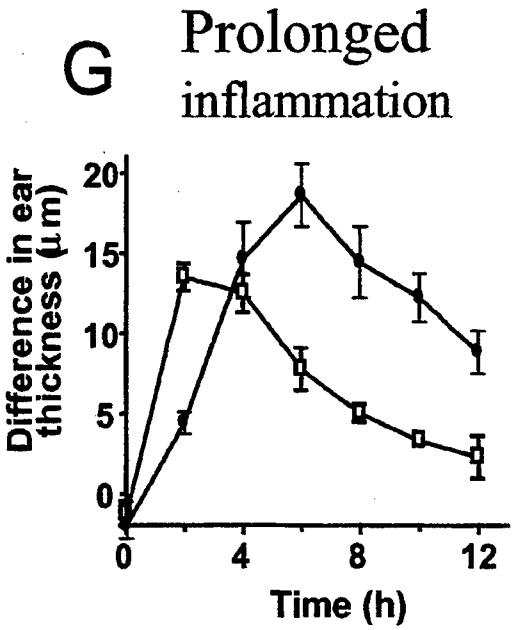
G
Prolonged
inflammation
Difference in ear
thickness (μm)
20
15
10
5
0
0
4
8
12
Time (h)

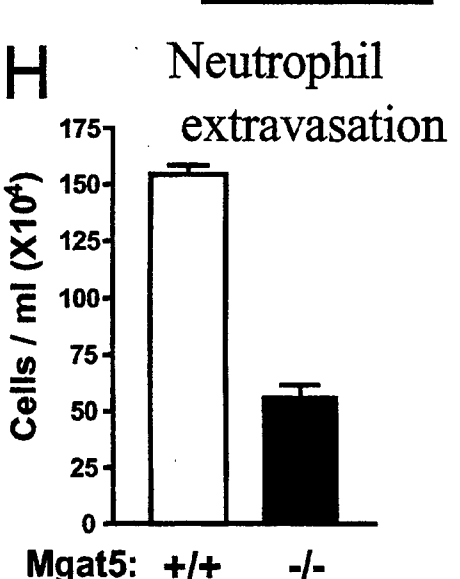
H
Neutrophil
extravasation
Cells / ml (X10⁴)
175
150
125
100
75
50
25
0
Mgat5: +/+ -/-

Figure 8

Cell volume is reduced in Mgat5$^{-/-}$ PyMT cells

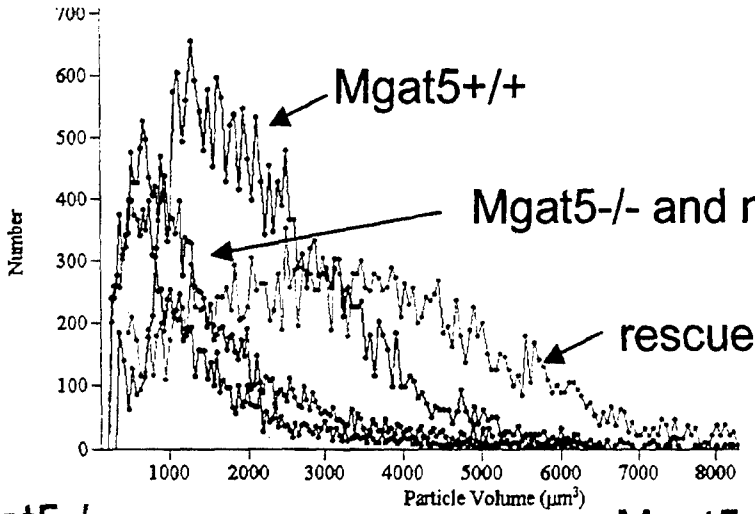

Mgat5-/-

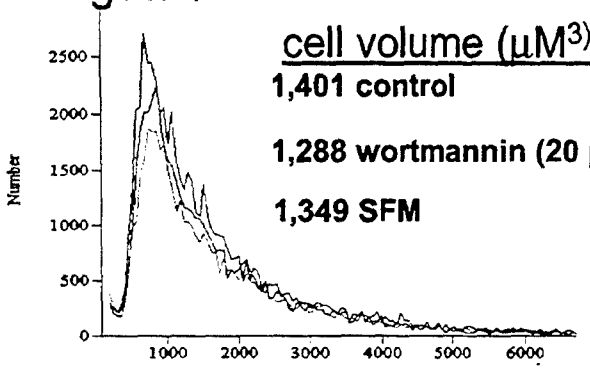

Mgat5+/+

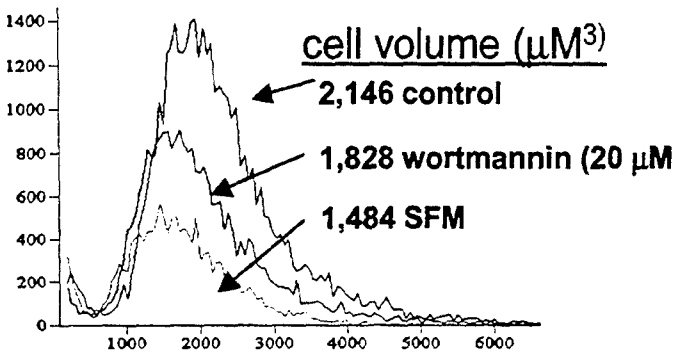

cell volume (μM3)

Altered cell cycle regulation in Mgat5 PyMT cells

Mgat5$^{-/-}$ cells pass G1/S prematurely

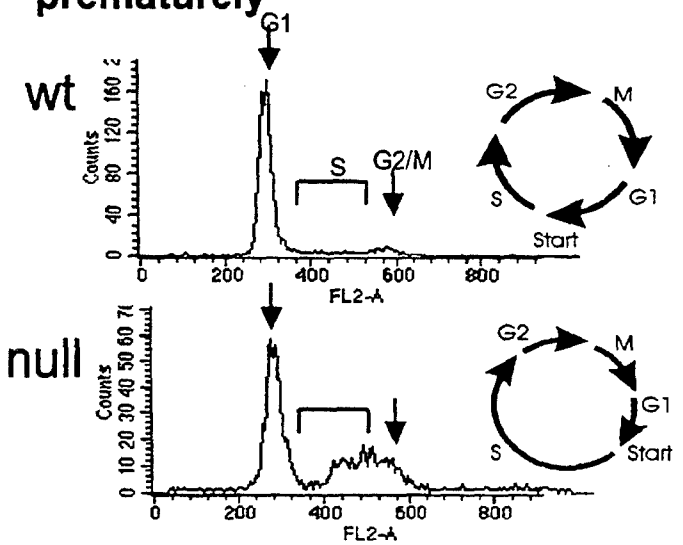

Mgat5$^{-/-}$ cells fail to arrest

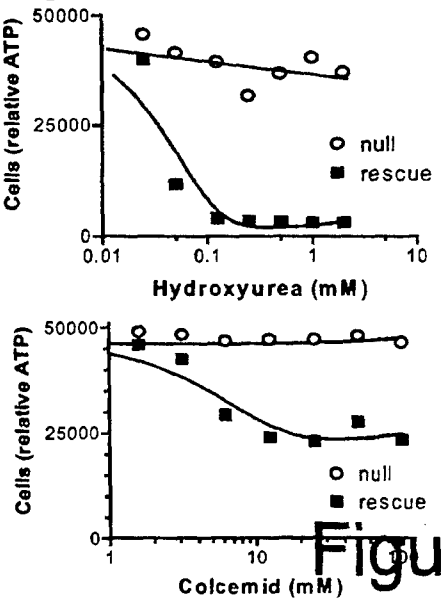

Figure 9

Glucose and insulin tolerance tests

Glucose tolerance tests were performed in awake mice after a 12-h fast[5]. Insulin tolerance tests were performed in awake mice after a 6-h fast[6].

Whole-body, skeletal muscle and liver glucose flux *in vivo*

Hyperinsulinaemic–euglycaemic clamp studies with uptake of [^{14}C]2-deoxyglucose into individual tissues were performed as described[25] in awake female mice at 6 months of age. Insulin was infused continuously for 120 min at 2.5 mU per kg (body weight) per min. Basal and insulin-stimulated rates of glucose turnover were measured with continuous [3-^{3}H]glucose infusion.

Phosphoinositide-3-OH kinase activity

Mice were fasted for 16–18 h, injected i.v. with saline or insulin (10 U per kg (body weight)) and killed 3 min after injection. Tissues were collected and frozen. PI(3)K activity was measured in phosphotyrosine immunoprecipitates (monoclonal antibody PY99, Santa Cruz Biotechnology, Santa Cruz, CA) from muscle and liver lysates as described[24].

Tissue triglyceride content

Triglyceride content in quadriceps muscle and liver was determined as described[25].

Adipocyte TNF-α mRNA and serum TNF-α levels

RNA was extracted from WAT and BAT using Trizol (GibcoBRL) and the expression of TNF-α mRNA relative to GAPDH mRNA or 18S ribosomal RNA was determined by real-time PCR (TaqMan, PE Systems). Serum TNF-α levels were determined in serum samples (50 μl) using the mouse TNF-α ELISA (Endogen). Both mRNA and serum levels were assessed in age- and sex-matched male and female mice at 12–13 and 26 weeks of age.

Statistical analysis

Data are expressed as mean ± s.e.m. Differences between two groups were assessed using the unpaired two-tailed *t*-test and among more than two groups by analysis of variance (ANOVA). Data involving more than two repeated measures (glucose and insulin tolerance tests) were assessed by repeated measures ANOVA. Analyses were performed using Statview Software (BrainPower, Calabasas, CA).

Received 29 August; accepted 14 November 2000.

1. Cline, G. W. *et al.* Impaired glucose transport as a cause of decreased insulin-stimulated muscle glycogen synthesis in type 2 diabetes. *N. Engl. J. Med.* **341**, 240–246 (1999).
2. Roden, M. & Shulman, G. I. Applications of NMR spectroscopy to study muscle glycogen metabolism in man. *Annu. Rev. Med.* **50**, 277–290 (1999).
3. Defronzo, R. A. Pathogenesis of type 2 diabetes: metabolic and molecular implications for identifying diabetes genes. *Diabetes Rev.* **5**, 177–269 (1997).
4. Shepherd, P. R. & Kahn, B. B. Glucose transporters and insulin action–implications for insulin resistance and diabetes mellitus. *N. Engl. J. Med.* **341**, 248–257 (1999).
5. Abel, E. D. *et al.* Cardiac hypertrophy with preserved contractile function after selective deletion of GLUT4 from the heart. *J. Clin. Invest.* **104**, 1703–1714 (1999).
6. Zisman, A. *et al.* Targeted disruption of the glucose transporter 4 selectively in muscle causes insulin resistance and glucose intolerance. *Nature Med.* **6**, 924–928 (2000).
7. Ross, S. R. *et al.* A fat-specific enhancer is the primary determinant of gene expression for adipocyte P2 *in vivo*. *Proc. Natl Acad. Sci. USA* **87**, 9590–9504 (1990).
8. Zambrowicz, B. P. *et al.* Disruption of overlapping transcripts in the ROSA β geo 26 gene trap strain leads to widespread expression of β-galactosidase in mouse embryos and hematopoietic cells. *Proc. Natl Acad. Sci. USA* **94**, 3789–3794 (1997).
9. Soriano, P. Generalized lacZ expression with the ROSA26 Cre reporter strain. *Nature Genet.* **21**, 70–71 (1999).
10. Katz, E. B., Stenbit, A. E., Hatton, K., Depinho, R. & Charron, M. J. Cardiac and adipose tissue abnormalities but not diabetes in mice deficient in GLUT4. *Nature* **377**, 151–155 (1995).
11. Donoghue, M. J., Alvarez, J. D., Merlie, J. P. & Sanes, J. R. Fiber type- and position-dependent expression of a myosin light chain- CAT transgene detected with a novel histochemical stain for CAT. *J. Cell Biol.* **115**, 423–434 (1991).
12. West, D. B., Boozer, C. N., Moody, D. L. & Atkinson, R. L. Dietary obesity in nine inbred mouse strains. *Am. J. Physiol.* **262**, R1025–R1032 (1992).
13. Boden, G. Role of fatty acids in the pathogenesis of insulin resistance and NIDDM. *Diabetes* **46**, 3–10 (1997).
14. Muoio, D. M. *et al.* Leptin directly alters lipid partitioning in skeletal muscle. *Diabetes* **46**, 1360–1363 (1997).
15. Barzilai, R. *et al.* Acute intravenous leptin infusion increases glucose turnover but not skeletal muscle glucose uptake in ob/ob mice. *Diabetes* **48**, 1264–1269 (1999).
16. Hotamisligil, G. S. & Spiegelman, B. M. Tumor necrosis factor alpha: a key component of the obesity-diabetes link. *Diabetes* **43**, 1271–1278 (1994).
17. Griffin, M. E. *et al.* Free fatty acid-induced insulin resistance is associated with activation of protein kinase C theta and alterations in the insulin signaling cascade. *Diabetes* **48**, 1270–1274 (1999).
18. Dresner, A. *et al.* Effects of free fatty acids on glucose transport and IRS-1-associated phosphatidylinositol 3-kinase activity. *J. Clin. Invest.* **103**, 253–9 (1999).
19. Mueller, W. M. *et al.* Evidence that glucose metabolism regulates leptin secretion from cultured rat adipocytes. *Endocrinology* **139**, 551–558 (1998).
20. Sivitz, W. I., Walsh, S. A., Morgan, D. A., Thomas, M. J. & Haynes, W. G. Effects of leptin on insulin sensitivity in normal rats. *Endocrinology* **138**, 3395–3401 (1997).
21. Tozzo, E., Gnudi, L. & Kahn, B. B. Amelioration of insulin resistance in streptozotocin diabetic mice by transgenic overexpression of GLUT4 driven by an adipose-specific promoter. *Endocrinology* **138**, 1604–1611 (1997).
22. Cushman, S. W. & Salans, L. B. Determinations of adipose cell size and number in suspensions of isolated rat and human adipose cells. *J. Lipid Res.* **19**, 269–273 (1978).
23. Kim, J. K., Gavrilova, O., Chen, Y., Reitman, M. L. & Shulman, G. I. Mechanism of insulin resistance in A-ZIP/F-1 fatless mice. *J. Biol. Chem.* **275**, 8456–8460 (2000).
24. Kim, Y. B. *et al.* Glucosamine infusion in rats rapidly impairs insulin stimulation of phosphoinositide 3-kinase but does not alter activation of Akt/protein kinase B in skeletal muscle. *Diabetes* **48**, 310–320 (1999).
25. Storlien, L. H. *et al.* Influence of dietary fat composition on development of insulin resistance in rats. Relationship to muscle triglyceride and omega-3 fatty acids in muscle phospholipid. *Diabetes* **40**, 280–289 (1991).

Acknowledgements

This work was supported by NIH Grants (to E.D.A., G.I.S. and B.B.K.) and an American Diabetes Association award to B.B.K. E.D.A. was the recipient of awards from the Robert Wood Johnson Foundation and the Eleanor and Miles Shore Scholars in Medicine Fellowship (Harvard Medical School). O.P. was supported by grants from the ALFEDIAM Society and Nestlé, France; and O.B. by the Human Frontier Sciences Program. We thank H. Chen for performing the TaqMan assays; P. She and M.A. Magnusen for breeding *aP2–Cre* mice with *Rosa26–lacZ* floxed mice; G. Hotamisligil for helpful advice; and C. Oberste-Berghaus and M. Pham for expert assistance.

Correspondence and requests for materials should be addressed to B.B.K. (e-mail: bkahn@caregroup.harvard.edu).

Negative regulation of T-cell activation and autoimmunity by *Mgat5 N*-glycosylation

Michael Demetriou*†‡, Maria Granovsky*‡, Sue Quaggin* & James W. Dennis*§

** Samuel Lunenfeld Research Institute, Mount Sinai Hospital, 600 University Avenue, R988, Toronto, Ontario M5G 1X5, Canada*
† Division of Neurology, Department of Medicine, University of Toronto
§ Department of Molecular & Medical Genetics, University of Toronto
‡ These authors contributed equally to this work

T-cell activation requires clustering of a threshold number of T-cell receptors (TCRs) at the site of antigen presentation, a number that is reduced by CD28 co-receptor recruitment of signalling proteins to TCRs[1–5]. Here we demonstrate that a deficiency in β1,6 *N*-acetylglucosaminyltransferase V (Mgat5), an enzyme in the *N*-glycosylation pathway, lowers T-cell activation thresholds by directly enhancing TCR clustering. Mgat5-deficient mice showed kidney autoimmune disease, enhanced delayed-type hypersensitivity, and increased susceptibility to experimental autoimmune encephalomyelitis. Recruitment of TCRs to agonist-coated beads, TCR signalling, actin microfilament re-organization, and agonist-induced proliferation were all enhanced in *Mgat5*$^{-/-}$ T cells. *Mgat5* initiates GlcNAc β1,6 branching on *N*-glycans, thereby increasing *N*-acetyllactosamine[6], the ligand for galectins[7,8], which are proteins known to modulate T-cell proliferation and apoptosis[9,10]. Indeed, galectin-3 was associated with the TCR complex at the cell surface, an interaction dependent on Mgat5. Pre-treatment of wild-type T cells with lactose to compete for galectin binding produced a phenocopy of *Mgat5*$^{-/-}$ TCR clustering. These data indicate that a galectin–glycoprotein lattice strengthened by Mgat5-modified glycans restricts TCR recruitment to the site of antigen presentation. Dysregulation of Mgat5 in humans may increase susceptibility to autoimmune diseases, such as multiple sclerosis.

Specific glycan structures regulate lymphocyte adhesion, recirculation and maturation, as demonstrated by the GDP-fucose deficiency in LADII patients[11], and immune defects associated with C2 *N*-acetylglucosamine (GlcNAc)-T(L)[12] or ST3Gal-I (ref. 13)

mutant mice. Depletion of the Mgat5-modified glycans by swainsonine, an inhibitor of α-mannosidase II, potentiates antigen-dependent T-cell proliferation[14]. Mgat5 catalyses the addition of β1,6-GlcNAc to *N*-glycan intermediates found on newly synthesized glycoproteins that transit the medial Golgi[15] (Fig. 1a). The glycans are elongated in *trans*-Golgi to produce tri (2,2,6) and tetra (2,4,2,6) antennary *N*-glycans, which are extended with *N*-acetyllactosamine (Gal-β1,4-GlcNAc) and polymeric forms of *N*-acetyllactosamine[6]. To further explore the function of Mgat5 in T-cell immunity, we examined Mgat5-deficient mice for evidence of immune dysfunction. *Mgat5*$^{-/-}$ mice are born healthy, and lack Mgat5 *N*-glycan products in all tissues examined[16]. At 3 months of age, peripheral white blood cells, erythrocyte and serum levels of immunoglobulin (Ig)M and IgG were comparable in Mgat5$^{-/-}$, *Mgat5*$^{+/-}$ and *Mgat5*$^{+/+}$ mice (data not shown). The CD4 and CD8 reactive T-cell populations in the spleen and thymus were also in the normal range (Fig. 1b, c). At 12–20 months of age, an increased incidence of leukocyte colonies in kidney and enlarged spleens was observed in *Mgat5*$^{-/-}$ mice. Furthermore, 32% of the *Mgat5*$^{-/-}$ (6 out of 19 mice) had macroscopic haematuria, mononuclear infiltrates and extensive accumulation of fibrin within Bowman's space, characteristic of proliferative glomerulonephritis (Fig. 1d). This form of renal injury is often observed in autoimmune-mediated glomerulonephritis. Milder renal defects were observed in 68% of the *Mgat5*$^{-/-}$ mice but not in the *Mgat5*$^{+/-}$ or Mgat5$^{+/+}$ mice.

To examine T-cell responses in the mice, we induced a type IV delayed-type hypersensitivity (DTH) reaction, and measured tissue swelling. The protein-reactive hapten oxazolone was applied topically to the backs of the mice, then again 4 d later to the right ear. Ear swelling in *Mgat5*$^{+/+}$ mice peaked 24 h after application, and swelling was completely gone by day 5. Ear swelling in *Mgat5*$^{-/-}$ mice attained a higher maximum between 48 and 72 h, and persisted for a longer time (Fig. 1e). To study T-cell-dependent autoimmunity *in vivo*[17], we induced experimental autoimmune encephalomyelitis (EAE) by immunizing mice with myelin basic protein (MBP) at three doses (25, 100 and 500 μg per mouse). At the lowest dose of MBP, the incidence of EAE was significantly greater in *Mgat5*-deficient mice. Furthermore, 25 and 100 μg doses of MBP produced more severe EAE in *Mgat5*$^{-/-}$ mice compared with wild-type littermates, characterized by an earlier onset, greater motor weakness and more days with disease (Table 1). Myelin injections of 500 μg induced disease in all mice with greater peak scores and no significant differences in disease incidence or severity between genotypes. These results indicate that mice lacking Mgat5-modified glycans are more susceptible to DTH and EAE autoimmune disease.

In vitro, splenic T cells from *Mgat5*$^{-/-}$ mice hyperproliferated in response to anti-TCRα/β antibody (Fig. 2a). To examine this hypersensitivity in more detail, purified *ex vivo* T cells were cultured at low density and stimulated with increasing concentrations of soluble anti-CD3ε antibody in the presence or absence of anti-CD28

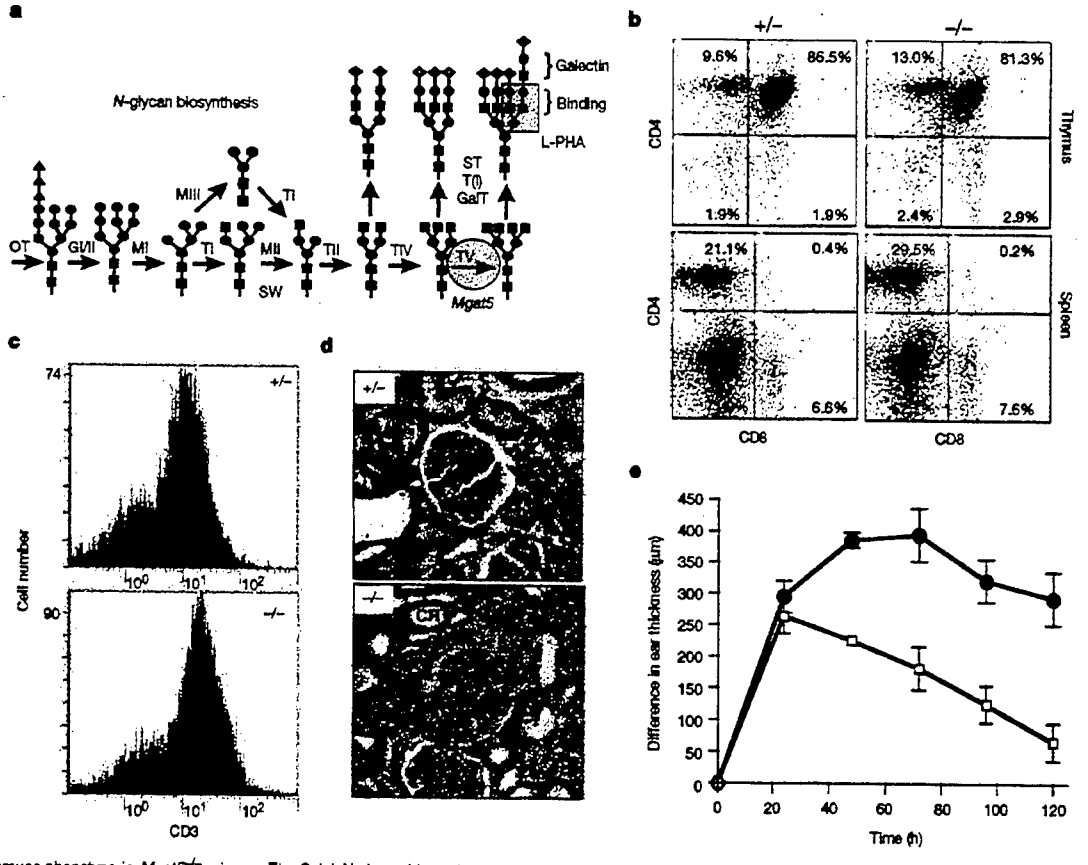

Figure 1 Immune phenotype in *Mgat5*$^{-/-}$ mice. **a**, The Golgi *N*-glycan biosynthesis pathway shows Mgat5 (TV) in the production of a tetra (2,4,2,6) antennary (numbers refer to the linkages of the antennae from left to right). OT, oligosaccharyltransferase; GI, GII, the α-glucosidases; TI, TII, TIV, TV, T(i), the β-*N*-acetylglycosaminyltransferases; MI, α1,3/6mannosidases MII, MIII, the α1,2mannosidases; Gal-T, β1,4-galactosyltransferases; ST, α-sialyltransferases; and SW, swainsonine block. The boxed structure Gal-β1,4-GlcNAc-β1,6(Gal-β1,4-GlcNAc-β1,2)Manα binds L-PHA. The galectin-binding disaccharide *N*-acetyllactosamine (Gal-β1,4-GlcNAc) is present in all antennae, and units are marked with red brackets in polylactosamine. **b**, Distribution of CD4$^+$ and CD8$^+$ cells in spleen and thymus by FACS analysis using FITC- or phycoerythrin-conjugated antibodies (Pharmingen) reactive to CD3ε, CD4 and CD8. **c**, TCR complex staining of spleen cells by FITC-anti-CD3ε antibodies and FACS analysis. **d**, Light microscopy of kidney showing cresentic glomerulonephritis with a large crescent (CR) of mononuclear cells and fibrin obliterating the Bowman's space (BS) in *Mgat5*$^{-/-}$ mice. **e**, DTH inflammatory response in *Mgat5*$^{-/-}$ (circles) and *Mgat5*$^{+/+}$ (squares) mice exposed to oxazolone (see Methods). The results are plotted as mean change ± standard error in ear thickness relative to the vehicle-treated left ear for seven *Mgat5*$^{-/-}$ and six *Mgat5*$^{+/+}$ control littermates. $P < 0.01$ with a student *t*-test comparing the genotypes at 2–5 d.

Table 1 Clinical observations of experimental autoimmune encephalomyelitis

Groups (dose)	Incidence of EAE	Peak score	Onset (days)	Days with disease	Deaths
Mgat5$^{+/+}$ (25 μg)	3/11	0.45 ± 0.24	24.0 ± 3.9	7.0 ± 3.9	0
Mgat5$^{-/-}$ (25 μg)	9/11*	1.82 ± 0.39†	19.8 ± 3.3†	11.5 ± 3.0†	1
Mgat5$^{+/+}$ (100 μg)	10/10	1.6 ± 0.22	25.0 ± 2.2	18.5 ± 2.2	0
Mgat5$^{-/-}$ (100 μg)	10/10	2.1 ± 0.34†	17.6 ± 2.9†	23.3 ± 3.5†	1
Mgat5$^{+/+}$ (500 μg)	12/12	3.0 ± 0.43	8.9 ± 1.2	27.9 ± 4.0	3
Mgat5$^{-/-}$ (500 μg)	12/12	2.83 ± 0.38	9.3 ± 0.95	27.2 ± 2.9	2

Disease severity was scored on a scale of 0–5 with: 0, no illness; 1, limp tail; 2, limp tail and hindlimb weakness; 3, hindlimb paralysis; 4, forelimb weakness/paralysis and hindlimb paralysis; and 5, moribundity or death. Means ± standard error of incidence, peak score and days with disease were calculated using the total number of mice injected per dose as the denominator. The mean ± standard error for day of onset was determined by only using those mice that developed diseases.
*Contingency test, $P < 0.001$.
†Mann–Whitney *U*-test comparing genotypes for significant differences at $P < 0.05$.

antibody (Fig. 2b). Both the Mgat5 deficiency and CD28 engagement reduced the requirements for TCR agonist as indicated by D_{50} values, and were additive when combined (Fig. 2c). Furthermore, the apparent Hill coefficient (n_H), a measure of synchrony in the responding cell population, was increased by both the Mgat5 deficiency and by CD28 engagement. Therefore, the stimulatory effects of the *Mgat5* mutation and CD28 co-receptor engagement were additive and similar in potency.

Alterations in cell-surface TCR complex levels and intracellular signalling potential of T cells were examined and discounted as possible causes of the *Mgat5*$^{-/-}$ hypersensitivity. The Mgat5 deficiency did not significantly alter cell-surface expression of CD3, CD4, CD8, TCRα/β, CD28 or CTLA-4 glycoproteins in resting T cells (Fig. 1b, c; and data not shown). Intracellular signalling potential in *Mgat5*$^{-/-}$ T cells is normal, as treatment with the phorbol ester 12-*O*-tetradecanoylphorbol-13-acetate (TPA) and the Ca^{2+} ionophore ionomycin stimulated T cells equally well from mice of both genotypes (Fig. 2d).

We next examined the relationship between cell-surface *Mgat5*-modified glycans and T-cell activation. Leukoagglutinin (L-PHA) is a tetravalent plant lectin and is a commonly used T cell mitogen that binds specifically to Mgat5-modified glycans. *Mgat5*$^{-/-}$ T cells were completely unresponsive to L-PHA, confirming that Mgat5-modified glycans are required for stimulation by this lectin (Fig. 2e). L-PHA reactive *N*-glycans are also present on B cells, but L-PHA is not a B cell mitogen. Furthermore, B-cell responses to anti-IgM antibody, lipopolysaccharide and interleukin (IL)-4 plus anti-CD40 antibody were similar for cells from *Mgat5*$^{-/-}$ and *Mgat5*$^{+/+}$ mice (Fig. 2f; and data not shown). In T cells, L-PHA induces signalling common to TCR engagement, including phosphorylation of CD3ζ, Ca^{2+} mobilization, PKC-γ and Ras/mitogen-activated protein kinase (Mapk) activation[18,19]. The TCRα/β chains have seven *N*-glycans in total, and some are branched, complex-type structures with L-PHA reactivity[20,21]. These data indicate that Mgat5-modified glycans are present on glycoproteins of the TCR complex and are required for L-PHA mitogenesis.

When bound to major histocompatibility complex (MHC)/peptide, TCRs cluster with an inherent affinity greater than unligated TCRs, and the stability of these clusters is critical for intracellular signalling[22]. However, the density of TCRs measured at the site of T cell–APC (antigen-presenting cell) contact is only marginally increased relative to the remaining cell surface, leaving most of the TCRs unengaged by MHC/peptide[4]. It is possible that ligand-induced TCR clustering in the plane of the membrane may be increased in the absence of Mgat5-modified glycans, thus lowering *Mgat5*$^{-/-}$ T-cell activation thresholds. Therefore, to visualize TCR re-organization in response to an antigen-presenting surface, we coated polystyrene beads with anti-CD3ε antibody and incubated them with purified *ex vivo* T cells. After 10 min of contact, TCRs in *Mgat5*$^{-/-}$ cells were markedly more concentrated at the bead surface compared with *Mgat5*$^{+/+}$ cells (Fig. 3a, b). TCRs on wild-type cells could not be induced to cluster to the same extent as *Mgat5*$^{-/-}$ cells, even with longer incubations (20 min) or using anti-CD3ε plus

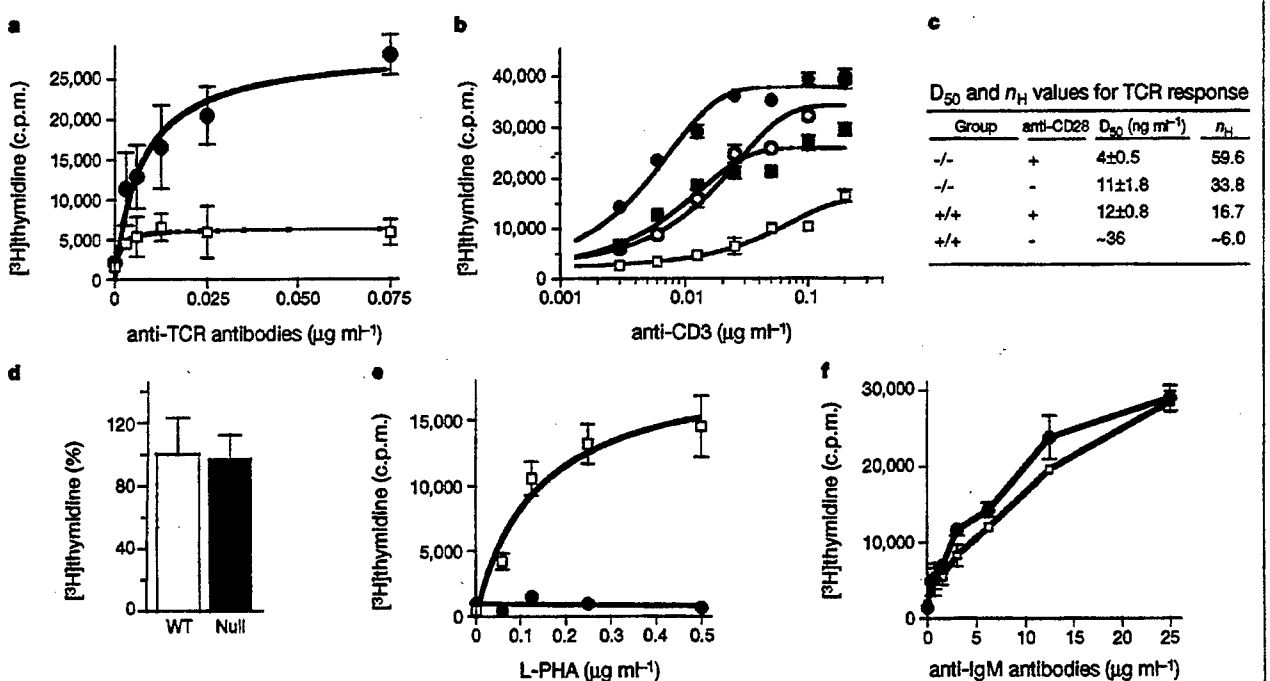

Figure 2 *Mgat5*$^{-/-}$ T cells are hypersensitive to TCR agonists. **a**, Spleen cells were cultured with anti TCRα/β antibodies for 48 h. Filled circles, *Mgat5*$^{-/-}$; open squares, *Mgat5*$^{+/+}$. **b**, Purified T cells from spleen were stimulated for 48 h with anti-CD3ε antibody in the absence (open circles and squares) or presence (filled squares and circles) of anti-CD28 antibody. *Mgat5*$^{-/-}$ and *Mgat5*$^{+/+}$ cells are indicated by circles and squares, respectively. **c**, The Hill slope (n_H) of the sigmoidal curve is calculated using $Y = x^{n_H}/(k^{n_H} + x^{n_H})$. **d**, Stimulation of splenic T cells with TPA plus ionomycin for 48 h. **e**, Stimulation of splenic T cells from *Mgat5*$^{-/-}$ (filled circles) and *Mgat5*$^{+/+}$ (open squares) mice with L-PHA. **f**, Stimulation of splenic B cells from *Mgat5*$^{-/-}$ (filled circles) and *Mgat5*$^{+/+}$ (open squares) mice with anti-IgM antibody for 48 h. The means ± standard deviation of triplicate determinations are used.

anti-CD28-coated beads (data not shown). Actin microfilaments were more concentrated at the bead contact site in *Mgat5*$^{-/-}$ cells, and overlapped more extensively with TCRs in the merged images compared with *Mgat5*$^{+/+}$ T cells (Fig. 3a, b). TCRs are internalized after productive TCR clustering[1], and this was significantly greater in *Mgat5*$^{-/-}$ compared with *Mgat5*$^{+/+}$ cells (Fig. 3c, solid lines). Intracellular signalling mediated by TPA treatment induces TCR internalization but at similar rates in *Mgat5*$^{-/-}$ and *Mgat5*$^{+/+}$ cells (Fig. 3c, dotted lines). Microfilament reorganization was more rapid in Mgat5-deficient T cells after soluble anti-CD3ε antibody stimulation (Fig. 3d). Akt/protein kinase B (PKB) phosphorylation is dependent on phosphoinositide 3-OH kinase activity, which stimulates Rac/CDC42 GTPases and actin filament reorganization[23]. Phosphorylated Akt/PKB showed a greater fold increase in *Mgat5*$^{-/-}$ compared with *Mgat5*$^{+/+}$ T cells (Fig. 3d). Mobilization of intracellular Ca^{2+} after stimulation with soluble anti-CD3ε antibody was enhanced in the absence of Mgat5-modified glycans (Fig. 3e). Tyrosine phosphorylation of multiple proteins was increased and persisted longer in *Mgat5*$^{-/-}$ T cells exposed to anti-CD3ε antibody coated beads. (Fig. 3e). Immunoprecipitation of Zap-70 revealed increased phosphorylation in *Mgat5*$^{-/-}$ cells 1–5 min after stimulation. Zap-70 kinase binds to dual phosphorylated immunoreceptor tyrosine-based activation motif domains of CD3ζ, and association of the latter with Zap70 was increased in *Mgat5*$^{-/-}$ compared with *Mgat5*$^{+/+}$ T cells (Fig. 3g). Thus, the Mgat5 deficiency enhanced ligand-dependent TCR aggregation, and

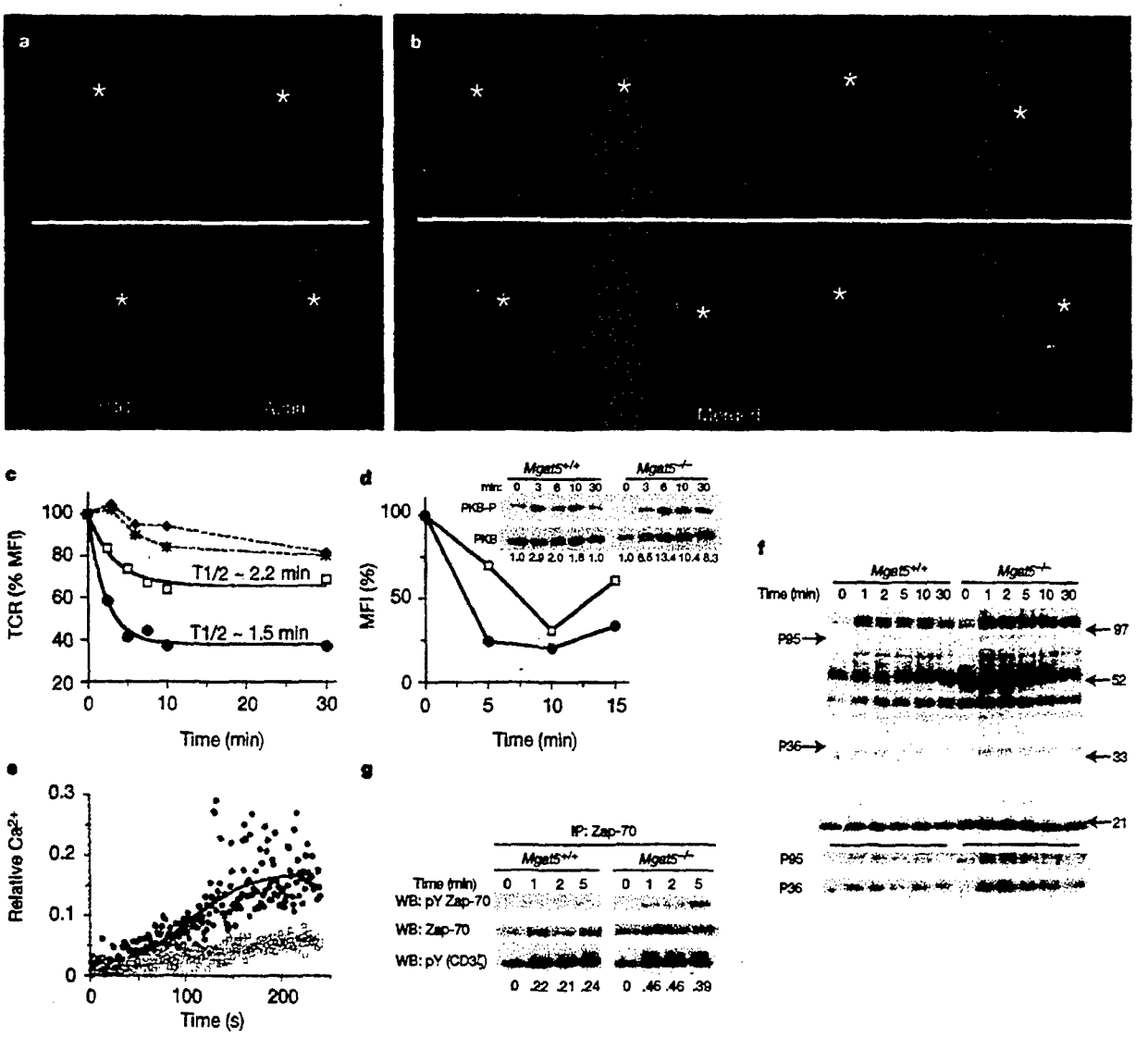

Figure 3 TCR clustering, actin re-organization and signalling in T cells from *Mgat5*$^{-/-}$ and *Mgat5*$^{+/+}$ mice. **a**, TCR and actin microfilament distribution in T cells stimulated by anti-CD3ε-coated beads. **b**, Merged images of *Mgat5*$^{-/-}$ and *Mgat5*$^{+/+}$ cells. Clustering was observed in 5 of 6 and 0 of 6 randomly photographed cells, respectively. **c**, TCR internalization by FACS analysis using FITC-anti-TCRα/β antibodies to measure cell-surface TCRs after addition of anti-CD3ε antibody. Changes in MFI with time are shown. T cells from *Mgat5*$^{-/-}$ (filled circles and squares) or *Mgat5*$^{+/+}$ (open squares and asterisks) mice were treated with anti-CD3ε antibody (filled circles (*Mgat5*$^{-/-}$) and open squares (*Mgat5*$^{+/+}$)); or with TPA (filled squares (*Mgat5*$^{-/-}$) and asterisks (*Mgat5*$^{+/+}$)). Similar results were obtained when the stimulation and detection roles of anti-TCRα/β and anti-CD3 were reversed. **d**, Actin polymer content in T cells from *Mgat5*$^{-/-}$ (filled circles), or *Mgat5*$^{+/+}$ (open squares) mice after stimulation with anti-CD3ε antibody, measured by FACS. Western blot for phospho-Akt/PKB in T-cell lysates after addition of anti-CDε antibody is shown (top). The values below are fold increase in PKB-P normalized to PKB protein. **e**, Ca^{2+} mobilization in purified T cells from *Mgat5*$^{-/-}$ (filled circles), and *Mgat5*$^{+/+}$ (open squares) mice stimulated with anti-CD3ε antibody. **f**, Western blot with anti-phosphotyrosine antibody detecting phosphorylated proteins in T-cell lysates after incubation with anti-CD3ε antibody-coated beads. A longer exposure was used to show bands (arrowheads at left) migrating as p95 and p36 shown below. Arrows at the right indicate the positions of molecular mass markers. **g**, Immunoprecipitation of Zap-70 and western blotting for phosphotyrosine (pY) to detect Zap-70 and CD3ζ (values below are CD3ζ ratio P23/P21).

consequently, signal transduction and microfilament re-organization.

The larger size of Mgat5-modified glycans may limit the geometry and spacing of TCR clusters in the plane of the membrane[24]. Alternatively, Mgat5-modified glycans may bind cell-surface galectins, which restrict TCR mobility and thereby antigen-induced TCR clustering. The galectins are a widely expressed family of mammalian lectins defined as *N*-acetyllactosamine-binding proteins. The poly *N*-acetyllactosamine sequences preferentially added to Mgat5-modified glycans[6] enhance the affinity for galectin binding (Fig. 1a). Galectins bind to lactosamine and lactose with dissociation constants in the 10^{-4} M range[7,8], an affinity comparable to MHC/peptide-induced oligomerization of TCRs in solution[22]. Therefore, the avidity of a multivalent galectin–Mgat5 glycoprotein lattice at the cell surface may be sufficient to restrict TCR clustering. To probe for the presence of galectin–glycoprotein interactions, wild-type *ex vivo* T cells were preincubated with various disaccharides for 20 min before a 10 min stimulation with anti-CD3ε antibody-coated beads. Preincubation with lactose increased TCR clustering at the bead interface and reduced TCR density elsewhere on the cells (Fig. 4c), which is similar to the behaviour of untreated *Mgat5*$^{-/-}$ T cells (Fig. 3a, b). TCR clustering was not altered by preincubation with the control disaccharide sucrose (Fig. 4b). Lactosamine and lactose both enhanced protein phosphorylation induced by anti-CD3ε antibody-coated beads, but sucrose and maltose had no effect (Fig. 4d; and data not shown). Lactose did not enhance signalling in *Mgat5*$^{-/-}$T cells (data not shown).

Galectin-3 was detected on the surface of naïve T cells by labelling with sulphosuccinimidobiotin, capture with streptavidin beads and western blotting with anti-galectin-3 antibodies (Fig. 4e). Chemical crosslinking of the cell surface to stabilize complexes followed by western blotting of galectin-3 immunoprecipitates showed that galectin-3 is associated with TCR complex proteins. This interaction was disrupted by either Mgat5 deficiency or incubating wild-type T cells with 2 mM lactose (Fig. 4e). Taken together, the data demonstrate that a multivalent cell-surface galectin–glycoprotein lattice limits TCR clustering in response to agonist, the avidity of which is dependent on Mgat5-modified glycans (Fig. 4f). The full complement of glycoproteins and lectins present in the T-cell lattice remains unknown, but at a minimum includes galectin-3 and the TCR complex. Exogenously added galectin-1 binds CD2, CD3, CD4, CD7, CD43 and CD45, and these proteins may also participate in the lattice[25]. Indeed, exogenous galectin-1 modulates T-cell activation *in vitro*[9,25], antagonizes TCR signalling[26], and when injected into mice it suppresses the pathology of EAE[27].

The gene replacement vector used to produce our Mgat5-deficient mice contained the reporter gene *LacZ*, replacing the first exon, which was expressed with the same tissue specificity as *Mgat5* transcript[16]. Both the *LacZ* expression and cell-surface Mgat5-modified glycans in *Mgat5*$^{-/-}$ and *Mgat5*$^{+/+}$ T cells, respectively,

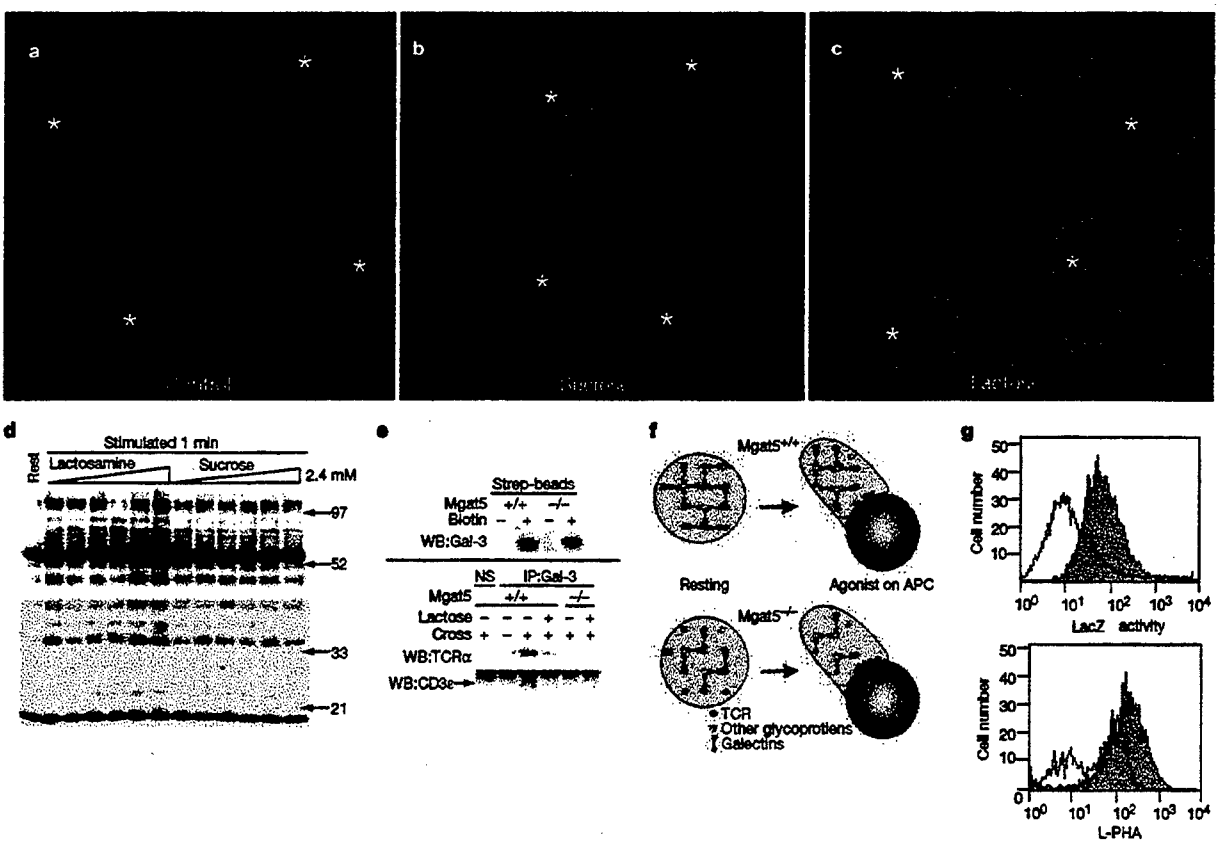

Figure 4 Lactose stimulates TCR aggregation and signalling in *Mgat5*$^{+/+}$ mice. **a–c**, Purified T cells preincubated for 20 min with buffer (**a**), 2 mM sucrose (**b**), or 2 mM lactose (**c**), then stimulated with anti-CD3ε antibody-coated beads for 10 min and stained for TCRs. Enhanced TCR clustering was observed in 0 of 10, 1 of 10 and 9 of 10 cases, respectively. **d**, *Mgat5*$^{+/+}$ T cells incubated with increasing concentrations of disaccharide (1/3 serial dilution from 2.4 mM) and stimulated for 1 min with anti-CD3ε antibody-coated beads compared for phosphotyrosine. Arrows at the right indicate the positions of molecular mass markers. A longer exposure of the lower molecular weight portion of the blot is shown. **e**, Galectin-3 detected by surface labelling with NHS-biotin on T cells. Association of galectin-3 with CD3ε and TCRα chain, and its disruption by Mgat5 deficiency and lactose is shown (bottom). **f**, Model showing restricted mobility of TCRs by interaction with a galectin–glycoprotein network, which is stronger in Mgat5-expressing cells. **g**, Upper panel shows *LacZ* activity in untreated (white) and anti-CD3 and anti-CD28-stimulated (grey) T cells from *Mgat5*$^{-/-}$ mice. Lower panel, L-PHA-binding to *Mgat5*$^{+/+}$ T lymphocytes either untreated (white) or stimulated with anti-CD3 and anti-CD28 for 48 h (grey).

increased 48 h after stimulation, demonstrating regulation of Mgat5 by transcriptional means (Fig. 4g). This suggests that Mgat5 enzyme activity and glycan production are limiting in resting T cells, and with stimulation, increases in Mgat5-modified glycans and galectins may dampen TCR sensitivity to antigen. Negative feedback by Mgat5-modified glycans on TCR sensitivity is delayed as it requires Mgat5 gene expression, which is dependent on T-cell activation status, and only indirectly on antigen concentrations. This form of slow-negative regulation governed by steady-state activity of the system is a key feature of robust and adaptive biochemical pathways[28], and Mgat5-modified glycans may contribute this feature to T-cell regulation.

It has been estimated that sustained clustering of roughly 8,000 TCRs is required for T-cell activation[2], but other molecular interactions clearly alter this threshold. With CD28 co-stimulation, only about 1,500 TCRs are required[2]. Co-signalling through CD28 decreases the extent of TCR clustering needed for activation predominantly by recruiting protein kinase-enriched GM1 ganglioside rafts to the site of TCR engagement, thereby amplifying signalling[3,5]. We show that Mgat5 deficiency increases the number of TCRs recruited to the antigen-presenting surface, thereby reducing the requirement for CD28 co-receptor engagement. This may lead to T-cell activation in the absence of CD28 co-signalling, failure of anergy and loss of immune tolerance. $CD28^{-/-}$ mice are resistant to induction of EAE by low dose MBP, whereas $Mgat5^{-/-}$ mice are hypersensitive, but both mutants develop clinical signs of EAE comparable to wild-type littermates with high doses of MBP[29]. In this regard, CD28 and Mgat5 function as opposing regulators of T-cell activation thresholds and susceptibility to autoimmune disease. Mgat5-dependent glycosylation limits agonist-induced TCR clustering by sequestering receptors in a cell-surface galectin–glycoprotein lattice. However, the glycosylation deficiency in $Mgat5^{-/-}$ mice affects other pathways and cell types that may also contribute to the observed autoimmunity. Indeed, Mgat5-modified glycans also reduce clusters of fibronectin receptors, causing accelerated focal adhesion turnover in fibroblasts and tumour cells; a functionality that may affect leukocyte motility[16]. Finally, glycosylation of Notch receptor by Fringe, a fucose-specific β1,3-GlcNAc-transferase, provides another example of regulation by differential receptor glycosylation[30]. In a broad context, our results suggest a general mechanism for the regulation of receptor clustering through differential glycosylation and interaction with cell-surface lectins. □

Methods

Delayed-type hypersensitivity skin reaction

To induce DTH, 100 μl of 5% (w/v) 4-ethoxymethilene-2-phenyl-2-oxazolin-5-one (oxazolone) (Sigma) in ethanol/acetone (3:1, v/v) was injected epicutaneously to the shaved backs of the 129 mice. Four days after sensitization, 25 μl of 1% (w/v) oxazolone was applied on each side of the right ear, and the left ear received 25 μl of olive oil/acetone on each side. Ear swelling was measured with a micrometer at 24 h intervals for the next 5 d, and swelling was reported as the difference between the ear thickness of the right minus the left ears.

EAE model

Mice (129) 8–12 weeks of age were injected subcutaneously with 100 μl of rabbit MBP (Sigma) emulsified 1:1 with complete Freund's adjuvant at three different total doses (25, 100 and 500 μg per mouse). Mice were observed from day 5 to day 50, and observations were blinded with respect to the genotype until day 36. For lower doses of 25 and 50 μg, half the total was injected on day 0 in the right flank and the other half on day 7 in the left flank. The high dose of 500 μg per mouse was injected all on day 0 at the base of the tail, and 500 ng of pertussis toxin was injected through the tail vein on day 0 and day 2.

T-cell proliferation

Naïve T-cells were purified from spleens of 8–12-week-old mice by negative selection using $CD3^+$ T-cell purification columns. T-cell proliferation was measured by culturing cells for 48 h in RPMI, 10% FCS, 10^{-4}M 2-mercaptoethanol in the presence of one or more of the following soluble antibodies: hamster anti-mouse CD3ε (clone 2C11; Cedarlane), hamster anti-mouse TCRα/β (clone H59.72; Pharmingen) or 0.5 μg ml^{-1} anti-mouse CD 28 (Pharmingen). TPA (10 ng ml^{-1}) and ionomycin (0.5 μg ml^{-1}) were also used to stimulate cells. We added 2 μCi of [^{3}H]thymidine for the last 20 h of incubation, and we collected cells on fibreglass filters and measured radioactivity in a β-counter.

TCR clustering

Six-micro polystyrene beads (Polysciences) in PBS were coated with hamster anti-mouse CD3ε antibody (Clone 2C11; Cederlane) at 2 μg ml^{-1} antibody followed by coating with 200 μg ml^{-1} bovine serum albumin. To measure TCR clustering, 5×10^4 T cells were incubated with 2.5×10^5 anti-CD3ε antibody-coated beads in 100 μl RPMI 1640 + 10% FCS at 37 °C for 10 min, placed on poly-L-lysine-coated cover slips. The cells were fixed with 10% formalin, stained with 2 μg ml^{-1} fluorescein isothiocyanate (FITC)-labelled anti-TCRα/β antibody (Pharmingen), solubilized with 0.2% Triton X-100, labelled with rhodamine-phalloidin and Hoechst, and then visualized by deconvolution microscopy. To measure TCR internalization, purified splenic T cells stimulated with either 0.1 μg ml^{-1} anti-CD3 antibody or with 10 ng ml^{-1} TPA for varying lengths of time were collected and stained with FITC–anti-TCRα/β. TPA concentrations were not limiting as 10, 50 and 100 ng ml^{-1} produced similar internalization and cell activation results. To measure actin reorganization, purified splenic T cells stimulated with 0.1 μg ml^{-1} anti-CD3 for varying lengths of time were fixed with 4% paraformaldehyde for 10 min, washed with PBS and stained with rhodamine-phalloidin, and mean fluorescence intensity (MFI) was determined by FACS.

TCR signalling

T cells (10^6) and anti-CD3ε antibody-coated beads (5×10^6 at 0.4 ng ml^{-1} antibody) in 100 μl RPMI 1640 were pelleted, incubated at 37 °C for various times, then solubilized with ice-cold 50 mM Tris pH 7.2, 300 mM NaCl, 0.5% Triton X-100, protease inhibitor cocktail (Boehringer Mannheim) and 2 mM orthovanadate. Zap-70 was immunoprecipitated by incubating whole-cell lysates with rabbit polyclonal anti-Zap-70 agarose conjugate (Santa Cruz) overnight at 4 °C, followed by one wash with lysis buffer and three washes with PBS. Western blotting was done with whole-cell lysates or immunoprecipitates separated on SDS–polyacrylamide gel electrophoresis gels under reducing conditions, transferred electrophoretically to polyvinylidene difluoride membranes, and immunoblotted with antibodies to Akt/PKB (NEB), phospho-Akt/PKB (NEB), phosphotyrosine (clone 4G10; Upstate Biotechnology), Zap-70 (clone Zap-70-6F7; Zymed), TCRα (polyclonal; Santa cruz) and rabbit anti-galectin-3 (a gift from A. Raz, University of Michigan). Cell-surface proteins were biotinylated using sulphosuccinimidobiotin (NHS-biotin) for 30 min, PBS pH 8.0. Cells were lysed and labelled protein was captured on streptavidin-agarose beads. To crosslink surface proteins on purified naïve T cells, the homobifunctional crosslinker dithio-bis(sulphosuccinimydylpropionate) (DTSSP) was used at 0.1 mg ml^{-1} with 10^6 cell per ml in PBS pH 8.0 for 10 min at 20 °C. T cells were preincubated for 20 min with or without 2 mM lactose, and reacted with DTSSP in the presence of the same. Aliquots of cell lysate were immunoprecipitated with rabbit anti-galectin-3 antibody or non-immune rabbit serum (NS), separated on reducing SDS–PAGE, and western blotted for CD3ε and TCRα chain. The band above CD3ε is a cross-reactivity of secondary antibody with light-chain.

To measure Ca^{2+} mobilization, purified T cells were loaded with 10 μM AM ester of Fluo-3 (Molecular Probes), washed and stimulated with 10 μg ml^{-1} anti-CD3ε antibody at 37 °C. We took emission at 525 nm using a spectrofluorimeter with excitation at 488 nm. Data is plotted as a fraction of the Ca^{2+} mobilized by addition of 2 μg ml^{-1} of ionomycin. *LacZ* activity in $Mgat5^{-/-}$ T cells was detected by loading cells with fluorescein-di-β-D-galactopyranoside (FDG) (Molecular Probes) at 10 °C, and allowing the reaction to proceed for 30 min. The reaction was stopped by the addition of 1 mM phenyl-β-thiogalactoside.

Received 11 September; accepted 29 November 2000.

1. Valitutti, S., Muller, S., Cella, M., Padovan, E. & Lanzavecchia, A. Serial triggering of many T-cell receptors by a few peptide–MHC complexes. *Nature* 375, 148–151 (1995).
2. Viola, A. & Lanzavecchia, A. T cell activation determined by T cell receptor number and tunable thresholds. *Science* 273, 104–106 (1996).
3. Viola, A., Schroeder, S., Sakakibara, Y. & Lanzavecchia, A. T lymphocyte costimulation mediated by reorganization of membrane microdomains. *Science* 283, 680–682 (1999).
4. Monks, C. R., Freiberg, B. A., Kupfer, H., Sciaky, N. & Kupfer, A. Three-dimensional segregation of supramolecular activation clusters in T cells. *Nature* 395, 82–86 (1998).
5. Wulfing, C. & Davis, M. M. A receptor/cytoskeletal movement triggered by costimulation during T cell activation. *Science* 282, 2266–2269 (1998).
6. Cummings, R. D. & Kornfeld, S. The distribution of repeating Gal β1-4GlcNAc β1-3 sequences in asparagine-linked oligosaccharides of the mouse lymphoma cell line BW5147 and PHAR 2.1. *J. Biol. Chem.* 259, 6253–6260 (1984).
7. Sato, S. & Hughes, R. C. Binding specificity of a baby hamster kidney lectin for H type I and II chains, polylactosamine glycans, and appropriately glycosylated forms of laminin and fibronectin. *J. Biol. Chem.* 267, 6983–6990 (1992).
8. Knibbs, R. N., Agrwal, N., Wang, J. L. & Goldstein, I. J. Carbohydrate-binding protein 35. II. Analysis of the interaction of the recombinant polypeptide with saccharides. *J. Biol. Chem.* 268, 14940–14947 (1993).
9. Perillo, N. L., Pace, K. E., Seilhamer, J. J. & Baum, L. G. Apoptosis of T cells mediated by galectin-1. *Nature* 378, 736–739 (1995).
10. Vespa, G. N. *et al.* Galectin-1 specifically modulates TCR signals to enhance TCR apoptosis but inhibit IL-2 production and proliferation. *J. Immunol.* 162, 799–806 (1999).
11. Karsan, A. *et al.* Leukocyte Adhesion Deficiency Type II is a generalized defect of de novo GDP-fucose biosynthesis. Endothelial cell fucosylation is not required for neutrophil rolling on human non-lymphoid endothelium. *J. Clin. Invest.* 101, 2438–2445 (1998).
12. Ellies, L. G. *et al.* Core 2 oligosaccharide biosynthesis distinguishes between selectin ligands essential for leukocyte homing and inflammation. *Immunity* 9, 881–890 (1998).
13. Priatel, J. J. *et al.* The ST3Gal-I sialyltransferase controls CD8+ T lymphocyte homeostasis by modulating O-glycan biosynthesis. *Immunity* 12, 273–283 (2000).

14. Wall, K. A., Pierce, J. D. & Elbein, A. D. Inhibitors of glycoprotein processing alter T-cell proliferative responses to antigen and to interleukin 2. *Proc. Natl Acad. Sci. USA* **85**, 5644–5648 (1988).
15. Cummings, R. D., Trowbridge, I. S. & Kornfeld, S. A mouse lymphoma cell line resistant to the leukoagglutinating lectin from *Phaseolus vulgaris* is deficient in UDP-GlcNAcα-D-mannoside β1,6 N-acetylglucosaminyltransferase. *J. Biol. Chem.* **257**, 13421–13427 (1982).
16. Granovsky, M. *et al.* Suppression of tumor growth and metastasis in Mgat5-deficient mice. *Nature Med.* **6**, 306–312 (2000).
17. Lafaille, J. J., Nagashima, K., Katsuki, M. & Tonegawa, S. High incidence of spontaneous autoimmune encephalomyelitis in immunodeficient anti-myelin basic protein T cell receptor transgenic mice. *Cell* **78**, 399–408 (1994).
18. Downward, J., Graves, J. D., Warne, P. H., Rayter, S. & Cantrell, D. A. Stimulation of p21^{ras} upon T-cell activation. *Nature* **346**, 719–723 (1990).
19. Trevillyan, J. M., Lu, Y. L., Aituru, D., Phillips, C. A. & Bjorndahl, J. M. Differential inhibition of T cell receptor signal transduction and early activation events by a selective inhibitor of protein-tyrosine kinase. *J. Immunol.* **145**, 3223–3230 (1990).
20. Wang, J. *et al.* Atomic structure of an αβ T cell receptor (TCR) heterodimer in complex with an anti-TCR fab fragment derived from a mitogenic antibody. *EMBO J.* **17**, 10–26 (1998).
21. Hubbard, S. C., Kranz, D. M., Longmore, G. D., Sitkovsky, M. V. & Eisen, H. N. Glycosylation of the T-cell antigen-specific receptor and its potential role in lectin-mediated cytotoxicity. *Proc. Natl Acad. Sci. USA* **83**, 1852–1856 (1986).
22. Reich, Z. *et al.* Ligand-specific oligomerization of T-cell receptor molecules. *Nature* **387**, 617–620 (1997).
23. Reif, K. & Cantrell, D. A. Networking Rho family GTPases in lymphocytes. *Immunity* **8**, 395–401, (1998).
24. Rudd, P. M. *et al.* Roles for glycosylation of cell surface receptors involved in cellular immune recognition. *J. Mol. Biol.* **293**, 351–366 (1999).
25. Pace, K. E., Lee, C., Stewart, P. L. & Baum, L. G. Restricted receptor segregation into membrane microdomains occurs on human T cells during apoptosis induced by galectin-1. *J. Immunol.* **163**, 3801–3811 (1999).
26. Chung, C. D., Patel, V. P., Moran, M., Lewis, L. A. & Carrie Miceli, M. Galectin-1 induces partial TCR zeta-chain phosphorylation and antagonizes processive TCR signal transduction. *J. Immunol.* **165**, 3722–3729 (2000).
27. Offner, H. *et al.* Recombinant human beta-galactoside binding lectin suppresses clinical and histological signs of experimental autoimmune encephalomyelitis. *J. Neuroimmunol.* **28**, 177–184 (1990).
28. Barkai, N. & Leibler, S. Robustness in simple biochemical networks. *Nature* **387**, 913–917 (1997).
29. Oliveira-dos-Santos, A. J. *et al.* CD28 costimulation is crucial for the development of spontaneous autoimmune encephalomyelitis. *J. Immunol.* **162**, 4490–4495 (1999).
30. Moloney, D. J. *et al.* Fringe is a glycosyltransferase that modifies Notch. *Nature* **406**, 369–375 (2000).

knowledgements

thank S. Kulkarni and J. Tsang for technical assistance. This research was supported by nts from NCI of Canada, the Mizutani Foundation, the National Science and gineering Research Council of Canada, and GlycoDesign, Toronto.

rrespondence and requests for materials should be addressed to J.W.D.
mail: dennis@mshri.on.ca).

rystal structure of photosystem II om *Synechococcus elongatus* at .8 Å resolution

ina Zouni*, Horst-Tobias Witt*, Jan Kern*, Petra Fromme*, bert Krauß†, Wolfram Saenger†, Peter Orth†

x-Volmer-Institut für Biophysikalische Chemie und Biochemie, nische Universität Berlin, Straße des 17, Juni 135, D-10623, Berlin, Germany stitut für Chemie, Kristallographie, Freie Universität Berlin, Takustrasse 6, 4195 Berlin, Germany

rgenic photosynthesis is the principal energy converter on h. It is driven by photosystems I and II, two large protein–ictor complexes located in the thylakoid membrane and acting eries. In photosystem II, water is oxidized; this event provides overall process with the necessary electrons and protons, and atmosphere with oxygen. To date, structural information on architecture of the complex has been provided by electron roscopy of intact, active photosystem II at 15–30 Å resolution[1], by electron crystallography on two-dimensional crystals of D2-CP47 photosystem II fragments without water oxidizing rity at 8 Å resolution[2]. Here we describe the X-ray structure of photosystem II on the basis of crystals fully active in water oxidation[3]. The structure shows how protein subunits and cofactors are spatially organized. The larger subunits are assigned and the locations and orientations of the cofactors are defined. We also provide new information on the position, size and shape of the manganese cluster, which catalyzes water oxidation.

Conversion of light to chemical energy at photosystem II (PSII) is associated with charge separation across the thylakoid membrane (for review see ref. 4). It is initiated by ejection of an electron from the excited primary donor P680, a chlorophyll *a* located towards the luminal side of the membrane at the heart of the PSII reaction centre that is formed by protein subunits D1 and D2. When the cationic radical $P680^{+\bullet}$ is formed, the electron moves by means of a pheophytin to the electron stabilizing acceptor Q_A, a plastoquinone that is tightly bound at the stromal side of subunit D2. After each of four successive charge separating steps that are light induced, $P680^{+\bullet}$ abstracts one electron from a manganese cluster (generally assumed to contain four manganese ions) by means of the redox-active tyrosine residue Tyr_Z. In turn, the four positive charges accumulated in the manganese cluster oxidize two water molecules, coupled with the release of one O_2 and four H^+. In the first two charge separations, Q_A^- doubly reduces one mobile molecule Q_B docked to the binding site B on D1. After uptake of two protons, Q_BH_2 is released into the plastoquinone pool that is embedded in the membrane, and replaced by a new Q_B from the pool for another round of reduction and release.

We isolated PSII from the thermophilic cyanobacterium *Synechococcus elongatus* in the form of homodimers as shown by electron microscopy (E. J. Boekema, unpublished observations). With these preparations, three-dimensional crystals were grown[5] that are suitable for X-ray analysis (see Methods). According to SDS–polyacrylamide gel electrophoresis and mass-spectrometry (MALDI-TOF) (data not shown), this PSII is composed of at least 17 subunits[6] of which 14 are located within the photosynthetic membrane: the reaction centre proteins D1 (PsbA) and D2 (PsbD); the chlorophyll-containing inner-antenna subunits CP43 (PsbC) and CP47 (PsbB); α- and β-subunits of cytochrome *b*-559 (PsbE and PsbF); and the smaller subunits PsbH, PsbI, PsbJ, PsbK, PsbL, PsbM, PsbN and PsbX. The membrane-extrinsic cytochrome *c*-550

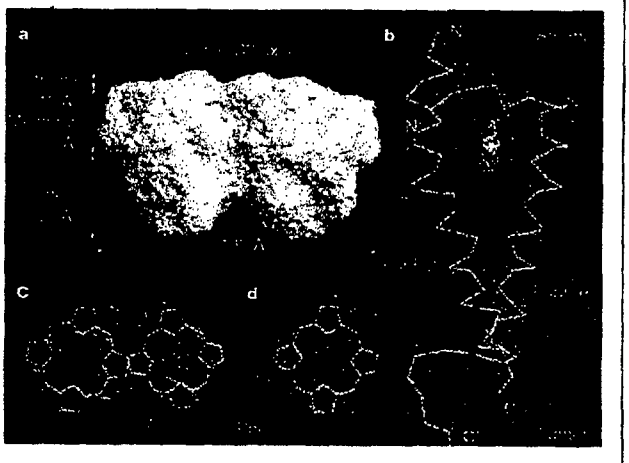

Figure 1 Electron densities of PSII after density modification and their interpretation. **a**, Surface of PSII homodimer drawn from the averaging mask generated during density modification. View direction along the membrane plane; the position of local-C2 rotation axis, is shown. **b**, Cytochrome (Cyt) *b*-559 heterodimer with electron densities contoured at 1.2 σ (r.m.s. deviation above the mean electron density) for protein and haem group, and at 4.0 σ for Fe^{2+}. The termini of the α-helices are labelled N, C for the α-subunit, and N′, C′ for the β-subunit. **c**, Head groups of P680 chlorophyll (Chl) *a* P_{D1} and P_{D2} with view perpendicular to their planes. Mg^{2+} are depicted as red spheres. **d**, Head group of pheophytin $Pheo_{D1}$.

Genetic defects in *N*-glycosylation and cellular diversity in mammals

James W Dennis*, Charles E Warren†, Maria Granovsky† and Michael Demetriou†

Glycoproteins in mammalian cells are modified with complex-type aspargine-linked glycans of variable chain lengths and composition. Observations of mice carrying mutations in glycosyltransferase genes imply that *N*-glycan structures regulate T-cell receptor clustering and hence sensitivity to agonists. We argue that the heterogeneity inherent in *N*-glycosylation contributes to cellular diversity and, thereby, to adaptability in the immune system.

Addresses
*Department of Molecular & Medical Genetics, University of Toronto, Toronto, Canada; e-mail: dennis@mshri.on.ca
†Samuel Lunenfeld Research Institute, Mount Sinai Hospital, R988, 600 University Avenue, Toronto, Ontario M5G 1X5, Canada

Current Opinion in Structural Biology 2001, 11:601–607

0959-440X/01/$ – see front matter

Abbreviations

APC	antigen-presenting cell
CDG	congenital disorder of glycosylation
CRD	carbohydrate-recognition domain
peptide–MHC	antigenic peptide bound to major histocompatibility complex
PyMT	polyomavirus middle T oncogene
TCR	T-cell receptor

Introduction

N- and *O*-linked glycans are found on both cell-surface and secreted proteins, many of which control proliferation and cell fate decisions in animals. Tissue-specific expression of glycosyltransferases is a significant factor controlling the glycan profiles observed in differentiated cells [1]. In addition, many glycosyltransferases compete for acceptor intermediates, causing bifurcations of the pathways and additional structural complexity [2]. Heterogeneity at specific Asn-X-Ser/Thr sites on individual glycoproteins is very common and diversifies the molecular population into glycoforms. The protein environment of each Asn-X-Ser/Thr influences access by processing enzymes and inefficiencies in this process result in only a fraction of *N*-glycans receiving certain substitutions. As a result, each Asn-X-Ser/Thr site of a glycoprotein is commonly populated by a set of biosynthetically related *N*-glycan structures.

The specific activity with respect to a particular functional property can vary between individual glycoforms and thus the potency of a glycoprotein is actually the weighted average of the specific activities of the glycoform population. For example, the peptide hormones lutropin and erythropoietin are produced with structurally diverse glycans, and the discrete glycoforms differ in their affinity for hepatic lectins, thereby determining serum half-lives and potency *in vivo* [3,4]. By balancing the proportions of glycoforms with different serum half-life, the potency and kinetics of a cytokine response can be modified or adapted to extrinsic conditions. In a similar manner, variation in receptor glycosylation has the potential to modify their physical associations in the membrane and thereby the ligand occupancy thresholds for signal transduction. The terminal portions of mature *N*-glycans are generally not held close to the glycoprotein on which they reside. This leaves them free to bind to multivalent lectins at the cell surface. Various receptor glycoforms would have differing affinities for cell-surface lectins. The interaction of receptors with such lectins could potentially serve as an adjustable means of linking various signaling systems and hence tuning the cellular responses to various stimuli, as previously suggested by Feizi and Childs [5]. Receptor systems that form highly cooperative macromolecular clusters in response to agonists, such as T-cell receptors (TCRs) and cell adhesion receptors, appear to be sensitive to glycoform variation. Herein we discuss phenotypes associated with mutations in enzymes of the glycosylation pathways and their implications concerning the molecular functions of cell-surface *N*-glycans.

Congenital disorders of glycosylation

The first stage of protein *N*-glycosylation, conserved from yeast to man, is the synthesis of $Glc_3Man_9GlcNAc_2$-PP-dolichol and transfer of the oligosaccharide to proteins in the ER. Five congenital disorders of glycosylation (CDGs) are known, each with a characteristic enzymatic defect either in the biosynthesis of $Glc_3Man_9GlcNAc_2$-PP-dolichol or in its transfer to asparagine. These are known as type I CDGs. Infants with these defects share clinical features, including developmental delay, multiple organ abnormalities and severe neurologic dysfunction [6•,7]. These deficiencies result from the partial failure to glycosylate proteins with oligosaccharides at the usual Asn-X-Ser/Thr sites. A complete deficit of *N*-glycosylation is expected to be incompatible with life, as the inhibition of oligosaccharyltransferase by tunicamycin is toxic to yeast and mammalian cells. $Glc_1Man_{7-9}GlcNAc_2$ on newly synthesized glycoproteins binds calnexin, calreticulin and ER α-glucosyltransferase. The last acts as a sensor of glycoprotein conformations and, combined with the action of α-glucosidase II, a deglucosylation/reglucosylation cycle continues and retains the glycoprotein until proper folding occurs, thus fulfilling a function analogous to that of chaperones [8•,9].

CDG type I patients display a remarkable variability in clinical phenotypes, even, for example, between patients that have the same mutant alleles of the phosphomannomutase gene *PMM2* [6•]. The genetic background of each

patient can presumably influence the expressivity of a phenotype in a complex manner. The chaperone function of $Glc_1Man_{7-9}GlcNAc_2$ may vary depending on polymorphism in the underlying polypeptides and this could influence the clinical phenotype. 'Silent' polymorphisms are common in the population, such as the underglycosylated state present in CDG patients, and may be innocuous until revealed by a 'molecular stress'. This is analogous to the inactivation of the chaperone Hsp90 in *Drosophila*, which revealed the accumulated genetic variation between strain backgrounds as morphological mutations [10]. In an evolutionary context, environmental stresses that compromise the buffering capacity of protein chaperones, including those that rely on *N*-glycans, may reveal a reservoir of genetic diversity for rapid adaptation [10].

Complex-type *N*-glycans in embryogenesis and immune regulation

The position and specificity of key enzymes in the *N*-glycan biosynthesis pathway are depicted in Figure 1a. The GlcNAc-TI gene *Mgat1* is ubiquitously expressed and required in the biosynthesis of all hybrid and complex-type *N*-glycans (Figure 1a). *Mgat1*$^{-/-}$ mouse embryos die at around embryonic day E9.5 with failures of neural tube formation, vascularization and determination of left/right body plan asymmetry [11,12]. Maternal sources of the Mgat1 enzyme and its *N*-glycan products are present in pre-E6 day embryos, and may support development until E9.5, after which complex-type glycans are largely depleted [13]. In chimeric embryos, *Mgat1*$^{-/-}$ cells contribute to various tissues, with the exception of lung bronchial epithelium [14]. Consistent with this observation, the *Mgat1*$^{-/-}$ embryos display a severe failure to organize bronchial epithelium. As Mgat1 mutant Chinese hamster ovary cells grow normally in culture, the *in vivo* data on the failure of *Mgat1*$^{-/-}$ embryos support the notion that complex-type *N*-glycans mediate cell–cell interactions in the animal. However, when growth conditions are limiting, as in low-serum cultures, mutant tumor cells with defects in either GlcNAc-TV (Mgat5) or the Golgi UDP-Gal transporter were observed to grow at reduced rates and displayed an increased dependency on autocrine growth factors [15].

These studies suggested that complex-type *N*-glycans on certain cell-surface receptors affect their sensitivity to growth factors and/or adhesion signals. Indeed, some glycosyltransferase mutant mice may appear normal at birth. Phenotypes can be revealed, however, by stress and aging, as well as by expressing the mutations in different inbred strains of mice. In this regard, there was a relatively low incidence of mammary tumor growth and metastases induced by the polyomavirus middle T oncogene (PyMT) in *Mgat5*$^{-/-}$ mice on the 129/sv x FVB background. The PyMT protein is an intracellular docking protein that transforms cells by activating the Ras signaling pathways, as well as phosphatidylinositol 3-kinase and protein kinase B (PKB/Akt). The activation of these latter enzymes is the downstream effect of focal adhesion signaling, which appears to be impaired in *Mgat5*$^{-/-}$ tumor cells and embryonic fibroblasts. Glycans modified by Mgat5 are present on integrin α5β1 and their depletion may stabilize substratum attachment and result in an impairment of PyMT signaling and tumor growth in *Mgat5*$^{-/-}$ mice [16••]. A cancer phenotype has also been revealed in *Mgat3*$^{-/-}$ mice by treating them with a carcinogen. Diethylnitrosamine-induced hepatocarcinomas progress more slowly in *Mgat3*$^{-/-}$ mice compared with wild-type littermates. Further analysis of the mice revealed that a paracrine growth factor dependent upon Mgat3 promotes tumor growth in the mice [17•].

In the absence of GlcNAc-TII (Mgat2), complex-type *N*-glycans are replaced by hybrid-type glycans (Figure 1a). Mis-sense mutations have been identified in *Mgat2* that reduce enzyme activity by >95% in two CDG type IIa patients [18]. This is a rare autosomal recessive disorder characterized by multisystemic involvement and severe impairment of the nervous system. *Mgat2*$^{-/-}$ mice are runted and die at variable times after birth with multiple organ defects (D Chui, JD Marth, personal communication), further evidence that complex-type *N*-glycans are required for normal embryogenesis.

Mutations disrupting fewer glycan structures generally result in viable animals with tissue-restricted or conditional phenotypes. These include mutations that affect either late steps in the processing pathway or enzymes with functional redundancies. Immune phenotypes have been detected in a number of viable glycosyltransferase mutant mice, indicating a particular sensitivity of immune cells to changes in glycosylation. Sialyltransferase ST6Gal modifies *N*-linked glycans with α2-6-linked sialic acid; mice lacking this enzyme display impaired B-cell proliferation [19]. Mice deficient in ST3Gal-1, a sialyltransferase that substitutes core 1 (Galβ1-3GalNAc) *O*-glycans, also display the subtle phenotype of $CD8^+$ T-cell depletion by apoptosis, but retention of $CD8^+$ memory T cells [20]. The E-, P- and L-selectins and their ligands control leukocyte traffic. Mutations in several glycosyltransferases that produce selectin ligands disrupt trafficking, but mutant phenotypes differ qualitatively, presumably because of the details of glycan structure and their tissue distribution. These include Fuc-TIV, Fuc-TVII [21], the *O*-linked core 2 GlcNAc-T(L) branching enzyme [22] and a β3GlcNAc-T that extends core 1 *O*-glycans with 6-sulfo sialyl-LeX [23]. Mice deficient in the *N*-linked processing enzymes α-mannosidase II [24] or Mgat5 both develop autoimmune kidney disease with age [25••].

Mgat5-modified glycans regulate TCR sensitivity to antigen

Mgat5$^{-/-}$ mice lack detectable GlcNAcβ1,6Manα1,6-branched *N*-glycan products and are born healthy from CD1 outbred and 129/sv inbred mouse strains [16••].

Figure 1

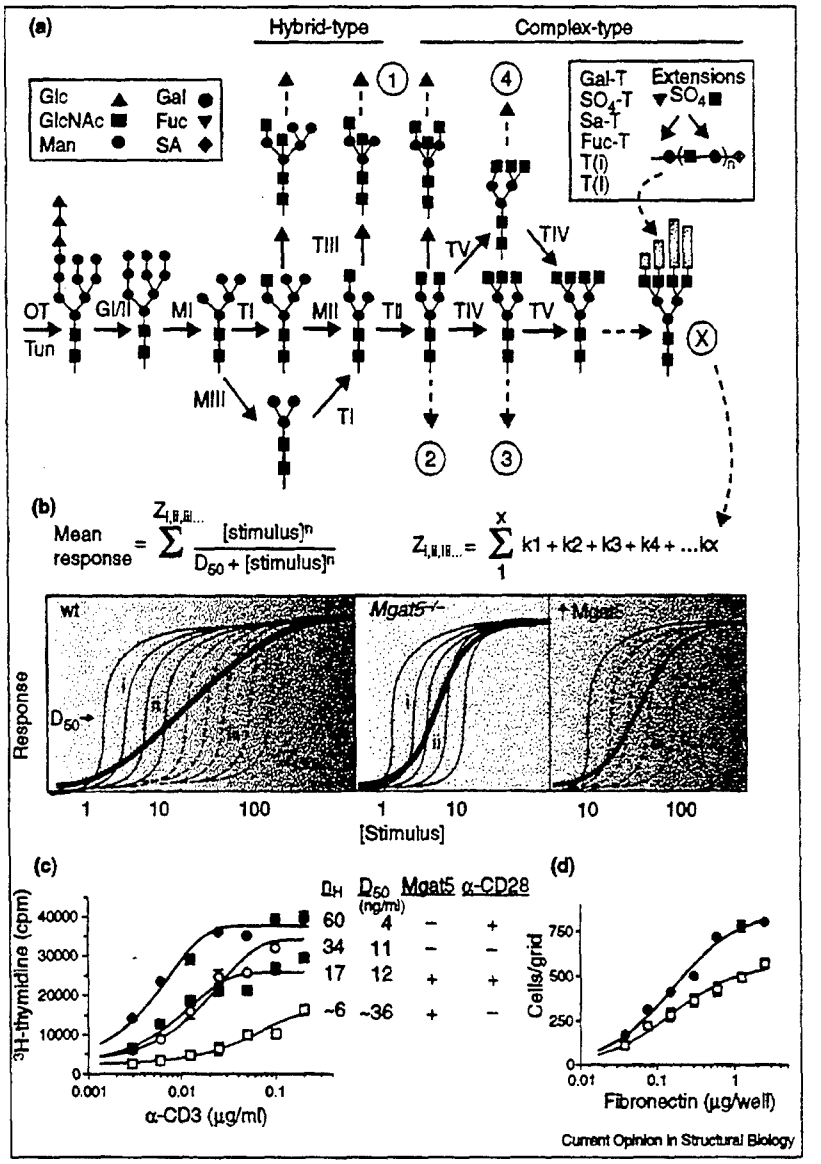

Glycosylation, signaling thresholds and cell population diversity. **(a)** Scheme of the *N*-glycan biosynthesis pathway. Oligosaccharyltransferase, OT; α-glucosidases, GI and GII; β-*N*-acetylglucosaminyltransferases, TI, TII, TIII, TIV, TV, T(i); α1,2-mannosidases, MI; α1,3/6-mannosidases, MII and MIII; β1,4-galactosyltransferases, Gal-T; α-fucosyltransferases, Fuc-T; α-sialyltransferases, Sa-T; sulfotransferase, SO_4-T. Gene names for TI to TV are *Mgat1* to *Mgat5*, respectively. Tun, tunicamycin. The circled numbers 1 to x represent biosynthetically related subsets of glycans labeled here only to illustrate the model shown below. **(b)** Hypothetical model to represent variability or plasticity within the T-cell population. For each T cell, entry into S phase is a switch-like event that initiates activation and several rounds of cell division. Each black line represents individual cells or groups of cells that share a similar *N*-glycan structural profile. The weighted contributions of glycoforms (k1–kx) determine the cell phenotype (Z_i), the response to agonist. The mean response to agonists is the sum of responses for the population over all Z_i. The dashed lines depict the influence of Mgat5 glycans. The mean response has a D_{50} and Hill slope as depicted by the colored line for the wild-type (wt), Mgat5 deficiency (*Mgat5*$^{-/-}$) and Mgat5 overexpression (↑ Mgat5). The last panel may also apply to ST6Gal-deficient cells. Note the variance in the cell population is largest for the wild-type and reduced in the mutants. **(c)** Purified T cells were stimulated at low density for 48 h with increasing concentrations of soluble anti-TCR antibody in the presence or absence of anti-CD28 antibody (data from [25••]). The code for genotypes and stimulation in each curve are indicated in the table on the right, along with the ligand concentration providing a 50% response (D_{50}) and the Hill coefficient (n_H). **(d)** Adhesion of *Mgat5*$^{-/-}$ (solid) and wild-type (open) leukocytes to increasing concentrations of fibronectin. Mgat5-modified glycans on the TCR complex and adhesion receptors impair TCR clustering and formation of focal adhesions, respectively, in both cases reducing the cooperativity (n_H) and increasing the ligand threshold (D_{50}).

However, small litter sizes and higher perinatal mortality have been observed with the *Mgat5* mutation on a PLJ mouse background, a hyperimmune mouse strain (J Pawling, M Demetriou *et al.*, unpublished data). *Mgat5*$^{-/-}$ mice displayed an age-dependent autoimmune disease characterized by glomerulonephritis [25••]. T-cell-dependent immune reactions were exaggerated in *Mgat5*$^{-/-}$ mice and T cells in culture were hypersensitive to TCR agonists. Delayed type hypersensitivity was more severe and susceptibility to experimental autoimmune encephalomyelitis, a model for human multiple sclerosis, was greater in mutant mice. In contrast, *Mgat5*$^{-/-}$ B cells responded normally to a variety of stimuli, indicating that the defect is restricted to selected cell types.

TCRs are recruited into 'immune synapses' by peptide–MHC complexes on antigen-presenting cells (APCs). A threshold number of receptors are required in the immune synapse to sustain intracellular signaling and trigger entry into S phase [26]. This rate-limiting event of sustained TCR clustering was enhanced in *Mgat5*$^{-/-}$ cells (Figure 2). TCR-dependent tyrosine phosphorylation,

Figure 2

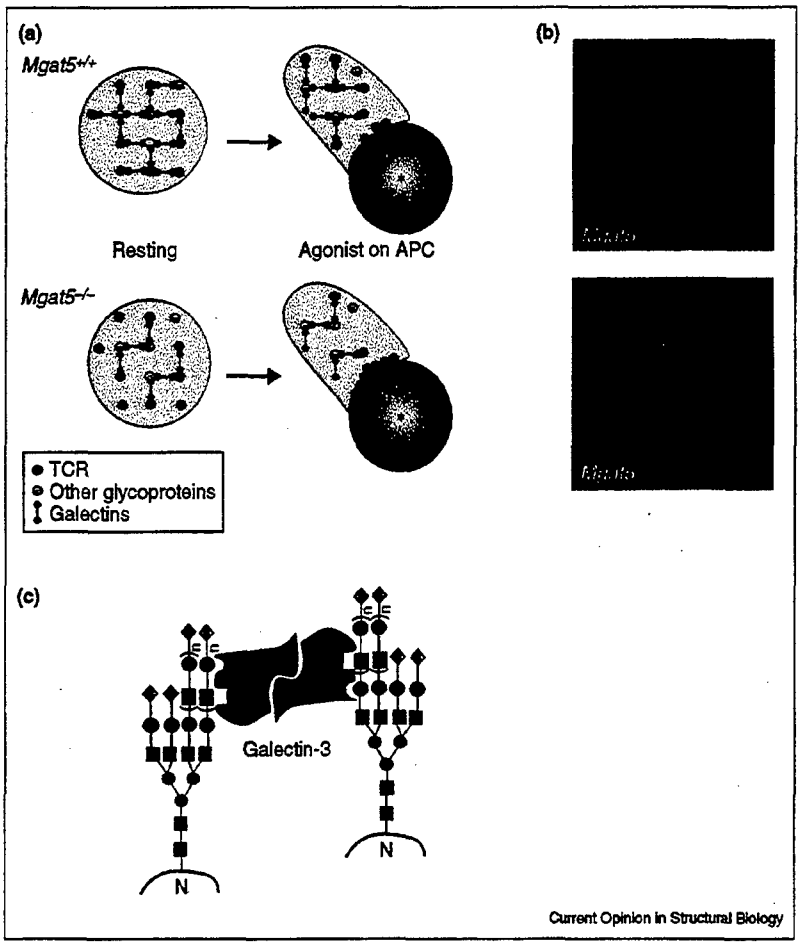

Restriction of receptor clustering by galectins. **(a)** A model depicting restricted mobility of TCR by interaction with a galectin–glycoprotein network. The lattice has more binding interactions and therefore greater avidity in *Mgat5*$^{+/+}$ cells. The ball marked by an asterisk represents an APC or an anti-TCR antibody-coated bead. **(b)** Merged images of *Mgat5*$^{-/-}$ and *Mgat5*$^{+/+}$ cells, showing the TCR (green) and actin microfilament (red) distribution in T cells stimulated by anti-CD3ε coated beads (marked with an asterisk) (taken from [25••]). **(c)** Schematic diagram of a galectin-3 homodimer, represented as a red dumbbell in (a), binding to *N*-glycans and cross-linking two glycoproteins.

actin microfilament reorganization and Ca^{2+} mobilization were enhanced in *Mgat5*$^{-/-}$ T cells, but intracellular signaling downstream of TCR induced by phorbol ester was unchanged. These results indicate that T-cell hypersensitivity in *Mgat5*$^{-/-}$ cells is due to change at the cell surface [25••]. In quiescent T cells, Mgat5 gene expression is low and rate limiting in the production of cell-surface *N*-glycans with β1,6GlcNAc branches. *Mgat5* gene transcription, enzyme activity and glycan products increase following activation [25••]. Mgat5 gene expression is positively regulated by Ras–Raf–Ets activation downstream of TCR. Therefore, Mgat5 glycans are regulated during T-cell maturation and are also determinants of TCR sensitivity to agonists.

Some glycoproteins recycle through the endocytic pathway and back to the cell surface, but this does not appear to involve remodeling of *N*-glycan branching [27]. As such, changes in *N*-glycan branching at the cell surface occur through *de novo* synthesis of glycoproteins. The timescale of this process is hours, whereas TCR-dependent tyrosine phosphorylation, Ca^{2+} mobilization and actin rearrangement occur in minutes after agonist-induced receptor clustering. Therefore, Mgat5-dependent regulation of TCR sensitivity to antigen is a long timescale, slow form of negative feedback, governed by the steady-state activity of signaling pathways that are downstream of TCR. This type of delayed negative feedback has been observed in other pathways and provides a mechanism to adjust or tune receptor sensitivity to match ambient conditions [28]. T cells in different tissue environments may alter Mgat5-modified glycan levels, thereby adapting the TCR sensitivity and response threshold.

Lectin–glycan interactions modulate lymphocyte receptor signaling

The TCR α and β chains together have seven *N*-glycans and CD3 γ and δ each have one chain. Glycosylation is necessary for the assembly of these peptides into a mature TCR complex. The *N*-glycans protrude ~30 Å from the protein surface and a fraction of these glycans appear, by their positive leukoagglutinin L-PHA reactivity, to be β1,6GlcNAc-branched complex-type structures [29], which are preferentially substituted with poly *N*-acetyllactosamine

[30]. Electron density for the chitobiose core ($GlcNAc_2$) of *N*-glycans is often observed in high-resolution X-ray structures [31••]. However, density for distal *N*-glycan sequences is generally not visible in X-ray structures, consistent with their mobility and lack of order in the crystal. Biantennary complex-type *N*-glycans have been modeled onto TCR complex. Based on their size and positions, it has been proposed that *N*-glycans may limit nonspecific receptor aggregation and thereby also spurious T-cell activation [31••]. The glycans may also align the geometry for TCR binding towards peptide–MHC complexes on the APC [31••].

We recently reported that glycoproteins of the TCR complex bind to galectins at the cell surface, which impedes TCR clustering in response to agonist [25••]. The galectin family is conserved in metazoans and features either one or two carbohydrate-recognition domains (CRDs) per molecule. Galectin-1 and galectin-3 have one CRD and form homodimers with CRDs spaced ~50 Å apart and oriented in opposing directions [32], a feature ideally suited for cross-linking glycoproteins with multiple glycans [33] (Figure 2). Treating wild-type T cells with lactose or lactosamine to dissociate the galectins from their endogenous ligands enhanced TCR clustering and tyrosine phosphorylation in response to agonist, in essence creating a phenocopy of *Mgat5*$^{-/-}$ [25••]. Furthermore, cell-surface galectin-3 was found physically associated with TCR complex, an interaction enhanced by the expression of Mgat5 glycans. Monomeric affinities of galectins for lactosamine and lactose are in the 10^{-3} M range [34], which is comparable to peptide–MHC-induced oligomerization of TCR measured in solution and lower than TCR affinity for peptide–MHC to form an immune synapse [26]. Poly *N*-acetyllactosamine, a slightly higher affinity ligand (10^{-4} M) for galectin-3 [34], is preferentially added to Mgat5-modified glycans [30] (Figure 1a). Therefore, Mgat5 glycans on the TCR complex and other glycoproteins appear to form a multivalent lattice held together by galectins, which slow the migration of the TCR into clusters at the immune synapse (Figure 2a,c).

There are at least ten mammalian galectins with overlapping expression patterns. Mice deficient in galectin-1 or galectin-3 are healthy, but have not yet been examined for T cell or stress-related phenotypes [35]. Galectin-3 and the TCR complex are present in the T-cell lattice and galectin-1 has been reported to bind to glycoproteins designated CD2, CD3, CD4, CD7, CD43 and CD45 on T cells [36], but other components of the lattice remain to be defined. Exogenous galectin-3 and galectin-1 modulate T-cell activation *in vitro* [36], antagonize TCR signaling [37•] and, when injected into mice, galectin-1 can suppress autoimmune disease [38]. The expression of galectin-3 at the cell surface of cancer cells is associated with an increase in tumor growth, invasion and metastasis [39•], possibly as a result of enhanced turnover of integrin–substratum contacts, which would give rise to an increase in focal adhesions.

Siglecs are sialic-acid-binding lectins implicated in lymphoid and myeloid cell functions. CD22 (siglec-2) binds ST6Gal products (SAα2,6Galβ) in *cis* on the B-cell surface. Unlike galectins, CD22 is a transmembrane protein with a phosphorylated cytosolic domain, and recruits Grb2, Shc, SHP1 and SHIP, causing reduced B-cell receptor signaling [40]. B cells of CD22-deficient mice are hypersensitive to antigen stimulation. However, ST6Gal-deficient mice display impaired B-cell proliferation, attenuated antibody production and, although cell-surface CD22 is present, it is not bound to ligand [41]. This suggests that the recruitment of CD22 into B-cell receptor signaling complexes is inhibited by SAα2,6Galβ. Therefore, SAα2,6Galβ appears to be a negative regulator of a negative regulator (i.e. CD22) and loss of SAα2,6Galβ allows CD22 to dampen the B-cell response. Such a possible scenario is depicted by the model in Figure 1b (represented by the right panel). ST6Gal activity [42] and CD22 occupancy with sialic acid are regulated with B-cell activation [43]. Similar to Mgat5 regulation in T cells, this suggests that the signaling threshold for B-cell receptors may be regulated by differential sialylation, which controls the availability of CD22.

Structural diversity of glycans increases functional diversity

Individual cells typically show small variances of many molecular parameters that, together, confer a Gaussian spectrum of responsiveness in the cell population. The protein glycosylation machinery appears to be designed to increase molecular heterogeneity and, presumably in some instances, functional diversity within cell populations as well. Although different receptor glycoforms may vary only slightly in their affinities for lectins and signal transduction, exponential amplification of lymphocyte clones can convert small differences into large systemic events [44]. T-cell clones undergo multiple rounds of cell division once triggered by peptide–MHC binding above a threshold affinity. Once this stochastic event occurs, strong positive feedback by cytokines creates a highly cooperative and sustained expansion of cells. Many other interactions between cells influence the balance of Th1/Th2 helper T cells, development of memory T cells and cessation of the response. The immune system appears to be particularly sensitive to small functional differences at the cellular level.

Sustained clustering of ~8000 TCRs results in an increase in the concentration of protein kinases and of docking proteins on the inner surface of the membrane; this results in the triggering of T-cell activation [45]. CD28 is a co-receptor of the TCR. Binding of CD28 to CD80 on APCs enhances the recruitment of intracellular signaling molecules, thereby reducing by fivefold the number of TCRs required for activation [46,47]. The Mgat5 deficiency sensitizes this system still further and lowers the threshold for the TCR response to agonists; this is independent of the ligation of CD28 [25••] (Figure 1c). In addition, the apparent Hill coefficient (n_H) was increased in Mgat5-deficienct cells and this represents the synchrony of the responding cell population in this

Suppression of tumor growth and metastasis in Mgat5-deficient mice

MARIA GRANOVSKY[1,2], JIMMIE FATA[3], JUDY PAWLING[1], WILLIAM J. MULLER[4], RAMA KHOKHA[3] & JAMES W. DENNIS[1,2]

[1]*Samuel Lunenfeld Research Institute, Mount Sinai Hospital 600 University Ave. R988, Toronto, Ontario, Canada M5G 1X5*
[2]*Department of Molecular & Medical Genetics, University of Toronto, Toronto, Ontario, Canada*
[3]*Department of Medical Biophysics, University of Toronto, Ontario Cancer Institute, Princess Margaret Hospital, 620 University Ave., Toronto, Ontario, Canada M5G 2C1*
[4]*Institute for Molecular Biology and Biotechnology, McMaster University, Hamilton, Ontario, Canada L8S 4K1*
Correspondences should be addressed to: J.W.D.; email: Dennis@mshri.on.ca

Golgi β1,6N-acetylglucosaminyltransferase V (MGAT5) is required in the biosynthesis of β1,6GlcNAc-branched N-linked glycans attached to cell surface and secreted glycoproteins. Amounts of MGAT5 glycan products are commonly increased in malignancies, and correlate with disease progression. To study the functions of these N-glycans in development and disease, we generated mice deficient in Mgat5 by targeted gene mutation. These *Mgat5*$^{-/-}$ mice lacked Mgat5 products and appeared normal, but differed in their responses to certain extrinsic conditions. Mammary tumor growth and metastases induced by the polyomavirus middle T oncogene was considerably less in *Mgat5*$^{-/-}$ mice than in transgenic littermates expressing Mgat5. Furthermore, Mgat5 glycan products stimulated membrane ruffling and phosphatidylinositol 3 kinase–protein kinase B activation, fueling a positive feedback loop that amplified oncogene signaling and tumor growth *in vivo*. Our results indicate that inhibitors of MGAT5 might be useful in the treatment of malignancies by targeting their dependency on focal adhesion signaling for growth and metastasis.

Malignant transformation is accompanied by increased β1,6GlcNAc-branching of N-glycans attached to Asn-X-Ser/Thr sequences in mature glycoproteins[1,2]. The β1,6GlcNAc-branched N-glycans are tri (2,2,6)- and tetra (2,4,2,6)-antenna-like oligosaccharides that constitute a subset of the 'complex-type' N-glycans (Fig. 1*a*). The medial Golgi enzyme β1,6N-acetylglucosaminyltransferase V (MGAT5 (mannoside acetyl glucosaminyl transferase 5) or GlcNAc-TV) catalyzes the addition of β1,6-linked GlcNAc and defines this subset of N-glycans[3,4] (Fig. 1*a*). The plant lectin leukoagglutinin (L-PHA) binds specifically to mature MGAT5 products (Fig. 1*a*)(ref. 5). L-PHA has been used to measure these N-glycans in tissue sections (Fig. 1*b* and ref. 6). MGAT5 products in breast and colorectal carcinomas correlate with poor prognosis and decreased survival time[6,7].

MGAT5 enzyme activity increases in fibroblast and epithelial cell lines with expression of the oncogenes *v-src*, T24-*H-ras* and *v-fps*, and in cells infected with polyomavirus or rous sarcoma virus[2,8,9,10]. Transcription of the *MGAT5* gene is positively regulated by signaling downstream of these oncogenes, notably by the Ras–Raf–Ets pathway[11,12]. Studies on transplantable tumors in mice have indicated that Mgat5 products contribute directly to the cancer growth and metastasis. For example, somatic tumor cell mutants deficient in Mgat5 activity produce fewer spontaneous metastases and tumors grow slower than wild-type cells[10,13]. In addition, forced expression of Mgat5 in epithelial cells results in loss of contact inhibition, increased cell motility, morphological transformation in culture, tumor formation in athymic nude mice[14], and enhanced metastasis[15].

MGAT5 selectively substitutes only a subset of N-glycan intermediates, presumably specified by the structural features of the glycoprotein substrates[16]. Structural analysis of glycans on specific glycoproteins remains incomplete, but has shown that MGAT5 products are present on the integrins LFA-1 and $\alpha_1\beta_5$ (refs. 17,18). The amount of MGAT5 product on integrin subunits α_5, α_v and β_1 increase in cells transfected with *MGAT5*, and the cells show increased motility and decreased substratum adhesion[14]. The larger size of MGAT5 products may impede or alter the kinetics of protein–protein interactions that mediate cell–cell and cell–substratum adhesion. Indeed, large N-glycans present on CD44 (ref. 19), intracellular adhesion molecule-1 (ref. 20) and CD43 (ref. 21) decrease the ligand-binding activity of these cell adhesion receptors, although the *in vivo* importance of these observations has been unclear.

Here, we generated Mgat5-deficient mice by targeted gene mutation in embryonic stem (ES) cells to assess the function of Mgat5 products in normal development and cancer progression. Activating mutations in *Ras* genes, as well as mutations leading to activation of protein kinase B (PKB; also known as Akt) are commonly found in human tumors[22,23]. The *Polyomavirus* middle T antigen (PyMT) viral oncogene activates these pathways[24,25], which together contribute to transformation and multifocal tumors in mice expressing PyMT from a transgene in mammary epithelium[26-29]. Here, PyMT-induced tumor growth and metastasis were considerably suppressed in Mgat5-deficient mice compared with that in their PyMT-transgenic littermates expressing Mgat5. Moreover, *Mgat5* gene expression was induced by the

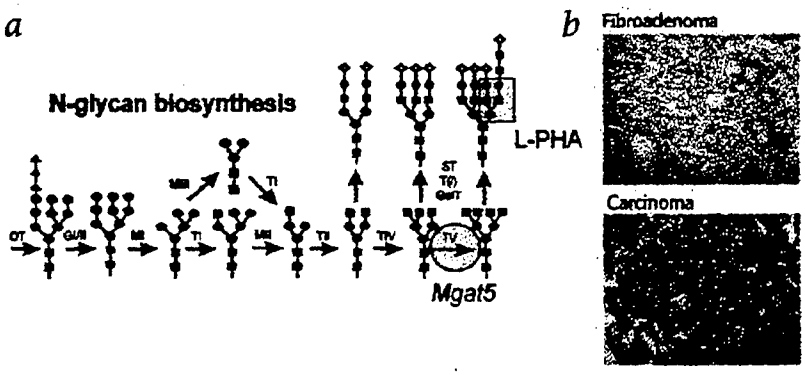

Fig. 1 MGAT5 in N-glycan biosynthesis, and overexpression of its products in human cancers. *a*, Golgi N-glycan biosynthesis pathway, showing MGAT5 (TV) in the production of a tetra (2,4,2,6)-antenna-like oligosaccharide (numbers in brackets represent linkages of the 'antennae', left to right). OT, oligosaccharyltransferase; GI and GII, the α-glucosidases; TI, TII, TIV, TV T(i), the β-N-acetylglycosaminyltransferases; MI, the α1,2mannosidases; MII, MIII, α1,3/6mannosidases; Gal-T, β1,4-galactosyltransferases; ST, α-sialyltransferases. The boxed structure Galβ1,4GlcNAcβ1,6(Galβ1,4GlcNAcβ1,2)Manα binds L-PHA (ref. 5). *b*, L-PHA lectin histochemical staining of a human benign fibroadenoma and breast carcinoma using steptoavidin–horseradish peroxidase for detection as described[6].

PyMT oncogene. Finally, the products of Mgat5 promoted focal adhesion turnover, which amplified PyMT-dependent activation of phosphatidylinositol 3 (PI3) kinase–PKB, and promoted tumor growth and metastasis.

Mgat5$^{-/-}$ mice are viable and lack Mgat5 products

We designed the *Mgat5* targeting vector to replace the coding portion of the first exon of *Mgat5* with the *lacZ* reporter gene (Fig. 2*a* and *b*). We isolated two independent homologous recombinant ES clones and injected them into blastocytes to produce chimeric mice. Alleles from both ES cell lines were successfully transmitted from chimeric mice to progeny. *Mgat5*$^{-/-}$ mice were generated from heterozygous parents with a normal frequency of 25%. We determined the *Mgat5* genotypes of the mice by Southern blot analysis (Fig. 2*b*) and by PCR analysis (data not shown). Mgat5 enzyme activity was approximately 50% in heterozygous mice, and below the level of detection in *Mgat5*$^{-/-}$ mice (Fig. 2*c* and *d*). We did not detect Mgat5 products in *Mgat5*$^{-/-}$ tissues by L-PHA lectin probing of western blots, indicating that mutation of the *Mgat5* locus had eliminated essentially all catalytic activity and Mgat5 products in the *Mgat5*$^{-/-}$ mice (Fig. 2*e*). Mgat5-deficient mice developed normally, producing normal numbers of pups, but adult *Mgat5*$^{-/-}$ mice had several phenotypic abnormalities, including leukocyte recruitment into inflamed tissues, an age-related decrease in the cellularity of kidney glomeruli, an apparent deficiency in nurturing behavior, and T-cell hypersensitivity to T-cell receptor agonists. These phenotypes are now being analyzed. Peripheral white cell and erythrocyte counts were normal, and populations of T and B cells in spleen, thymus and lymph nodes were also in the normal range, as assessed by fluorescence-activated cell sorting analysis (data not shown). There was no weight loss or premature mortality in the *Mgat5*$^{-/-}$ mice up to 18 months of age.

LacZ activity in *Mgat5*$^{+/-}$ embryos was distributed like that of *Mgat5* transcripts (Fig. 3*a* and *b*), indicating the reporter gene faithfully reflected *Mgat5* transcription in mouse tissues[30]. LacZ activity, *Mgat5* transcripts and L-PHA reactivity also co-localized in adult tissues. In the cerebellum, the neuronal cell bodies stained for lacZ and the neural dendritic trees stained with L-PHA; the latter is consistent with localization of glycoproteins to plasma membrane and secretory compartments (Fig. 3*c* and *d*). Therefore, lacZ activity in mice with *Mgat5*-mutant alleles could be used to monitor *Mgat5* promoter activity *in vivo*.

Cancer growth and metastasis are reduced in *Mgat5*$^{-/-}$ mice

We crossed PyMT-transgenic mice with *Mgat5*-mutant mice and measured tumor latency, tumor growth and the incidence of lung metastases in the progeny. We first detected mammary tumors in PyMT *Mgat5*$^{+/-}$ and PyMT *Mgat5*$^{+/+}$ female mice at 8 weeks of age, and by 16 weeks 50% of the mammary pads had tumors (Fig. 4*a* and *b*). In contrast, 50% tumor incidence in the PyMT *Mgat5*$^{-/-}$ mice occurred at 24 weeks, and by 27 weeks of age, tumors were detected in all mammary fat pads. PyMT *Mgat5*$^{+/+}$ male

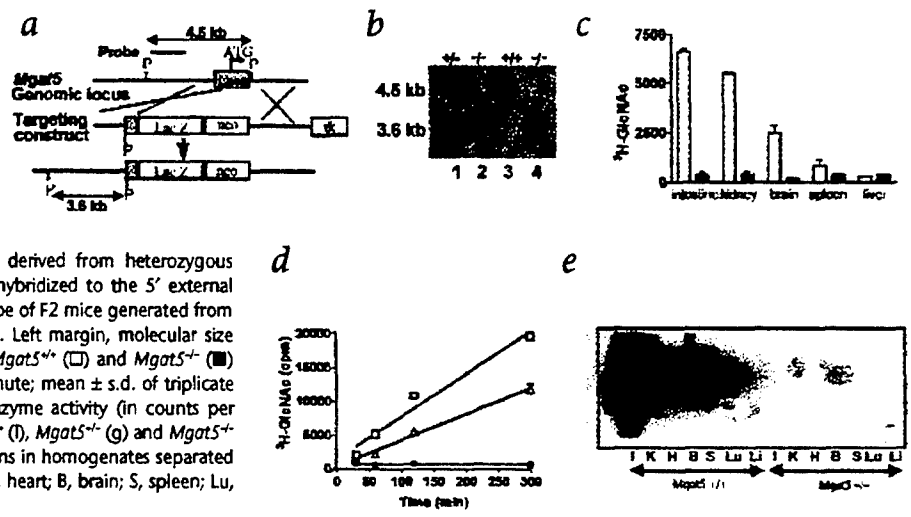

Fig. 2 Targeted mutation of the *Mgat5* locus in mice. *a* and *b*, The wild-type *Mgat5* locus, the targeting vector, and the resulting targeted locus. Nucleotides −22 to 241 of the first coding exon were replaced with *lacZ* and a neomycin-resistant gene. ■, exon; ■ (above *Mgat5* genomic locus), 5′ external probe; P, *Pst*I restriction site. *b*, Southern blot analysis of genomic DNA of F2 offspring derived from heterozygous crosses. DNA digested with *Pst*I was hybridized to the 5′ external probe. Lanes 2 and 4, *Mgat5*$^{-/-}$ genotype of F2 mice generated from two independently targeted ES clones. Left margin, molecular size markers *c*, Mgat5 enzyme activity in *Mgat5*$^{+/+}$ (□) and *Mgat5*$^{-/-}$ (■) tissue homogenates (in counts per minute; mean ± s.d. of triplicate samples).*d*, Time course of Mgat5 enzyme activity (in counts per minute) in small intestine from *Mgat5*$^{+/+}$ (l), *Mgat5*$^{+/-}$ (g) and *Mgat5*$^{-/-}$ (P) mice. *e*, L-PHA-reactive glycoproteins in homogenates separated by SDS–PAGE. I, intestine; K, kidney; H, heart; B, brain; S, spleen; Lu, lung; Li, liver.

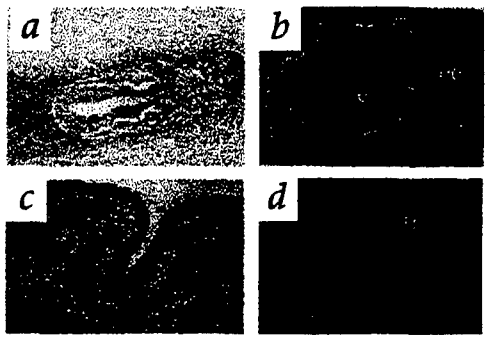

Fig. 3 Mouse embryo at embryonic day 7.5. *a* and *b*, Section through the center of embryo. *a*, lacZ expression, visualized by X-gal staining (blue). *b*, Darkfield microscopy, showing *Mgat5* transcripts detected by RNA *in situ* hybridization. *c* and *d*, Cerebella of mice at postnatal day 6. *LacZ* expression from the targeted *Mgat5* allele corresponds to L-PHA staining. The neuronal cell bodies stain for *lacZ* (*c*) and the neural dendritic trees stain with L-PHA (*d*); the latter is consistent with localization of glycoproteins to plasma membrane and secretory compartments. t, trophoblasts; e, embryonic tissue; ee, extraembryonic tissue; p, Purkinje cells.

mice developed tumors between 6 and 9 months and tumor development in *Mgat5*$^{-/-}$ male mice was delayed until 10–13 months (data not shown). Tumors in PyMT *Mgat5*$^{-/-}$ mice grew more slowly than those in heterozygous and wild-type mice (Fig. 4*c*). At 28–30 weeks of age, the tumor burden in PyMT *Mgat5*$^{-/-}$ mice was 3.4 ± 0.8 g, compared with 15.1 ± 1.8 g and 13 ± 2.8 g in the PyMT *Mgat5*$^{+/-}$ and PyMT *Mgat5*$^{+/+}$ mice, respectively. The fraction of cells staining positive for proliferating cell nuclear antigen was substantially less in PyMT *Mgat5*$^{-/-}$ neoplastic and carcinoma tissues than in similar tissues in PyMT *Mgat5*$^{+/-}$ mice (Fig. 4*d*). The frequency of apoptotic cells in the tumors was 1–2% and did not vary substantially with *Mgat5* genotype (data not shown). Northern blot analysis indicated that PyMT transcript amounts were similar in tumors from the three *Mgat5* genotypes (data not shown).

The incidence of lung metastases in PyMT *Mgat5*$^{-/-}$ mice was about 5% that in wild-type and heterozygous littermates (Fig. 4*e*). The metastatic tumor nodules in lung were smaller in the PyMT *Mgat5*$^{-/-}$ mice, and tumor burden in the lung did not cause cardiac hypertrophy (0 of 15 mice), which was common in the PyMT *Mgat5*$^{+/+}$ and PyMT *Mgat5*$^{-/+}$ mice at late stages of tumor growth (13 of 27 mice).

Before overt tumor formation, the branching morphology of ductal epithelium was similar in PyMT *Mgat5*$^{-/-}$ and PyMT *Mgat5*$^{+/-}$ mice (Fig. 5*a* and *b*). In mammary fat pads lacking overt tumors at 14 weeks, there were multiple microscopic tumor foci in mice of all *Mgat5* genotypes. This indicates that although tumor growth was considerably less, multiple focal initiation was not suppressed in Mgat5-deficient mice. At 26 weeks, tumors in *Mgat5*$^{+/-}$ and *Mgat5*$^{+/+}$ PyMT-transgenic mice had completely replaced the ductal epithelium, whereas mammary fat pads from PyMT *Mgat5*$^{-/-}$ mice contained areas of normal tissue, hyperplasia and neoplasia (Fig. 5*c* and *d*).

LacZ activity was absent in normal and hyperplastic mammary tissues of PyMT *Mgat5*$^{+/-}$ and PyMT *Mgat5*$^{-/-}$ mice (Fig. 5*e*). PyMT *Mgat5*$^{-/-}$ tumors expressed small amounts of *LacZ* activity with some foci of intensely staining tumor cells, whereas PyMT *Mgat5*$^{+/-}$ tumors stained strongly. We found that 5 of 140 tumors in PyMT *Mgat5*$^{-/-}$ mice had acquired a fast-growth phenotype, similar to tumors in transgenic mice expressing Mgat5. These tumors, which had escaped growth suppression dependent on *Mgat5*$^{-/-}$, also expressed more *lacZ* activity (Fig. 5*f* and *g*). This indicates that the *Mgat5* promoter was activated in concert with the molecular event(s) leading to a fast-growth phenotype. L-PHA-reactive N-glycans were not re-expressed in the fast-growing PyMT *Mgat5*$^{-/-}$ tumors (data not shown).

Mgat5$^{-/-}$ stabilizes focal adhesions and actin stress fibers

Overexpression of MGAT5 in cultured epithelial cells blocks contact inhibition of growth, and cell–substratum adhesion on collagen and fibronectin[14]. Therefore, we removed mammary tumor cells from PyMT-transgenic mice and cultured them on fibronectin-coated cover slips in serum-free medium to assess cell spreading, microfilament organization and focal adhesions. PyMT *Mgat5*$^{-/-}$ tumor cells showed impaired membrane ruffling compared with that of PyMT *Mgat5*$^{+/+}$ cells. The former cells showed actin stress fiber networks with paxillin in a punctate distribution of focal adhesions beneath the cells, whereas paxillin in the PyMT *Mgat5*$^{+/-}$ cells was very concentrated in ruffled

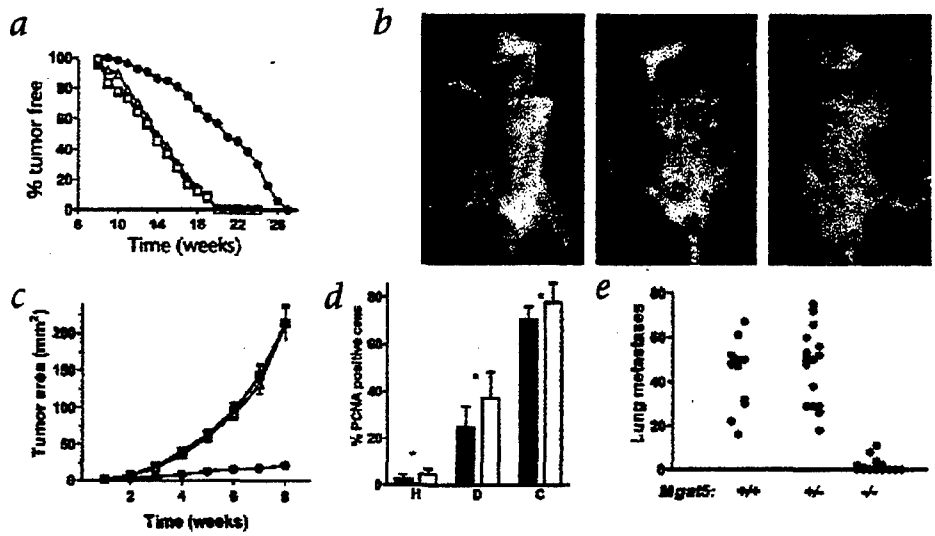

Fig. 4 PyMT-dependent tumor growth is suppresses in *Mgat5*$^{-/-}$ mice. *a*, Fraction of mammary pads free of palpable tumors in PyMT-transgenic littermates with either *Mgat5*$^{+/+}$ (□; *n* = 9), *Mgat5*$^{+/-}$ (△; *n* = 17) or *Mgat5*$^{-/-}$ (●; *n* = 14) genotypes. *b*, PyMT-transgenic mice at 26 weeks of age. *c*, Tumor growth (omitting the 5 of 140 fast-growing tumors), plotted as mean tumor surface area ± s.e.m.; time 0, initial detection by palpation. *d*, Sections of mammary fat pad from *Mgat5*$^{+/-}$ (■) and *Mgat5*$^{+/+}$ (□), stained with antibodies against proliferating cell nuclear antigen to quantify the proliferating cell fraction in hyperplasia (H), dysplastia (D) and carcinoma (C). *e*, Incidence of lung metastases per mouse at 24–30 weeks of age, when mammary tumor burden necessitated killing of the mice expressing Mgat5.

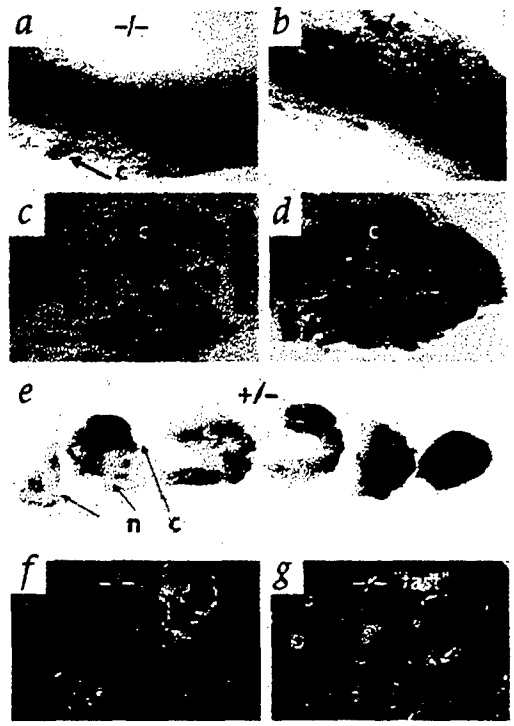

Fig. 5 Mammary fat pads and tumors. *a–d*, Whole mounts of mammary fat pads without palpable tumor at 19 weeks (*a* and *b*) and histological sections of tumors at 26 weeks stained with hematoxylin and eosin (*c* and *d*) from *Mgat5*$^{-/-}$ (left column) and *Mgat5*$^{+/-}$ (right column) mice. *e*, *LacZ* activity in mammary fat pads with low to high (left to right) tumor burden in PyMT *Mgat5*$^{+/-}$ mice. *f* and *g*, PyMT *Mgat5*$^{-/-}$ tumors, one with low *LacZ* activity (*f*) and a fast-growing PyMT *Mgat5*$^{-/-}$ tumor (*g*). d, dysplasia and hyperplasia; c, carcinoma; n, mammary fat pad.

edges, with fine radial actin fibers extending into the cells (Fig. 6*a* and *b*). PyMT activates c-Src kinase, which phosphorylates paxillin, allowing its recruitment into focal adhesions found at the ruffling edges in PyMT *Mgat5*$^{+/-}$ tumor cells. Paxillin in focal adhesion complexes is a docking protein for other signaling proteins, including FAK, Csk, c-Src and PI3 kinase[31]. Membrane ruffling and filapodia formation requires PI3 kinase activation[32], which is also a direct target of PyMT oncogenesis. Indeed, inhibition of PI3 kinase with wortmannin decreased membrane ruffling in PyMT *Mgat5*$^{+/-}$ cells and increased actin stress fibers, creating a morphology similar to that of PyMT *Mgat5*$^{-/-}$ cells (Fig. 6*c*). To measure actin filament turnover, we treated cells with latrunculin-A, a compound that binds actin monomers and renders them incompetent for filament formation[33]. The loss of rhodamine–phalloidin-staining filaments was more rapid in PyMT *Mgat5*$^{+/-}$ than in PyMT *Mgat5*$^{-/-}$ tumor cells, indicating a slower turnover of focal adhesions in cells with the latter genotype (Fig. 6*g*).

D3-phosphoinosotides produced by PI3 kinase stimulate phosphorylation and activation of PKB. The amounts of PKB protein and phosphorylated PKB were decreased in PyMT *Mgat5*$^{-/-}$ tumors, whereas amounts of phosphorylated mitogen-activated protein (MAP) kinase were not different (Fig. 6*h*). The amounts of phosphorylated PKB as well as membrane ruffling were restored in PyMT *Mgat5*$^{-/-}$ tumors with the fast-growth phenotype (Fig. 6*h*, far right lane). However, the tumor cell population was heterogenous for the membrane ruffling phenotype (Fig. 6*d*).

The *Mgat5*-null mutation also affected focal adhesions in the absence of an oncogene. *Mgat5*$^{+/-}$ fibroblasts spread extensively and pseudopodia showed fine actin microfilament, whereas there were cortical stress fibers characteristic of non-motile cells in *Mgat5*$^{-/-}$ cells (Fig. 6*e* and *f*). The amount of phosphorylated PKB was also decreased, but amounts of phosphorylated MAP kinase were similar in fibroblasts expressing Mgat5 (Fig. 6*h*). The addition of serum induced rapid phosphorylation of MAP kinase and PKB, indicating that signaling potential was similar in mutant and wild-type cells. Therefore, the intrinsic defect in *Mgat5*$^{-/-}$ cells seems to be an inability to accelerate focal adhesion turnover and signaling through PI3 kinase/PKB as required for full transformation by PyMT.

Discussion

Here, we have shown that Mgat5 products are not required for embryonic development, but when expressed in cancer cells, they contribute directly to tumor growth and metastasis. Using the PyMT transgenic model of breast cancer, we examined early events in tumor formation as well as metastasis and secondary events associated with tumor progression. The initial appearance of tumors was delayed in PyMT *Mgat5*$^{-/-}$ mice compared with that in either *Mgat5*$^{+/-}$ or *Mgat5*$^{+/+}$ PyMT-trangenic mice. Tumor initiation occurred efficiently, as indicated by multi-focal tumor formation and involvement of 10 of 10 mammary fat pads in PyMT-transgenic mice of all *Mgat5* genotypes. The fraction of apoptotic tumor cells was small and similar in all genotypes. However, the proportion of proliferating cells in hyperplasia, dysplasia and carcinoma was less in PyMT *Mgat5*$^{-/-}$ mice than in similar tissues in mice expressing Mgat5. Tumor diameters and weights at the end of the experiment showed decrease of about 500% in tumor burden in the PyMT *Mgat5*$^{-/-}$ mice compared with that in the mice expressing Mgat5. Similar delays in tumor appearance have been seen in PyMT-transgenic mice on a *Grb2*$^{+/-}$ genetic background (an adapter protein in the Ras pathway[34]) and also on an *Ets-2*$^{+/-}$ background (a transcription factor downstream of Ras; ref. 35). However, the decrease in tumor growth rates was more substantial here. The incidence of lung metastases was also considerably decreased, approximately 5% in Mgat5-deficient mice. Suppression of tumor growth and metastasis has been reported for somatic tumor cell mutants lacking Mgat5 transplanted into syngenic mice[10]. This indicates that decreased tumor growth in PyMT *Mgat5*$^{-/-}$ mice is likely a tumor-cell-autonomous phenotype rather than being host-mediated, and prompted further examination of the PyMT tumor cells.

The amounts of phosphorylated PKB were decreased in PyMT *Mgat5*$^{-/-}$ tumor cells, whereas phosphorylated MAP kinase amounts were unaffected, indicating that PyMT-dependent PI3 kinase and PKB activation is blocked by the *Mgat5*$^{-/-}$ mutation. The PyMT protein is tyrosine-phosphorylated at Y315/Y322, creating binding sites for p85, the regulatory subunit of PI3 kinase[25]. The Asn-Pro-Thr-Tyr motif at position 250 is also phosphorylated, creating a binding site for the phosphotyrosine-binding domain of Src homology 2 domain-containing (Shc) protein[29]. Mutations in either domain of PyMT compromise its transforming activity[27], creating a growth delay similar to that in PyMT *Mgat5*$^{-/-}$ mice. Integrin-mediated cell motility and invasion by mammary epithelial cells in culture depend on activation of PI3 kinase, which acts downstream of Rac and Cdc42 GTPases[36]. PI3 kinase increases the amounts of D-3 phosphoinositide, which is

required for PKB activation, actin microfilament re-organization, membrane ruffling, and cell motility[32,37]. Here, PyMT *Mgat5*$^{-/-}$ tumor cells on fibronectin-coated plastic were deficient in membrane ruffling, actin was organized as stress fibers and turnover was slower. The α and β chains of integrin receptors each have multiple N-glycosylation sites, and MGAT5 products are present at a fraction of the glycosylation sites on $\alpha_5\beta_1$ fibronectin receptor[17,18]. Overexpression of MGAT5 in epithelial cells enhanced cell motility and increased MGAT5 products on $\alpha_1\beta_5$, indicating that enzyme activity is not saturating in epithelial cells before transformation[14]. Therefore, integrins may be essential target glycoproteins modified by MGAT5 products to effect the increase in focal adhesion turnover, cell migration and tumor growth.

Our results show that in the absence of Mgat5 products, PyMT-induced activation of PI3 kinase and PKB is not sufficient for optimal tumor growth and metastasis. Furthermore, additional genetic or epigenetic event(s) in the tumor cells enabled 5 of 140 PyMT *Mgat5*$^{-/-}$ tumors to overcome growth suppression. This was accompanied by increased PKB activation and active membrane ruffling. Similarly, secondary events restoring tumor growth have been found in mice with a mutant PyMT transgene deficient in P85/PI3 kinase binding. Tumors in these mice express more c-ErbB2 and c-ErbB3 receptors, which may compensate for the loss of PyMT activity[27]. These results indicate that the dependence on MGAT5 products for tumor growth may be diminished with secondary mutations that amplify oncogene signals downstream of focal-adhesions, and might include increased activity of gene products such as c-Src, PI3 kinase, PKB or loss of phosphatase and tensin homolog.

LacZ expression from the *Mgat5* targeted locus was greater in tumors than in normal mammary fat pads, indicating that the PyMT oncogene is a positive regulator of the *Mgat5* promoter. Furthermore, LacZ expression was increased in the fast-growing *Mgat5*$^{-/-}$ tumors that overcame growth suppression. *LacZ* expression was considerably higher in PyMT *Mgat5*$^{+/-}$ tumors than in PyMT *Mgat5*$^{-/-}$ tumors, indicating that Mgat5 products also positively regulate *Mgat5* transcription.

The precise location of the MGAT5 products on specific glycoprotein(s) and their role in regulating tumor growth and metastasis remains to be determined. However, MGAT5 products on adhesion receptors may create steric hindrance that destabilizes agonist-dependent clusters in the plane of the membrane. Adhesion receptors are highly engaged and turnover is slow in quiescent substratum-attached cells. Cell motility requires a decrease in the proportion of stable receptor complexes to allow greater focal adhesion turnover. PyMT oncogenesis induces *Mgat5* gene expression and increases Mgat5 glycan products, which in turn stimulate focal adhesion turnover and tumor cell growth. Thus, Mgat5 glycan products seem to be potent downstream effectors of PyMT dependent oncogenesis. The role of MAGT5 products in normal physiological process is less apparent, but our observations of the *Mgat5*$^{-/-}$ mouse indicate they may regulate cell interactions affecting leukocyte migration, cell interactions with basement membranes in kidney glomeruli, and T-cell-receptor responses to antigens.

Our findings indicate that inhibitors of MGAT5 may be useful in the treatment of cancer by targeting their dependency on focal adhesion signaling for proliferation. Indeed, swainsonine, a competitive inhibitor of Golgi β-mannosidase II, has anti-cancer activity in mice[38,39]. This compound partially blocks Mgat5 products by diverting the biosynthesis pathway upstream of Mgat5 enzyme. In a phase I clinical trial of cancer patients, swainsonine treatment produced responses with mild side effects[40]. However, an MGAT5 inhibitor may provide a more-complete and specific block of the MGAT5 products. Our study

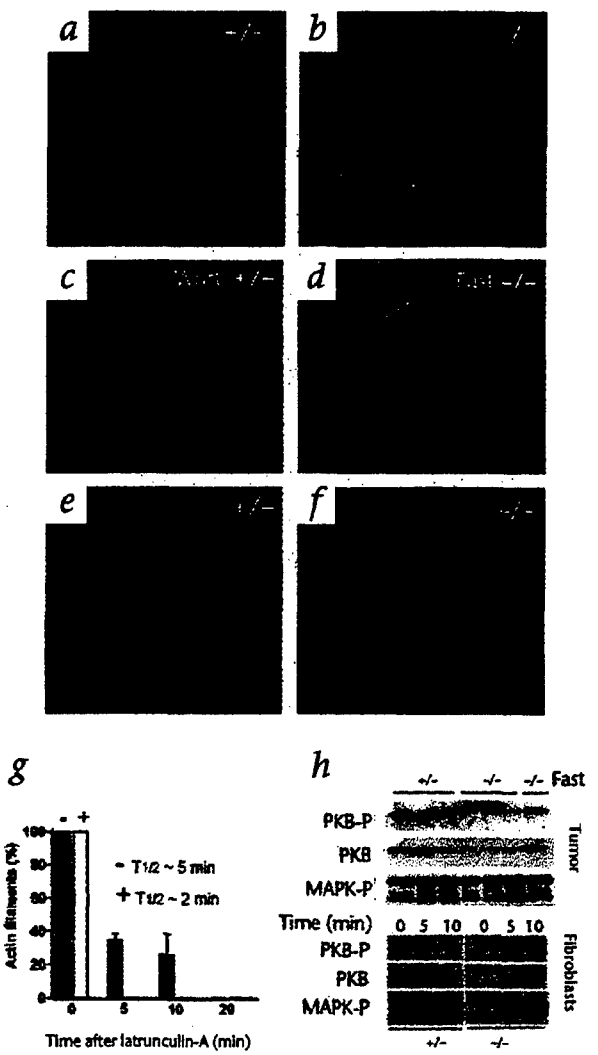

Fig. 6 Suppression of membrane ruffling, actin filament turnover and PKB phosphoprotein in PyMT *Mgat5*$^{-/-}$ tumor cells. *a–f*, Cells were plated on glass cover slips coated with fibronectin, fixed and stained with the nuclear stain Hoechst322, actin-specific rhodamine–phalloidin and FITC-conjugated antibody against paxillin. *a* and *b*, Paxillin (green) is present at the ends of microfilaments (red) in focal adhesions of *Mgat5*$^{+/-}$ (*a*) but not *Mgat5*$^{-/-}$ (*b*) fibroblasts. *c*, PyMT *Mgat5*$^{+/-}$ tumors on fibronectin treated with 100 nM wortmannin for 18 h. *d*, PyMT *Mgat5*$^{-/-}$ tumor cell from a fast-growing tumor (representative of 5 of 140 tumors) that escaped *Mgat5*$^{-/-}$ growth suppression. *e* and *f*, Embryonic fibroblasts. *Mgat5*$^{+/-}$ cells spread more extensively, therefore the nucleus in *e* is out of view to the left. *g*, Actin microfilament decay in the presence of 0.5 μM latrunculin-A, determined by the fraction of cells staining with rhodamine–phalloidin. *h*, Mouse tumors were homogenized and detergent extracts were separated by SDS–PAGE and assessed by western blot analysis with antibodies against phosphorylated MAP kinase (Thr202/Tyr204) and PKB and phosphorylated PKB. Fast, fast-growing tumor. Below, The procedure was repeated with primary embryonic fibroblasts growth-arrested in serum-free medium and re-stimulated with serum for 5 and 10 min.

shows that suppression of Mgat5 activity is not toxic, and sheds light on the molecular mechanism of tumor growth suppression, as well as the possibilities of acquired resistance to Mgat5 inhibition in tumors.

Methods

Mutation of the *Mgat5* gene. A genomic library from strain 129/sv mice was screened with a *Mgat5* cDNA probe. A 13.5-kb genomic clone containing the 205-nucleotide 5′ untranslated region and 241 nucleotides spanning the first coding exon was used to construct the *Mgat5* targeting vector. The *Mgat5* targeting vector was constructed with *lacZ* replacing the coding region of the first exon. The targeting vector was linearized by digestion with *Not*I and electroporated into R1 ES cells, and transfected cells were selected in the presence of G418 and gancyclovir as described[41]. DNA from drug-resistant colonies was digested with *Pst*I and screened for homologous recombination by Southern blot analysis using a 1.7-kb *Pst*I–*Xba*I genomic fragment external to the targeting vector. Two *Mgat5*$^{-/-}$ ES cell lines were aggregated with blastocysts from CD-1 mice and implanted into pseudo-pregnant CD-1 females. The resultant chimeras were mated with 129/sv females. Heterozygous progeny were intercrossed to generate *Mgat5*$^{-/-}$ mice, and experiments were done on the 129/sv background. For histology, mice were perfused with 10% phosphate-buffered formalin *in vivo* and tissues were embedded in paraffin, sectioned, and stained with hematoxylin and eosin. To detect β-galactosidase (*lacZ*) activity, tissues were fixed in 0.2% glutaraldehyde for 30 min, washed in phosphate-buffered saline, and incubated overnight in X-gal staining solution (1 mg/ml 4-chloro-5-bromo-3-indolyl-β-galactoside (X-gal), 4 mM $K_4Fe(CN)_6 \cdot 3H_2O$, 4 mM $K_3Fe(CN)_6$, 2 mM $MgCl_2$, 0.01% deoxycholate and 0.02% Nonidet P-40 in 0.1 M sodium phosphate, pH 7.3). After being stained, samples were further fixed in 10% phosphate-buffered formalin.

Tumor growth and metastasis in PyMT-transgenic mice. Transgenic mice expressed the PyMT oncogene under the control of the mouse mammary tumor virus long terminal repeat[28]. Male PyMT *Mgat5*$^{+/-}$ mice on a 129sv × FVB-129/sv background were crossed with 129sv *Mgat5*$^{+/-}$ female mice littermates lacking the PyMT gene. The progeny were genotyped by PCR, and examined by palpation for tumors on a weekly basis. Once tumors were detected, they were measured with callipers weekly. Mice were killed when their tumor burden reached about 50% of their body weight, and lungs were resected and surface metastatic foci were counted with a dissection microscope. Immunohistochemisty was done using a 1:1,000 dilution of biotinylated antibody against proliferating cell nuclear antigen (Novocastra, Newcastle, UK) and developed using strepavidin detection system (Signet, Dedham, Massachusetts). Apoptosis was assessed using DNA end-labeling and immunohistochemical detection.

L-PHA lectin, western blot analysis and Mgat5 assay. Tumors from the mice were homogenized in 10 volumes of RIPA buffer; 50 mM Tris-HCl, pH7.5, 150 mM NaCl, 1% Triton-X100, 1% deoxycholate, 0.1% SDS, 100 μM orthovanadate, 1 mM PMSF and protease inhibitor 'cocktail' (Boehringer). Cell lysates were prepared in the same buffer. Detergent extracts were clarified by centrifugation, and proteins were separated by SDS–PAGE, transferred electrophoretically to PVDF membrane and assessed by western blot analysis using 1:500 dilutions of antibodies against phosphorylated MAP kinase (Thr202/Tyr204), PKB and phosphorylated PKB (NEB). For lectin blots, membranes were probed with 0.5 μg/ml L-PHA, followed by incubation with a rabbit antibody against L-PHA (1:1,000 dilution) and with HRP-conjugated donkey antibody against rabbit (Amersham). Mgat5 enzyme activity in tissue homogenates was determined as transfer of ^{3}H-GlcNAc from UDP-6-^{3}H-GlcNAc (Amersham) to the synthetic acceptor GlcNAcβ1-2Manβ1-6Glcβ1-octyl per mg of lysate protein, as described[14].

Focal adhesion and actin microfilament turnover. PyMT mammary tumor cells and fibroblasts from embryos at embryonic day 13.5 were extracted from tissues samples with trypsin and cultured for 2 weeks in alpha-modified Eagle medium plus 10% FCS. Cells were plated overnight on glass slides coated with 1 μg/ml fibronectin in serum-free alpha-modified Eagle medium. The cells were then fixed in 3.7% paraformaldehyde, washed with 0.2% Nonidet P-40 in phosphate-buffered saline and stained with rhodamine–phalloidin, 1:50 dilution of antibodies against paxillin (Transduction Laboratories, Lexington, Kentucky), and Hoechst 33258 stain according to the manufacturer's instructions. Fluorescence images of the cells were obtained using a deconvolution microscope and digital capture of data. Latrunculin-A, an actin monomer-binding drug that renders the monomers incompetent for filament formation, was added to cells at a concentration of 0.5 μM, and the percentage of cells with actin microfilaments was determined by staining with rhodamine–phalloidin.

Acknowledgments

The authors thank C. Warren, S. Kulkarni and P. Cheung for suggestions. This research was supported by grants from National Cancer Institute of Canada, the Mizutani Foundation, the National Science and Engineering Research Council of Canada, and GlycoDesign (Toronto, Canada). W.J.M. is supported by a Medical Research Council Scientist Award.

RECEIVED 20 SEPTEMBER; ACCEPTED 29 DECEMBER 1999

1. Yamashita, K., Ohkura, T., Tachibana, Y., Takasaki, S. & Kobata, A. Comparative study of the oligosaccharides released from baby hamster kidney cells and their polyoma transformant by hydrazinolysis. *J. Biol .Chem.* **259**, 10834–10840 (1984).
2. Pierce, M. & Arango, J. Rous sarcoma virus-transformed baby hamster kidney cells express higher levels of asparagine-linked tri- and tetraantennary glycopeptides containing [GlcNAc-β(1,6)Man-α(1,6)Man] and poly-N-acetyllactosamine sequences than baby hamster kidney cells. *J. Biol. Chem.* **261**, 10772–10777 (1986).
3. Cummings, R.D., Trowbridge, I.S. & Kornfeld, S. A mouse lymphoma cell line resistant to the leukoagglutinating lectin from *Phaseolus vulgaris* is deficient in UDP-GlcNAc:α-D-mannoside β1,6 N-acetylglucosaminyltransferase. *J. Biol. Chem.* **257**, 13421–13427 (1982).
4. Shoreibah, M. *et al.* Isolation, characterization, and expression of cDNA encoding *N*-Acetylglucosaminyltransferase V. *J. Biol. Chem.* **268**, 15381–15385 (1993).
5. Cummings, R.D. & Kornfeld, S. Characterization of the structural determinants required for the high affinity interaction of asparagine-linked oligosaccharides with immobilized *Phaseolus vulgaris* leukoagglutinating and erythroagglutinating lectin. *J. Biol. Chem.* **257**, 11230–11234 (1982).
6. Fernandes, B., Sagman, U., Auger, M., Demetriou, M. & Dennis, J.W. β1-6 branched oligosaccharides as a marker of tumor progression in human breast and colon neoplasia. *Cancer Res.* **51**, 718–723 (1991).
7. Seelentag, W.K., *et al.* Prognostic value of β1,6-branched oligosaccharides in human colorectal carcinoma. *Cancer Res.* **58**, 5559–5564 (1998).
8. Yamashita, K., Tachibana, Y., Ohkura, T. & Kobata, A. Enzymatic basis for the structural changes of asparagine-linked sugar chains of membrane glycoproteins of baby hamster kidney cells induced by polyoma transformation. *J. Biol. Chem.* **260**, 3963–3969 (1985).
9. Dennis, J.W., Kosh, K., Bryce, D.-M. & Breitman, M.L. Oncogenes conferring metastatic potential induce increased branching of Asn-linked oligosaccharides in rat2 fibroblasts. *Oncogene* **4**, 853–860 (1989).
10. Dennis, J.W., Laferte, S., Waghorne, C., Breitman, M.L. & Kerbel, R.S. β1-6 branching of Asn-linked oligosaccharides is directly associated with metastasis. *Science* **236**, 582–585 (1987).
11. Kang, R. *et al.* Transcriptional regulation of the N-acetylglucosaminyltranserase V gene in human bile duct carcinoma cells (HuCC-T1) is mediated by Ets-1. *J. Biol.Chem.* **271**, 26706–26712 (1996).
12. Chen, L., Zhang, W., Fregien, N. & Pierce, M. The her-2/neu oncogene stimulates the transcription of N-acetylglucosaminyltransferase V and expression of its cell surface oligosaccharide products. *Oncogene* **17**, 2087–2093 (1998).
13. Lu, Y., Pelling, J.C. & Chaney, W.G. Tumor cells surface β1-6 branched oligosaccharides and lung metastasis. *Clin. Exp. Metastasis* **12**, 47–54 (1994).
14. Demetriou, M., Nabi, I.R., Coppolino, M., Dedhar, S. & Dennis, J.W. Reduced contact inhibition and substratum adhesion in epithelial cells expressing GlcNAc-transferase V. *J. Cell Biol.* **130**, 383–392 (1995).
15. Seberger, P.J. & Chaney, W.G. Control of metastasis by asn-linked, β1-6 branched oligosaccharides in mouse mammary cancer cells. *Glycobiology* **9**, 235–241 (1999).
16. Do, K.-Y., Fregien, N., Pierce, M. & Cummings, R.D. Modification of glycoproteins by *N*-acetylglucosaminyltransferase V is greatly influenced by accessibility of the enzyme to oligosacharide acceptors. *J. Biol. Chem.* **269**, 23456–23464 (1994).
17. Nakagawa, H., *et al.* Detailed oligosaccharide structures of human integrin alpha 5 beta 1 analyzed by a three-dimensional mapping technique. *Eur. J. Biochem.* **237**, 76–85 (1996).
18. Asada, M., Furukawa, K., Kantor, C., Gahmberg, C.G. & Kobata, A. Structural study of the sugar chains of human leukocyte cell adhesion molecules CD11/CD18. *Biochemistry* **30**, 1561–1571 (1991).
19. Skelton, T.P., Zeng, C., Nocks, A. & Stamenkovic, I. Glycosylation provides both stimulatory and inhibitory effects on cell surface and soluble CD44 binding to hyaluronan. *J. Cell Biol.* **140**, 431–446 (1998).
20. Diamond, M.S., Staunton, D.E., Martin, S.D. & Springer, T.A. Binding of the integrin Mac-1 (CD11b/CD18) to the third immunoglobulin-like domain of ICAM-1 (CD54) and its regulation by glycosylation. *Cell* **65**, 961–971 (1991).
21. McEvoy, L.M., Sun, H., Frelinger, J.G. & Butcher, E.C. Anti-CD43 inhibition of T cell

homing. *J. Exp. Med.* **185**, 1493–1498 (1997).
22. Verbeek, B.S. *et al.* c-Src protein expression is increased in human breast cancer. An immunohistochemical and biochemical analysis. *J. Pathol.* **180**, 383–388 (1996)
23. Liu, A.X., *et al.* AKT2, a member of the protein kinase B family, is activated by growth factors, v-Ha-ras, and v-src through phosphatidylinositol 3-kinase in human ovarian epithelial cancer cells. *Cancer Res.* **58**, 2973–2977 (1998).
24. Dilworth, S.M. *et al.* Transformation by polyoma virus middle T-antigen involves the binding and tyrosine phosphorylation of Shc. *Nature* **367**, 87–90 (1994).
25. Whitman, M., Kaplan, D.R., Schaffhausen, B., Cantley, L. & Roberts, T.M. Association of phosphatidylinositol kinase activity with polyoma middle-T competent for transformation. *Nature* **315**, 239–242 (1985).
26. Guy, C.T., Muthuswamy, S.K., Cardiff, R.D., Soriano, P. & Muller, W.J. Activation of the c-Src tyrosine kinase is required for the induction of mammary tumors in transgenic mice. *Genes Dev.* **1**, 23–32 (1994).
27. Webster, M.A. *et al*Requirement for both Shc and phosphatidylinositol 3' kinase signaling pathways in polyomavirus middle T-mediated mammary tumorigenesis. *Mol. Cell. Biol.* **18**, 2344–2359 (1998).
28. Guy, C.T., Cardiff, R.D. & Muller, W.J. Induction of mammary tumors by expression of polyomavirus middle T oncogene: a transgenic mouse model for metastatic disease. *Mol. Cell. Biol.* **12**, 954–961 (1992).
29. Bronson, R., Dawe, C., Carroll, J. & Benjamin, T. Tumor induction by a transformation-defective polyoma virus mutant blocked in signaling through Shc. *Proc. Natl. Acad. Sci. USA* **94**, 7954–7958 (1997).
30. Granovsky, M. *et al.* GlcNAc-transferase V and core 2 GlcNAc-transferase expression in the developing mouse embryo. *Glycobiology* **5**, 797–806 (1995).
31. Turner, C.E. Molecules in focus, paxillin. *Int. J. Biol. Macromol.* **30**, 955–959 (1998).
32. Reif, K., Nobes, C.D., Thomas, G., Hall, A. & Cantrell, D.A. phosphatidylinositol 3-kinase signals activate a selective subset of Rac/Rho dependent effector pathways. *Curr. Biol.* **6**, 1445–1455 (1996).
33. Spector, I., Shochet, N.R., Blasberger, D. & Kashman, Y. Latrunculins, novel marine macrolides that disrupt microfilament organization and affect cell growth: I. Comparison with cytochalasin D. *Cell Motil. Cytoskeleton* **13**, 127–124 (1989).
34. Cheng, A.M. *et al.* Mammalian Grb2 regulates multiple steps in embryonic development and malignant transformation. *Cell* **95**, 793–803 (1999).
35. Neznanov, N. *et al.* A single targeted Ets2 allele restricts development of mammary tumors in transgenic mice. *Cancer Res.* **59**, 4242–4246 (1999).
36. Keely, P.J., Westwick, J.K., Whitehead.I.P., Der, C.J. & Parise, L.V. Cdc42 and Rac1 induce integrin-mediated cell motility and invasiveness through PI(3)K. *Nature* **390**, 632–636 (1997).
37. King, W.G., Mattaliano, M.D., ChanT.O., Tsichlis, P.N. & Brugge, J.S. Phosphatidylinositol 3-kinase is required for integrin-stimulated AKT and Raf-1/mitogen-activated protein kinase pathway activation. *Mol. Biol. Cell* **17**, 4406–4418 (1997).
38. Humphries, M.J., Matsumoto, K., White, S.L. & Olden, K. Oligosaccharide modification by swainsonine treatment inhibits pulmonary colonization by B16-F10 murine melanoma cells. *Proc. Natl. Acad. Sci. USA* **83**, 1752–1756 (1986).
39. Dennis, J.W. Effects of swainsonine and polyinosinic-polycytidylic acid on murine tumor cell growth and metastasis. *Cancer Res.* **46**, 5131–5136 (1986).
40. Goss, P.E., Baptiste, J., Fernandes, B., Baker, M. & Dennis, J.W. A study of swainsonine in patients with advanced malignancies. *Cancer Res.* **54**, 1450–1457 (1994).
41. Hasty, P. & Bradley, A. In *Gene Targeting. A Practical Approach* (ed. Joyner, A.) 138–180 (IRL Oxford Press, 1993).

THE JOURNAL OF BIOLOGICAL CHEMISTRY
Vol. 277, No. 25, Issue of June 21, pp. 22829–22838, 2002
Printed in U.S.A.

The *Caenorhabditis elegans* Gene, *gly-2*, Can Rescue the *N*-Acetylglucosaminyltransferase V Mutation of Lec4 Cells*

Received for publication, February 11, 2002, and in revised form, March 28, 2002
Published, JBC Papers in Press, April 5, 2002, DOI 10.1074/jbc.M201390200

Charles E. Warren‡, Aldis Krizus‡, Peter J. Roy‡§¶, Joseph G. Culotti‡§, and James W. Dennis‡§‖

From the ‡Samuel Lunenfeld Research Institute, Mount Sinai Hospital, Toronto, Ontario M5G 1X5 and §Department of Molecular and Medical Genetics, University of Toronto, Toronto, Ontario, M55 1A8, Canada

UDP-*N*-acetylglucosamine:α-6-D-mannoside β-1,6-*N*-acetylglucosaminyltransferase V (GlcNAc-TV) is a regulator of polylactosamine-containing *N*-glycans and is causally involved in T cell regulation and tumor metastasis. The *Caenorhabditis elegans* genome contains a single orthologous gene, *gly-2*, that is transcribed and encodes a 669-residue type II membrane protein that is 36.7% identical to mammalian GlcNAc-TV (*Mgat-5*). Recombinant GLY-2 possessed GlcNAc-TV activity when assayed *in vitro*, and protein truncations demonstrated that the N-terminal boundary of the catalytic domain is Ile-138. *gly-2* complemented the *Phaseolus vulgaris* leucoagglutinin binding defect of Chinese hamster ovary Lec4 cells, whereas GLY-2(L116R), an equivalent mutation to that which causes the Lec4A phenotype, could not. We conclude that the worm gene is functionally interchangeable with the mammalian form. GlcNAc-TV activity was detected in wild-type animals but not those homozygous for a deletion allele of *gly-2*. Activity was restored in mutant animals by an extrachromosomal array that encompassed the *gly-2* gene. Green fluorescent protein reporter transgenes driven by the *gly-2* promoter were expressed by developing embryos from the late comma stage onward, present in a complex subset of neurons in larvae and, in addition, the spermathecal and pharyngeal-intestinal valves and certain vulval cells of adults. However, no overt phenotypes were observed in animals homozygous for deletion alleles of *gly-2*.

UDP-*N*-acetylglucosamine:α-6-D-mannoside β-1,6-*N*-acetylglucosaminyltransferase V (GlcNAc-TV)[1] is one of a set of sequence-unrelated GlcNAc-T enzymes that create branches in complex-type *N*-glycans (1). These branches can be further elongated by galactosyltransferase and other enzymes to create the mature glycoprotein oligosaccharides. The GlcNAcβ1,6 branch resulting from GlcNAc-TV action is distinct in that it is the preferred site for elongation with polylactosamine chains, repeating lactosamine units that themselves can be further branched and carry a variety of terminal structures. GlcNAc-TV is thus a potential regulator of polylactosamine containing *N*-glycan chains on target glycoproteins. GlcNAc-TV is also distinct from the other *N*-acetylglucosaminyltransferases in that it has a specific temporal and spatial expression pattern in the developing mouse embryo. Expression is concentrated in neuronal tissues, specialized epithelium, and regions with stem cell-like populations. Zygotic expression increases at about 9.5 days post coitus, which coincides with the onset of organogenesis (2).

Mice deficient in GlcNAc-TV activity through mutation of the *Mgat-5* locus are viable but develop glomerulonephritis with age, which is associated with T cell hypersensitivity, apparently as a result of altered activation kinetics of the T cell receptor complex (3). When the *Mgat-5*° allele is combined with a mouse mammary tumor virus-promoted *Polyomavirus* middle T antigen transgene, multifocal tumorigenesis is delayed, and metastasis caused by the *Polyomavirus* middle T antigen is dramatically suppressed (4). This result is consistent with prior observations that tumor cell lines selected by resistance to the cytotoxic lectin *Phaseolus vulgaris* leucoagglutinin (L-PHA) deficient in GlcNAc-TV also failed to metastasize in syngeneic mice (5).

Although the *Mgat-5*° mouse is highly informative, systematic analysis of a complex viable phenotype remains difficult, particularly the identification of the dependent molecules and pathways. We therefore sought a simpler model organism in which synthetic genetics could be carried out rapidly to characterize the complex pleiotropic phenotypes expected from disruption of the glycosylation machinery. Because of the cellular non-autonomy typical of glycosylation phenotypes and of the phylogenetic restriction of complex-type *N*-glycans to metazoans, a whole animal model is necessary. *Caenorhabditis elegans* is the simplest and most highly characterized animal, its adult anatomy and developmental lineage have been completely determined (6, 7), and its genome is essentially completely sequenced (8). *C. elegans* is highly tractable to experimental phenotypic and genetic analysis, and there are numerous examples demonstrating that genetic pathways found in mammals are also conserved in this nematode (9–13).

* This work was funded by a grant from the National Cancer Institute of Canada. The costs of publication of this article were defrayed in part by the payment of page charges. This article must therefore be hereby marked "*advertisement*" in accordance with 18 U.S.C. Section 1734 solely to indicate this fact.

The nucleotide sequence(s) reported in this paper has been submitted to the GenBank™/EBI Data Bank with accession number(s) AF154122 (gly-2), AY037800 (cm20c4), and AY037802 (yk126h8). Appropriate data have also been contributed to ACeDB.

¶ Present address: Dept. of Developmental Biology and Genetics, Stanford University, Palo Alto, CA 94305.

‖ To whom correspondence should be addressed: Samuel Lunenfeld Research Inst., Mount Sinai Hospital, 600 University Ave., Toronto, Ontario M5G 1X5, Canada. Tel.: 416-586-8233; Fax: 416-586-8857; E-mail: dennis@mshri.on.ca.

[1] The abbreviations used are: GlcNAc-TV, UDP-*N*-acetylglucosamine:α-6-D-mannoside β-1,6-*N*-acetylglucosaminyltransferase V; L-PHA, *P. vulgaris* leucoagglutinin; EST, expressed sequence tag; FACS, fluorescence-activated cell analysis; FITC, fluorescein isothiocyanate; PBSE, PBS with 0.1% w/v EDTA; PBSFN, PBS with 1% v/v fetal bovine serum and 0.1% w/v NaN_3; 5′ RACE, rapid amplification of 5′ cDNA ends; SL1, splice leader type 1; SL2, splice leader type 2; TMD, *trans*-membrane domain; BisTris, 2-[bis(2-hydroxyethyl)amino]-2-(hydroxymethyl)propane-1,3-diol; MES, 2-(*N*-Morpholino)ethanesulfonic acid; CHO, Chinese hamster ovary; GFP, green fluorescent protein; TBS, Tris-buffered saline; TBSTM, TBS with 0.1% v/v Tween 20 (TBST) and 5% skimmed milk; MOPS, 3-(*N*-morpholino)propanesulfonic acid.

Surveys of the *C. elegans* genome sequence revealed a coding potential for most known glycosyltransferase genes (14). Genes encoding active polypeptide GalNAc-transferases (15), GlcNAc-TI (16), and a fucosyltransferase (17) have been characterized. In addition, there are at least three *sqv* genes that are elements of a proteoglycan glycosylation pathway that when mutated cause severe and pleiotropic defects (18–21). A recent NMR-mass spectrometry study identified the abundant *N*- and *O*-glycans in *C. elegans* (22). The canonical oligomannose series of *N*-glycans were observed, but atypical *O*-glycans were found where polypeptide linked GalNAc was β1–6-branched as in mammals but substituted with glucose or galactose rather than GlcNAc. We characterized the 6 homologues of core 2 GlcNAc-T (23) and demonstrated that *gly-1* transfers glucose from UDP-glucose to core 1 acceptor consistent with the inference based on the structural analysis (24).

We observed that the *C. elegans* genome encodes a single gene, designated *gly-2*, which is homologous to mammalian GlcNAc-TV sequences. In this paper, we establish that the nematode orthologue is functionally equivalent to that from mammals and that *C. elegans* is an appropriate model in which to pursue investigations of the contributions to fitness made by β6-GlcNAc-branched *N*-glycans.

EXPERIMENTAL PROCEDURES

Strains and Materials—Primer sequences (ACGT Corp.) are available on request. The wild-type Bristol strain of *C. elegans* (N2) (25) and *him-5(e1490)* were available as laboratory stocks. CB1282 *dpy-20(e1282) IV*, DR466 *him-5(e1490) V*, and DR435 *dpy-5(e61) unc-13(e51) I* were supplied by T. Stiernagle (*C. elegans* Genetics Center, University of Minnesota). BC107 *bli-4(e937), dpy-14(e188) I* was the gift of Dr. D. Baillie (Simon Fraser University, Vancouver, Canada). Standard husbandry methods were used (7, 26). Cosmid C55B7 was obtained from Dr. A. Coulson (Sanger Centre, Cambridge, UK). pPD95.77 and pPD95.69 were from Dr. A. Fire (Carnegie Institute of Washington), pMH#6 was obtained from Dr. M. Han (University of Colorado), pRF4 originated in the laboratory of Dr. J. Kramer (Northwestern University Medical School), and pIMKF1 was the gift of Dr. F. Hagen (University of Rochester Medical School). pCMVCD20 was obtained from Dr. E. Harlow (Massachusetts General Hospital Cancer Center), and Dr. P. Stanley provided pLec4 and pCHO-K1 (Albert Einstein College of Medicine). The *C. elegans* EST cm20c4 (GB:M89265) was provided by Dr L. Hillier (Washington University Genome Sequencing Center), and yk126h8 (GB:D64875/D68132) was obtained from Dr. Y. Kohara (National Institute of Genetics, Mishima, Japan). The GlcNAc-TV acceptor, βGlcNAc(1,2)αMan(1,6)βGlc-O$(CH_2)_7CH_3$, was a gift from Glycodesign Inc.

Molecular Biology Procedures—Unless otherwise noted, standard molecular biology techniques were employed (27).

5′ RACE—Poly(A)$^+$ RNA was isolated from mixed populations of *C. elegans* using a QuickPrep Micro mRNA purification kit (Pharmacia). The 5′ RACE system (Invitrogen) was used according to the manufacturer's instructions. First strand cDNA synthesis was primed with yk5′rc0. First round PCR using AmpliTaq Gold (PerkinElmer Life Sciences) was primed with yk5′rc1. The second round PCR used *Pfu* DNA polymerase (CLONTECH) and yk5′rc2 as the gene-specific primer. Amplimer was sequenced directly and subcloned into the *Eco*RV site of pZErO-2 (Invitrogen). Independent recombinants were analyzed by colony PCR using SL1, SL2, or RACE anchor and yk5′rc2 primers.

Northern Analysis—Non-starved mixed stage animals from Bristol N2 and *him-5(e1490)* strains were used to prepare poly(A)$^+$ RNA using a Dynabeads kit (Dynal A. S.) after disruption in a Polytron (Kinematica). ~1 μg of mRNA was fractionated, blotted, probed with the α-^{32}P-labeled *SalI/SmaI* fragment of yk126h8, and analyzed with a PhosphorImager (Storm/ImageQuant, Molecular Dynamics).

Construction of Mammalian Expression Vectors—pISTH1 was constructed from pIMKF1 (15) by replacing the *NdeI-BamHI* segment upstream of the cloning site with an *NdeI-BglII* fragment from pCITE4b(+) (Novagen). N-terminal truncations of GLY-2 were generated by PCR from yk126h8 as template using *Pfu* DNA polymerase primed by yk*$_{670}$r and one of ykl_{28}f, gly2-Δ133, gly2-Δ137, or gly2-Δ138. Amplimers were subcloned into the *Eco*RV site of pZErO-2 (Invitrogen) and sequenced. *Bam*HI fragments of error-free subclones were ligated into the *Bam*HI site of pISTH1. Ligation junctions, frame, and orientation were checked by DNA sequencing. A yk5′rc2 and SL1-primed *Taq*DNA polymerase PCR product of the RACE amplimer was subcloned into *Eco*RV cut and T-tailed pGEM5zf(+) (Promega) forming pYS. pCDNA3::yk126h8(+) was created by subcloning the *PvuII-SmaI* fragment of yk126h8 into *Eco*RV cut pCDNA3 (Invitrogen). An expression construct for mature SL1 *trans*-spliced cDNA (pCSYK-1) was constructed by combining the *SpeI-NarI* fragment of pYS with the *NarI-NotI* fragment of pCDNA3::yk126h8(+) in *SpeI-NotI*-cut pZErO-2, the *BamHI-NotI* fragment of which was subcloned into pCDNA3. The amplified region and ligation junctions were checked by DNA sequencing. The GLY-2(L116R) mutation was introduced into pCSYK-1 by mutagenesis directed by primer GLY2-L116R using the Chameleon kit according to the manufacturer's instructions (Stratagene). The complete transcriptional unit of the resulting construct, pCSYK-L116R, was sequenced. pEGFP-GLY2 was constructed by subcloning the ykR_2f-yk*$_{670}$r product generated by PCR amplification with *Pfu* DNA polymerase from yk126h8 template into the *Bam*HI site of pEGFP-C3 (CLONTECH). The insert and ligation junctions were completely sequenced and found to be in-frame and error-free. pEGFP-L116R was derived by replacing the *BstXI-Eco*RV fragment with the equivalent section of pCSYK-L116R to generate pEGFP-L116R. The introduced segment was confirmed by sequencing.

Transient Expression and Secretion of GLY-2 in Lec4 Cells—3×10^5 Lec4 cells (ATCC) were plated in each well of 6-well tissue culture clusters (Costar). The following morning, 1 μg of DNA (QIAgen) of pISTH1-based truncation constructs were transfected at 37 °C in a humidified 5% CO_2 atmosphere for 5–6 h using 8 μl of LipofectAMINE (Invitrogen) in 1 ml of OptiMEM-I (Invitrogen)/well. One ml of α-minimal essential medium containing 20% fetal bovine serum was added to the wells, and the clusters were transferred to a humidified 5% CO_2 atmosphere at 30 °C overnight. The following day, well contents were aspirated and replaced with 2 ml of α-minimal essential medium containing 10% fetal bovine serum, and incubation was continued until 78 h post-transfection. Conditioned medium was clarified by centrifugation at 1800 × *g* for 10 min and stored at 4 °C after the addition of sodium azide to 0.05% w/v.

Immunopurification of Recombinant Proteins—Recombinant proteins directed by pISTH1-based plasmids bear an N-terminal S-tag that was assayed according to the manufacturer's instructions in conditioned media from the transient transfections (Novagen). 1.25 pmol of recombinant protein in conditioned medium was immunoprecipitated and diluted into 1 ml of dilution buffer (10 mM Tris-HCl, pH 8.0, 150 mM NaCl, 0.025% w/v NaN_3, 0.1% v/v Triton X-100, 0.1% w/v bovine serum albumin). Aliquots were preadsorbed with 35 μl of a 50% v/v slurry of goat anti-rabbit IgG polyclonal antibody-agarose (Sigma) overnight at 4 °C then centrifuged briefly before supernatants were transferred to fresh tubes. 1 μg of rabbit polyclonal anti-S-tag antibody and a fresh aliquot of anti-rabbit IgG polyclonal antibody-agarose were added for 2 h at 4 °C before the beads were pelleted by centrifugation at 3000 rpm for 10 s in a microcentrifuge. Beads were washed 3 times with 1-ml aliquots of dilution buffer before 3 more washes with 100 mM MES, pH 6.5, 0.1% v/v Triton X-100, 100 μg/ml bovine serum albumin. A final aspiration of supernatant left the beads as a 50% slurry in a total volume of 35 μl, which was used for assay of GlcNAc-TV enzyme activity.

Assay of GlcNAc-TV Enzyme Activity—Enzyme activity was measured using synthetic specific acceptors (28). Assays contained 1 mM βGlcNAc(1,2)αMan(1,6)βGlc-O$(CH_2)_7CH_3$ acceptor, 1 mM [6-^{3}H]UDP-GlcNAc (44,400 dpm/nmol) in 50 mM MES, pH 6.5, in total volumes between 30 and 100 μl. Enzyme sources were nematode microsomal membranes, cell lysates, conditioned media either directly or dialysates against 10 mM MES, pH 6.0, or immunoprecipitates. Assays using microsomal membranes contained 2 mM acceptor and donor, both, which was 10^5 dpm/nmol. In addition these samples contained 5 mM adenosine 5′-monophosphate and 500 μM 2-acetamido-1,2-dideoxynojirimycin (Toronto Research Chemicals). After 3 h at the appropriate incubation temperature, 1 ml of ice-cold water was added to stop further reaction, and assays were either frozen or processed immediately. Enzyme products were separated from radioactive substrates by binding them to 50 mg of C_{18} cartridges (Alltech) preconditioned with methanol rinsing and water washing. Reactions were loaded, and the columns were washed 5 times with 1 ml of water. Radiolabeled products were eluted directly into scintillation vials with 2 separately applied 0.5-ml aliquots of methanol, and the radioactivity was determined by liquid scintillation counting.

Fluorescence Analysis of Lec4 Cells Transfected with gly-2—Transient transfections were performed essentially as above except that

Lec4 or CHO-K1 cells were plated at 10^6 cells on 6-cm tissue culture dishes (Falcon) that were cotransfected with 0.5 μg of pCMVCD20 (29) and 2.5 μg of pLec4, pCHO-K1, pCSYK-1, or pCSYK-L116R DNA using 18 μl of LipofectAMINE in 3 ml of OptiMEM-I. At 71 h post-transfection, the media were aspirated, and the plates were rinsed with ice-cold PBS followed by ice-cold PBS, 0.1% w/v EDTA (PBSE). Cells were dissociated from the dish by incubation in 0.5 ml of PBSE for 10 min at room temperature before triturating with 4.5 ml of PBS, 1% v/v fetal bovine serum, 0.1% w/v NaN_3 (PBSFN). Aliquots of 1.2×10^6 transfected cells were transferred to 6-ml polypropylene tubes (Falcon) on ice, filled with PBSFN, and centrifuged at 500 × *g* for 5 min at 4 °C, and the supernatants were decanted. FITC-conjugated L-PHA (Sigma) was preadsorbed against Lec4 cells by incubating 40 μg of FITC-L-PHA with 4×10^7 untransfected Lec4 cells (harvested using PBSE) in a total volume of 800 μl of PBSFN for 15 min on ice, then clarified. Lec4-absorbed FITC-L-PHA (0.5 μg) and 10 μl of phycoerythrin-conjugated monoclonal anti-CD20 (BD PharMingen) were added to each sample, and the cells were resuspended. After a 30-min incubation on ice, tubes were filled with PBSFN and centrifuged at 500 × *g* for 5 min at 4 °C, and the supernatants were decanted. Washes were repeated twice more before a final resuspension in 1 ml of PBSFN. FACS was carried out on a FACStar (BD PharMingen). Live single cells were selected based on a forward and side scattering gates, and data acquisition and analysis used the CellQuest package. Transfected cells were gated based on the phycoerythrin anti-CD20 fluorescence, and the FITC L-PHA staining of at least 10^4 transfected live single cells was measured for each sample. 3 μg of pEGFP-C3, pEGFP-GLY2, or pEGFP-L116R were transfected into Lec4 or CHO-K1 similarly. After harvesting, cells were stained with 2 μg of biotinylated L-PHA (Sigma), washed four times with PBSFN, then developed with 1 μg of streptavidin-CyChrome (BD PharMingen). After 3 washes with PBSFN, CyChrome staining of 2×10^4 transfected GFP^+ cells was measured for each sample. The remaining cells after analysis were immediately washed twice in PBS before cell pellets were flash-frozen and stored at −70 °C. Cell pellets were lysed in 50 mM MES, pH 6.5, 0.5% v/v Triton X-100, 10 mM EDTA containing 1× Complete protease inhibitor mixture (Roche Molecular Biochemicals). After 5 min on ice, lysates were clarified at 14,000 rpm for 5 min in a microcentrifuge, and supernatants were transferred and assayed immediately for GlcNAc-TV activity.

Western Analysis—Conditioned media from Lec4 cells that had been transiently transfected with pISTH1-based truncation constructs were subjected to SDS-PAGE, electroblotted to polyvinylidene difluoride (Waters), and blocked with TBS, 0.1% v/v Tween 20, 5% skimmed milk (TBSTM). Filters were washed with TBS, 0.1% v/v Tween 20 (TBST), then incubated with 0.5 μg/ml polyclonal rabbit anti-S-tag (CLONTECH) at 4 °C overnight. The blot was washed again with TBST then developed with 1:12,500 horseradish peroxidase-conjugated donkey anti-rabbit Ig (Amersham Biosciences) in TBST for 2 h at room temperature before extensive washes with TBST then TBS and visualization of the signal by ECL (Amersham Biosciences), recorded using X-Omat Blue XB-1 film (Eastman Kodak Co.). Clarified lysates prepared from samples that had been subjected to FACS analysis and GlcNAc-TV assay were separated by electrophoresis in a MOPS buffer system on 4–12% BisTris NuPage gels (Novex) then electroblotted as above. After methanol washing and air-drying, filters were incubated with 1:5000 monoclonal anti-GFP (CLONTECH) in TBSTM for 30 min at room temperature. After 5 rinses in TBS, the blot was developed with 1:2000 horseradish peroxidase-conjugated sheep anti-mouse Ig (Amersham Biosciences) in TBSTM. After 5 rinses and a 15-min wash in TBS, chemiluminescence signals (Supersignal, Pierce) were recorded.

GFP Reporter Transgenes—The 7461-bp *NsiI* fragment of C55B7 was subcloned into the *PstI* site of pPD95.69 and pPD95.77. A partial *NarI* digest was performed, and the overhangs were blunted (Klenow). A *SmaI* digestion was used to excise the intervening fragment, and the construct was reclosed. The ligation junctions were found to be correct after DNA sequencing. This procedure created an in-frame fusion between the *NarI* site in codon 3 of GLY-2 and the GFP segment of the vector, preceded by 6.7 kbp of upstream genomic DNA corresponding to bases 19,280 to 25,991 of C55B7. CB1282 hermaphrodites were transformed by gonad injection (30) of a mixture of reporter construct and pMH#6, a plasmid containing a region of *C. elegans* genomic DNA capable of rescuing the *dpy-20(e1282)* mutation. Several non-Dpy F1 progeny were selected for each reporter construct, transgenic lines were established from them, and epifluorescence microscopy was performed using a Leica DMR photomicroscope. The inheritance of extra-chromosomal arrays is mosaic, and the fine structure of the array in each strain is different. Consequently, several individuals from each line were examined to compile consensus expression patterns. Cell identification was accomplished using the position and morphology of the expressing cells, the number and position of their nuclei, and by comparison to anatomical landmarks visualized by differential interference contrast microscopy.

Mutagenesis—The *gly-2* alleles, *ev581*, and *qa700* were generated by Tc1-mediated mutagenesis with minor modifications (31). *qa703* was isolated from ethylmethanesulfonate-induced deletion libraries using minor variances from published procedures (32). Tc1 mutagenesis relies on transposon mobilization, so the founding strain contains *mut-2* alleles. Animals bearing *qa700* were therefore crossed eight times with N2 before out-crossing with BC107 and recombination of the *dpy-14* locus with *gly-2* to break the chromosome between *gly-2* and *mut-2*. This strain was then further out-crossed an additional 4 times with N2 to remove the *dpy-14* allele and create strain XA728 *gly-2(qa700**14)* I. qa703-bearing animals were crossed three times with N2 then with DR435 to recombine the mutagenized chromosome with wild-type material either side of *gly-2*. *dpy-5(e61)*, *gly-2(qa703)*, and *unc-13(e51)* I animals were derived and subsequently crossed another 5 times with N2 to remove the markers and generate strain XA762 *gly-2(qa703**10)* I. Both alleles were mapped by recombination frequencies with *dpy-5* and *unc-13* using PCR to score for the presence of the qa700 or qa703 alleles. The deletion boundaries of the alleles were characterized by sequencing DNA that had been PCR-amplified from genomic DNA using primers that encompassed the deletions.

Genetic Mapping of gly-2—DR435 hermaphrodites were mated with XA728 males, and cross-progeny hermaphrodites were picked and allowed to segregate F2. Animals carrying chromosomes that had recombined between the dpy-5 and unc-13 loci were genotyped by single-worm PCR (26) using primer sets that specifically detected wild-type and deletion alleles to determine the frequency of recombination between *gly-2* and both marker loci, *dpy-5* and *unc-13*. Of 26 Dpy non-Unc chromosomes, 15 recombinations occurred in the *dpy-5-gly-2* interval, and of 28 Unc non-Dpy chromosomes, 13 recombinations occurred between *gly-2* and *unc-13*.

Construction of Precomplementation Lines—The 13,806-bp *XbaI* fragment corresponding to bases 17,188–30,994 of cosmid C55B7 was subcloned into the *XbaI* site of pZErO-2 to create pResLng-9E, and the structure was verified by restriction digests. This genomic region encompassed all *gly-2* sequences detected in transcripts as well as an additional 4248 bases upstream of the 5′ limit of yk126h8 and 1281 bases downstream of the site of polyadenylation. XA762 hermaphrodites were transformed by gonad injection (30) of a mixture of pResLng-9E and pRF4, a plasmid containing a region of *C. elegans* genomic DNA carrying the *rol-6*(su1006) mutation that acts dominantly by causing animals bearing the array to roll. Several independent rolling lines were established, and the percentage of rolling self-progeny from each was characterized. GlcNAc-TV activity was assayed using microsomal membranes prepared from 2 such lines, XA766 *gly-2*(qa703) I; qaEx743[*gly-2*(+), *rol-6*(su1006)] and XA768 *gly-2*(qa703) I; qaEx745[*gly-2*(+), *rol-6*(su1006)], both of which transmitted the array to 30–50% of their progeny.

Microsomal Membrane Preparation—Cultures were established by picking 50 rolling L4 hermaphrodites (or 20 animals from non-transgenic lines) to each of 5 100-mm diameter complete nematode growth medium plates that were then grown at room temperature until the animals cleared the *Escherichia coli* OP50 lawn. Nematodes were rinsed from the plates in cold 100 mM NaCl, washed twice, then floated on sucrose (60% w/v). After 2 washes with 100 mM NaCl, the pellet was snap-frozen in an ethanol-dry ice bath and stored at −70 °C. Samples were thawed by adding 1 ml of TSEC (20 mM Tris-HCl, 250 mM sucrose, 1 mM EDTA, 1× Complete™; Roche Molecular Biochemicals) then sonicated on ice 5 times using a 10-s pulse before dilution with a further 3 ml of TSEC. After centrifugal clarification for 10 min at 3000 rpm at 4 °C (Sorval RT6000), the supernatant was ultracentrifuged at 55,000 rpm for 1 h at 4 °C (Beckman L8–80 M with a 70.1Ti rotor). The microsomal pellet was suspended in a minimal volume of 100 mM MES, pH 6.5, 2% v/v Triton X-100, 2× Complete™, 20 mM EDTA, the protein concentration was determined by BCA assay (Pierce) standardized with bovine serum albumin, then 386 μg of each preparation was subjected immediately to GlcNAc-TV assay.

RESULTS

The gly-2 Gene of C. elegans—TBLASTN queries of the GenBank™ dBEST data base using rat GlcNAc-TV polypeptide (GB:AAA41665) revealed two homologous *C. elegans* ESTs,

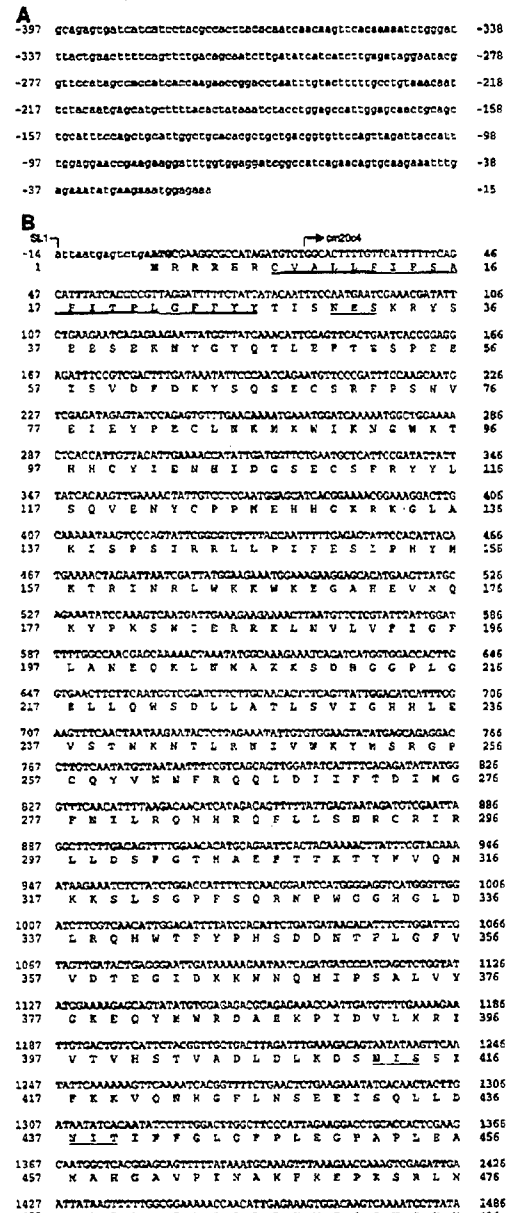

FIG. 1. **The sequence of *gly-2* cDNAs.** *A*, 5′-untranslated region of EST yk126h8 that is absent in the major *gly-2* mRNA. *B*, cDNA sequence and inferred polypeptide of mature *gly-2* mRNA numbered relative to the initiator residues. SL1 is *trans*-spliced to nucleotide −14. The start of EST cm20c4 is also indicated. Initiator and stop codons are shown in *bold*. The putative TMD is double-underlined. Potential *N*-linked glycosylation sites are *single-underlined*. The consensus polyadenylation signal is *boxed*. The run of eight adenines preceding the poly(A) (A_n) indicator is present in the genomic sequence. It is therefore not clear where transcription terminates precisely.

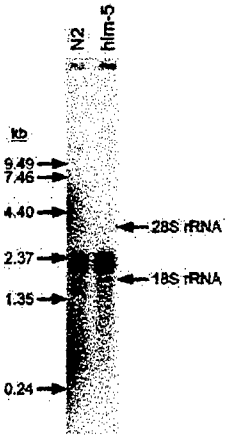

FIG. 2. **Northern analysis of poly(A)$^+$ RNA from *C. elegans* strains Bristol N2 and CB1490 *him-5(e1490)* probed with the *SalI-SmaI* fragment of yk126h8.** The data represent one of two independent experiments. The *arrows* indicate migration positions of size markers and the residual ribosomal RNAs in the preparations. The origins are marked by radioactive pencil lines at the *top*.

cm20c4 and yk126h8 (33),[2] which were obtained and sequenced (Fig. 1). A single reverse transcriptase-specific product after 5′ RACE was observed, and direct sequencing revealed a *trans*-spliced SL1 sequence attached to position −14, where a splice acceptor site occurs immediately upstream in the genomic sequence. Comparison of the genomic and yk126h8 sequences confirms an intron at this point. All 35 independent subclones of the RACE product that were tested for the presence of SL1 and SL2 sequences by colony PCR and 5 that were sequenced contained SL1. This transcript structure is concordant with the Northern analysis that indicated a single poly(A)$^+$ RNA species of ~2.25 kb (Fig. 2). Comparison of the cDNA and genomic sequences indicates that the gene organization is typical, with 10 exons of 82–589 bp separated by 44–882 bp of introns (Fig. 3*A*) (34). Notably, the majority of the exon boundaries in human and *C. elegans* genes occurs at equivalent residues, and in most cases, the phase is conserved too. We named the gene *gly-2* as a member of the GLYcosylation class. BLAST searches using the cDNA or deduced polypeptide sequences revealed that the *C. elegans* genome contains a single homologous region, implying that *gly-2* is the nematode orthologue of GlcNAc-TV.

The conceptual translation of the open reading frame encodes a 669-amino acid polypeptide that is 59.9% similar and 36.7% identical to rat GlcNAc-TV. When the sequence was queried against GenBank™ using BLAST, only mammalian GlcNAc-TV sequences were returned as significant hits. There are five potential *N*-linked glycosylation sites, but they are not conserved with the mammalian homologues. Hydropathy plots indicated that GLY-2 is a type II membrane protein with the secondary structural characteristics of Golgi glycosyltransferases (Fig. 4*A*). This plot reveals four distinct regions in GLY-2; a hydrophilic cytosolic tail precedes the putative TMD, whereas the lumenal part of the molecule consists of a consistently hydrophilic 112 residue stretch before an amphiphilic C-terminal portion. Consistent with this model, alignments between GLY-2 and mammalian homologues showed increased conservation in the C-terminal portion of the molecule (Fig. 4*B*). A conserved peptide (C^{110}–P^{124}) lies in the otherwise diverged stem that encompasses a conserved leucine residue equivalent to that mutated in the GlcNAc-TV gene of Lec4A cells (Fig. 3*B*) (35).

GLY-2 Has GlcNAc-TV Enzymatic Activity—Based on the

[2] Y. Kohara *et al.*, manuscript in preparation.

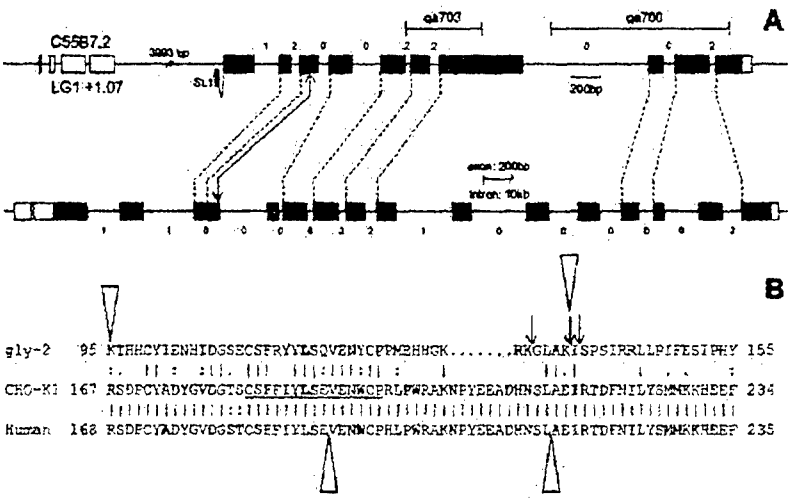

FIG. 3. **Genomic structure and alignment detail of *gly-2* with mammalian homologues.** *A*, inferred genomic structure of *gly-2* by comparison of cDNA and genomic sequence (cosmid C55B7, GB:AC006625, *top*) and human GlcNAc-TV cDNA and genomic sequence (52), GB:D17716 (53) and GB:S80050, *bottom*). *Dashed lines* indicate the alignment of the first amino acid of the *C. elegans* exons with the corresponding aligned residue in the human sequence. The *double-headed arrow* shows the position of the mislocalization mutations, and the exon containing the conserved stretch around this leucine is *shaded light gray*. The *darker gray exons* are those comprising the catalytic domains. The phase of each intron is indicated by the digits *0*, *1*, or *2*. Note that the intron scaling for the human sequence is different. Non-coding exons or portions are unshaded. The regions deleted by alleles qa700 and qa703 are demarcated with "I" bars. *B*, detail of the alignment between Ce-GLY-2 and CHO cell GlcNAc-TV (35) (GB:U62587). Mislocalization is caused by mutation of the emboldened leucine. The island of conservation surrounding this residue is *underlined*. The *triangles* indicate the in-frame boundary residues between exons. The *arrows* indicate the positions of truncations Δ133, Δ137, and Δ138.

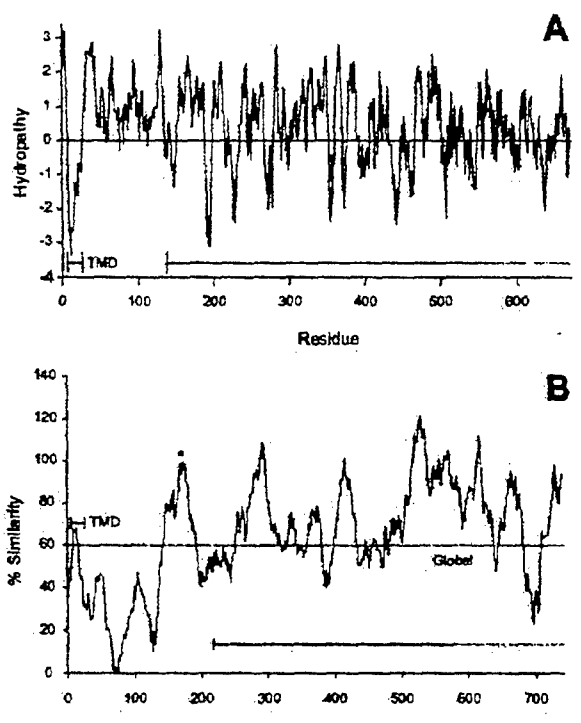

FIG. 4. **Hydropathy and conservation profiles of the GLY-2 protein sequence.** TMD marks the peak corresponding to the TMD, and the *solid/dotted line* indicates the catalytic portion of the molecule as determined by experiments reported here. The *dotted* portion of the line reflects that the C-terminal extent of the catalytically critical region was not investigated. *A*, Kyte-Doolittle profile generated using the GCG Peptidestructure program using a window of 7 residues (51). *B*, running similarity comparison to rat GlcNAc-TV (GB:L14284) aligned using the GCG Gap program averaging over a window of 25 residues. *Alignment position* refers to the numbering of the alignment, not a specific residue in either polypeptide. Global similarity is indicated by the *dashed line*. The *asterisk* marks the position of the mislocalization point mutations and the surrounding stretch of conserved residues.

hydropathy and similarity profiles, we postulated that the N-terminal limit of the catalytic domain is the boundary between exon 3 and 4, the first junction after the C^{110}–P^{124} peptide. This is the equivalent region to that observed to be essential for catalytic activity in rat GlcNAc-TV (36). Constructs directing the secretion into the medium of soluble, truncated versions of the protein (structures indicated in Fig. 3*B*) were transfected into Lec4 cells, a CHO-K1 derivative lacking endogenous GlcNAc-TV activity. Transfections were incubated at 30 °C to reduce the anticipated denaturation of GLY-2, which as a *C. elegans* enzyme is adapted for growth at 20 °C. The resulting conditioned medium contained soluble fusion protein at ~1 μg/ml, and GlcNAc-TV activity was detected from transfections with pISTH1-GLY2 series plasmids but not from vector-only controls. The nematode enzyme is markedly inhibited by NaCl above 50 mM (Fig. 5*A*). This is analogous to the suppression of rat GlcNAc-TV by NaCl above physiological levels (37). The pH optimum of GLY-2 is around pH 6.5 (Fig. 5*B*), typical of most Golgi glycosyltransferases, and is the ambient pH of the Golgi apparatus (38). As expected GLY-2 is progressively thermolabile, and no differences were apparent among truncation variants (Fig. 5*C*). As with other β6-*N*-acetylglucosaminyltransferases, GLY-2 was active in the presence of EDTA, and Mn^{2+} addition did not stimulate the reaction (data not shown).

Conditioned media from the truncation series containing equivalent amounts of S-tag fusion protein were assayed directly (Fig. 5*D*). The inferred initiator methionine and *trans*-membrane domain are confirmed by the detection of soluble enzyme from the construct that lacked the first 27 deduced residues. Deletion of more than 137 residues severely impaired the specific activity. Since all truncation variants were equally thermolabile, the most plausible reason is that the catalytic domain boundary resides at Ile-138. To confirm this and demonstrate that GlcNAc-TV activity was an intrinsic property of the recombinant polypeptide, the fusion protein was immunoprecipitated from the conditioned medium using anti-S-tag antibody. These assays were performed with equivalent amounts of S-tagged fusion protein, allowing direct comparisons between the various truncated forms (Fig. 5*E*). A band at the

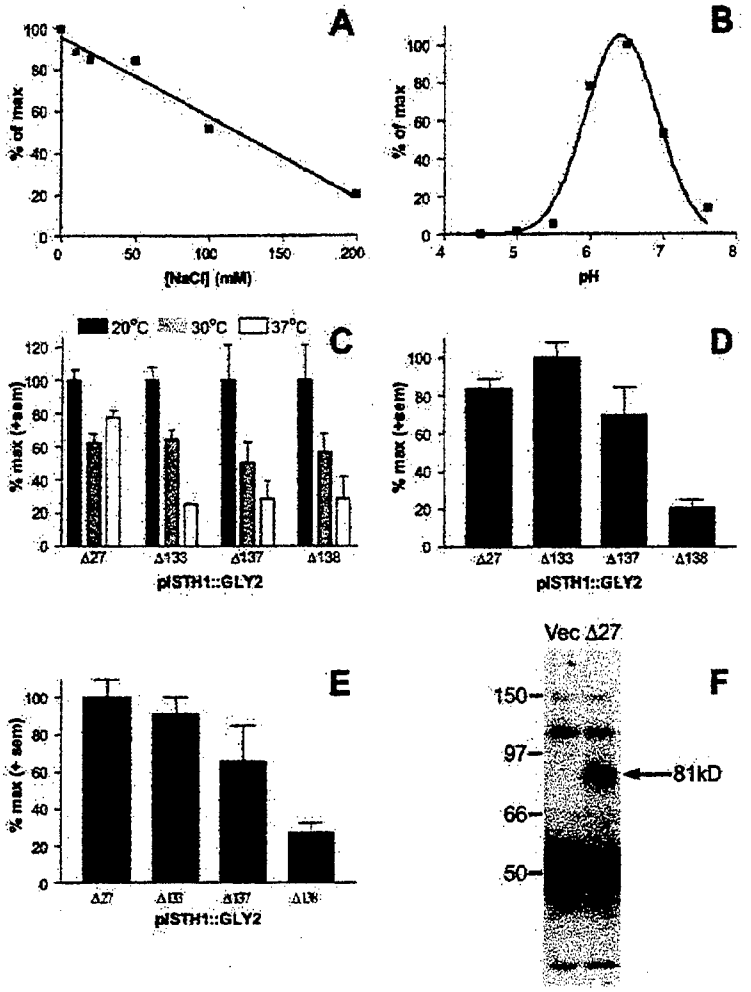

FIG. 5. **Enzymatic properties of GLY-2 produced by transient transfection of Lec4 cells.** Assay temperature was 22 °C unless indicated otherwise. In *panels A–E*, data are normalized to the negative control and maximal values. *A*, effect of NaCl on the activity of dialyzed conditioned medium from cells transfected with pISTH1::GLY2-Δ133. *B*, pH profile of catalytic activity for conditioned medium from cells transfected with pISTH1::GLY2-Δ27. Assays were performed in 50 mM MES buffer of various pH values. *C*, effect of temperature on the activity of conditioned medium from cells transfected with pISTH1::GLY2-Δ133. *D* and *E*, effect of truncation at the N terminus on catalytic activity of GLY2 fusion protein assayed in conditioned medium or immunoprecipitates, respectively, from Lec4 cells transfected with pISTH1::GLY2-Δ27, Δ133, Δ137, or Δ138. Data in *panels C–E* are the mean of independent triplicates with S.E. indicated by the *error bars*. *F*, specific detection by Western blotting of appropriately sized recombinant GLY-2 in conditioned medium from cells transfected with pISTH1::GLY2-Δ27.

expected size (~81 kDa) was observed when the immunoprecipitate of GLY-2Δ27 was Western-blotted for S-tag. In the other truncations an unavoidable background band masked the region at the expected size range (~60 kDa) (Fig. 5*F*). As with conditioned medium, deleting the first 137 residues of GLY-2, a region comprising the initiator methionine, the TMD, and the predicted stem region, including the C^{110}–P^{124} peptide, had little effect on specific activity. Removing a single additional residue reduced activity by 75%. Therefore, the boundary of the catalytic domain does indeed correspond to the 5′ limit of the exon initiated by Ile-138.

gly-2 Can Rescue the Cell Surface Phenotype of Chinese Hamster Ovary Lec4 Cells—The complementation of a genetic defect by a heterologous allele is a stringent test of equivalence since all the salient properties of the endogenous gene must be fulfilled by the introduced allele in the physiological environment. Lec4 mutant cells lack GlcNAc-TV activity and the mature glycan products, GlcNAcβ1,6 branched *N*-linked oligosaccharides on cell surface glycoproteins, which can be specifically detected as determinants of L-PHA binding (Fig. 6*A*). The parental phenotype was restored to Lec4 by transfecting the wild-type CHO-K1 GlcNAc-TV cDNA expression constructs (Fig. 6*B*). Transfection with wild-type *gly-2* also rescued the Lec4 phenotype, and the profile is qualitatively identical to that of Lec4 cells rescued by transfection of CHO-K1 GlcNAc-TV (Fig. 6*D*). The partially rescued population is probably the result of low levels of activity expressed in these cells, itself due to thermolability of the nematode enzyme at 30 °C. Thus, *gly-2* is functionally equivalent to the mammalian gene product, able to act on the natural glycoprotein substrates found in mammalian cells and create glycans recognized by L-PHA.

GlcNAc-TV must be present in the *medial*-Golgi because the elaboration of β6-GlcNAc-branched *N*-glycans and Lec4A mutant cells cannot bind L-PHA at the cell surface because they mislocalize active enzyme (35). The equivalent of the Lec4A missense mutation in GLY-2 was assayed. Protein truncations removing this region are catalytically active, yet GLY-2(L116R) failed to rescue the Lec4 phenotype in three independent experiments (Fig. 6*C*). Thus, although the wild-type GLY-2 enzyme complements Lec4 and, therefore, must be expressed and functional, the L116R mutant might not be. To address this, since attempts to raise anti-GLY-2 antibodies were unsuccessful, as were assays for activity in these transfected samples, constructs expressing GFP fused to the N terminus of GLY-2 were tested. Transfection of pEGFP-C3 alone does not affect the L-PHA binding properties of Lec4 or CHO-K1 (Fig. 7, *A* and *B*). GFP::GLY-2(+), however, results in complete restoration of the parental phenotype in Lec4 cells and is more effective than native GLY-2 (compare Figs. 7*D* to 6*D*). Consistent with this enhancement, GFP::GLY-2(L116R) can now partially rescue the cell surface phenotype and must therefore be catalytically competent (compare Figs. 7*C* to 6*C*). The FACS analysis indicated that transfection efficiencies were the same for all samples; therefore, cell extracts were Western-blotted for GFP epitopes, and GlcNAc-TV was assayed. Slightly more GFP epitope, as well as GlcNAc-TV enzyme activity, can be detected per cell transfected with GFP::GLY-2(L116R), but there is no indication of appreciable differences in specific activity (Fig. 7,

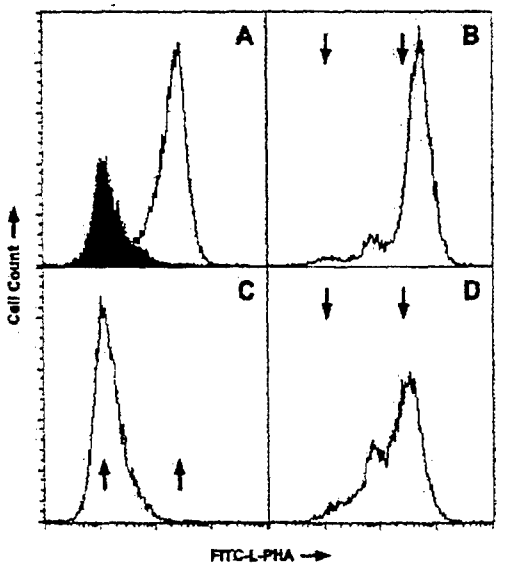

FIG. 6. **Rescue of the cell surface lectin binding phenotype of Lec4 cells by transient transfection of *Ce-gly-2* or CHO-derived GlcNAc-TV constructs.** FITC fluorescence of CD20-positive live single cells is graphed. *A*, the *solid line* is the profile of CHO-K1 parental cells, and the *gray solid* is the profile of Lec4 cells transfected with pLec4 plasmid. In *panels B–D* the positions of the peak channel fluorescence of these samples is indicated by the *arrows*. *B*, Lec4 cells transfected with pCHO-K1. *C*, Lec4 cells transfected with pCSYK-L116R. *D*, Lec4 cells transfected with pCSYK-1. Data are representative of independent triplicates.

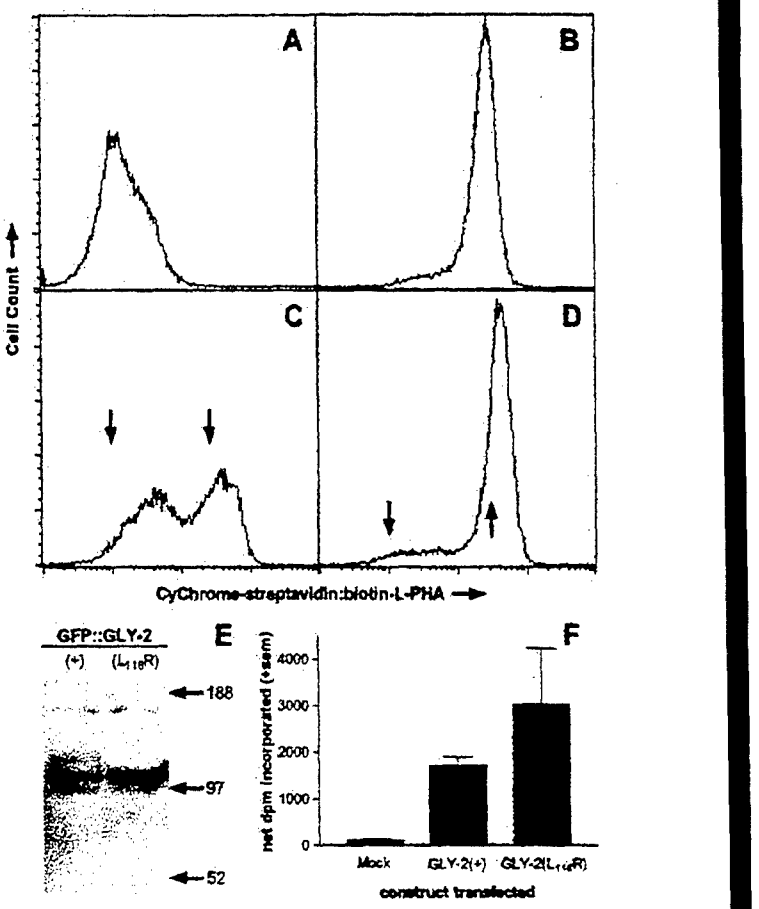

FIG. 7. **Rescue of defective L-PHA binding in Lec4 cells by transient transfection with GFP fusions of *Ce*-GLY-2 or CHO derived GlcNAc-TV constructs.** Fluorescence from CyChrome-streptavidin:biotin-L-PHA-stained GFP positive live single cells is graphed. *A*, the profile of Lec4 cells transfected with pEGFP-C3. *B*, CHO-K1 parental cells transfected with pEGFP-C3. In *panels C* and *D* the positions of the peak channel fluorescence of Lec4 and CHO-K1 from *A* and *B* are indicated by the *arrows*. *C*, Lec4 cells transfected with pEGFP-L116R. *D*, Lec4 cells transfected with pEGFP-GLY2. Data are representative of independent triplicates. *E*, immunoblot for GFP epitopes in extracts from cells that were subjected to the FACS analysis shown in *panels C* and *D*. Data are representative of independent duplicates. The expected size of GFP::GLY-2 is ~107 kDa. *F*, GlcNAc-TV enzyme activity in the extracts prepared as in *E*. The extract from the equivalent of $\sim 8 \times 10^5$ cells was assayed for 3 h at 30 °C in each case in the presence and absence of substrate to determine the net incorporation of [6-^{3}H]GlcNAc. Data are the mean of independent duplicates with S.E. indicated by the *error bars*.

E and *F*). Transfected cells were examined by deconvolution microscopy (data not shown), but fluorescent signals from both native and mutant forms were present in membranous compartments other than *medial*-Golgi. Overexpression by transient transfection may overwhelm retention and trafficking mechanisms, but nevertheless, GLY-2(+) and GLY-2(L116R) have different rescue behaviors.

Expression Pattern of gly-2p::GFP during Nematode Development—Transcriptional fusions of 6.7 kbp of upstream genomic DNA corresponding to bases 19,280–25,991 of cosmid C55B7 to nuclear localized and cytosolic forms of GFP provided by vectors pPD95.69 and pPD95.77, respectively, were used as reporter constructs. This stretch includes the 3′ end (base 19,436) of the next confirmed gene upstream on the same strand as *gly-2*. It encompasses all of the 5′-untranslated region sequences found in yk126h8 (which starts at base 21,436) as well as the region that is conserved in the genome of *Caenorhabditis briggsae*, a closely related species (alignment starts at base 23,114). By these criteria, the constructs should contain a fully qualified promoter of *gly-2*.

The distribution of signal in transgenic worms was unique and highly restricted with respect to tissue and/or stage of development but did not correspond to the descendants of a particular branch of the cell lineage. Fluorescence was first detectable at the comma stage (Fig. 8*A*) in cells that divided and appeared to migrate during the 2-fold (Fig. 8*B*) and 3-fold stages (Fig. 8*C*). Neuronal staining was obvious from L1 onward and by early L4 was seen to occur in both the dorsal and ventral nerve chords (Fig. 8*D*). During this stage, a strong signal was noted in the developing vulva (most likely the vulE and/or vulF cells). By late L4 an intense GFP signal in the spermathecal valve as well as other vulval and/or uterine structures was evident (Fig. 8*E*). Expression in the uv1 and uv2 cells was suggested by the pattern of fluorescence around the vulva. However, the nuclear-localized reporter construct stained more nuclei than can be accounted for by expression in these cells alone (Fig. 8*F*). With this construct, nuclear localized signal was observed in all four nuclei of the syncytial spermathecal valve cell (Fig. 8*G*). Although GFP fluorescence was seen to be strongest in the late L4 and early adult for the spermathecal valve and vulval/uterine structures previously noted, it was seen to persist throughout adulthood (Fig. 8, *H–J*). The M8 cell of the terminal bulb of the pharynx, all six cells of the pharyngeal-intestinal valve, and neuronal cell bodies within the metacorpus and around the isthmus of the pharynx also expressed *gly-2*p::GFP (Fig. 8*K*). At least 37 neurons with cell bodies lying next to the ventral nerve chord were positive for *gly-2*-directed reporter expression in the adult hermaphrodite, although with widely varying levels of staining. There was also GFP fluorescence present in other neurons associated with the pre-anal, dorso-rectal, and/or lumbar ganglia. In adult males, expression was similar in non-sexually dimorphic tissues and was also observed in axons that project into rays 2, 3, 5, 6, and either 8 or 9 of the copulatory bursa (data not shown).

gly-2 Is a Non-essential Gene—ev581 is a Tc1 insertion

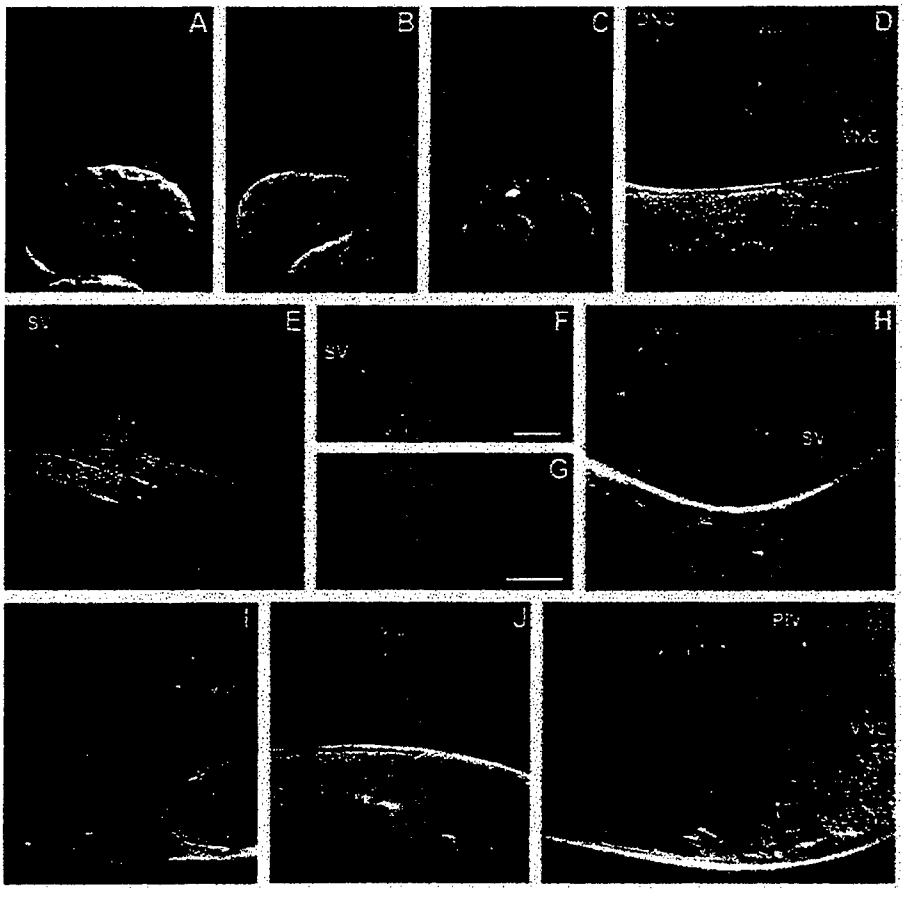

FIG. 8. **Pattern of *gly-2* promoter-directed GFP expression during nematode development.** Except for *panels F* and *G*, images are presented as pairs showing the epifluorescence from the cytosolic GFP reporter in the upper section and differential interference contrast images from the same field and focal plane in the lower section. The *emerald-green* light is emitted by GFP, the *yellow-green* signal is gut autofluorescence. *Scale bar* in all cases is 20 μm. *A*, comma stage embryo. *B*, 1.5-fold stage embryo. *C*, 3-fold stage embryo. *D*, lateral view of an early larval stage 4 hermaphrodite peri-vulval region. *DNC*, dorsal nerve cord; *VNC*, ventral nerve cord; *vul*, vulval cells vul E and/or vul F. *E*, ventral view of late larval stage 4 hermaphrodite peri-vulval region. *SV*, spermathecal valve; *v/u*, vulval and/or uterine structures. *F*, as *E*, but from a nuclear-localized reporter. *G*, detail in lateral view of the spermathecal valve staining by the nuclear-localized reporter expressed in an adult hermaphrodite. *H*, lateral view of an adult hermaphrodite mid-body showing continued expression in the spermathecal valve (*SV*) and vulval and/or uterine structures (*v/u*). *I* and *J*, lateral views in two different focal planes from adult hermaphrodites showing vulval/uterine staining (*v/u*). *K*, lateral view of the pharynx from an adult hermaphrodite showing GFP fluorescence from neurons (*N*) in the nerve ring and ventral nerve chord (*VNC*) and the staining of the pharyngeal-intestinal valve (*PIV*).

TABLE I
Genomic sequences of gly-2 alleles

Nucleotide numbering is the base position of the cosmid sequence C55B7 from the *C. elegans* sequencing consortium. Fusion junctions in deletion alleles *qa700* and *qa703* are indicated by double colons (::).

Allele	Genomic Sequence
gly-2(ev581)	28383 20384 TTTTCTAAAACACTATAAATATATTGATTGCCGTATTTCC
gly-2(qa700)	28371 29535 CACTTTACATACATTTTTCT::GCATTCCTTTTCAGTTGTGC
gly-2(qa703)	27255 27750 AGAATACTCTTAGAAAGTAT::TGGTATATGGAAAAGAGCAG

allele into the 7th intron of *gly-2* from which *qa700* was derived by imprecise excision, an event that deleted 1165 bp containing ~2.5 exons that contribute to the catalytic domain (Table I). *qa703* is a deletion created by ethylmethanesulfonate-induced deletion mutagenesis that removes 494 bp containing exon 6 and half of the largest exon, 7, both of which contribute to the catalytic domain. Both deletion alleles are probably null, but animals homozygous for either are viable. To check that no gross rearrangements occurred during mutagenesis, genetic mapping of the genotypes was performed. This placed the alleles on linkage group I between 1.07 and 1.18 map units to the right of *dpy-5*, exactly where expected from interpolations of the physical map.

GlcNAc-TV activity could be detected in microsomal extracts of wild-type *C. elegans* but not in the deletion mutant strain XA762 *gly-2*(qa703) (Fig. 9). Enzyme activity was restored in transgenic lines carrying a genomic region encompassing the *gly-2* gene on the deletion mutant background. Thus, *gly-2*, which is the sole cognate homologue of *Mgat-5* in *C. elegans*, encodes nematode GlcNAc-TV.

The strain XA728 *gly-2(qa700**14)* I had fertility defects arising from abnormal sperm function (Spe) that were not observed in XA762 *gly-2(qa703**10)* I. Compound heterozygotes of a qa700/qa703 genotype were non-Spe confirming that this defect is caused by a linked but extragenic mutation in a complementation group unrelated to *gly-2* (data not shown). Although *gly-2* is expressed in many neurons, the vulva, and spermatheca, XA762 was wild type with respect to morphology, egg laying and hatching, locomotion, brood size, dauer switching,

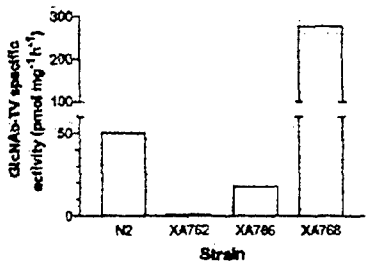

FIG. 9. **GlcNAc-TV activity in *C. elegans* is dependent on the *gly-2* gene.** N2 is the laboratory wild-type strain; XA762 is homozygous for the *gly-2* deletion allele qa703. XA766 and XA768 are independent strains carrying extrachromosomal arrays encompassing a *gly-2*(+) genomic region on a *gly-2*(qa703) background.

male incidence, developmental timing, and mechanosensory axon path-finding (data not shown). GFP reporter patterns were also unaffected by the mutant background.

DISCUSSION

The genomic structure of the *gly-2* gene is significantly related to that of human GlcNAc-TV. The majority of exon boundaries, particularly in the catalytic domain, occur at equivalent residues and are in-frame. The N-terminal boundary of the catalytic region starts at exon 4; exon 3 contains the "Lec4A" region. Retention of phase zero introns in ancient genes is a feature of the "introns-early" model (39). These observations support the notion that exon shuffling of functional domains may have been the mechanism by which the ancestral GlcNAc-TV gene originated.

The deduced polypeptide sequence of *gly-2* is stereotypical of Golgi glycosyltransferases, being a type II membrane protein with a 20-residue TMD starting six residues from the N terminus. This length is efficiently retained by the Golgi apparatus and is the sole element in the polypeptide that appears to have bilayer-spanning properties (40). The lumenal portion starts with a hydrophilic region that may position the following catalytic domain away from the membrane and so promote efficient interactions with macromolecular substrates. Heterologous expression of recombinant gene product demonstrated that GLY-2 does indeed possess GlcNAc-TV enzyme activity and other properties in common with the mammalian homologue. The putative initiator codon and the TMD were confirmed since soluble recombinant fusion proteins were produced when truncated. The proposed stem could also be removed without affecting GlcNAc-TV enzyme activity *in vitro*. Several other *C. elegans* glycosyltransferase-related sequences have been found to possess the catalytic activity expected from their homologies. *gly-3*, *gly-4*, and *gly-5* are polypeptide GalNAc-Ts (15), and *gly-12* and *gly-14* encode active GlcNAc-TI (16), whereas CeFT-1 is an α1,3-fucosyltransferase (17). *gly-1* and possibly the other core 2 GlcNAc-T homologues may be an exception (23). GLY-1 transfers glucose rather than GlcNAc to core 1 acceptors (24), an observation concordant with the available structural data on *C. elegans* glycoprotein glycans (22). The components of the proteoglycan pathway encoded by *sqv-3*, *sqv-7*, and *sqv-8* all possess the biochemical activity expected from their homologies (20, 21). The proper functioning of GlcNAc-TV depends not only on catalytic competence but also upon being able to interact with nascent glycoprotein substrates in the ambient milieu, correct localization, and domain structure (35). We found unequivocally that *gly-2* could rescue the surface lectin binding phenotype of Lec4 cells. Thus, GLY-2 retains all of the salient properties of the mammalian GlcNAc-TV despite being diverged for >500Myr (41).

Alignment of mammalian GlcNAc-TV and GLY-2 identified a region that is highly conserved despite being N-terminal to the catalytic domain. This region contains a leucine that is mutated in Lec4A cells, causing otherwise active GlcNAc-TV to mislocalize and fail to elaborate cell surface β6-GlcNAc-branched *N*-glycans in consequence (35). The equivalent mutation in native GLY-2 did not rescue the Lec4 defect, but a GFP fusion product could do so inefficiently. It may be that the fusion protein is better expressed than the native nematode enzyme in Lec4 cells or that the addition of GFP stabilizes the product (42). The simplest interpretation is that GFP::GLY-2(L116R) is mislocalized as in Lec4A, but due to overexpression typical of transient transfections, a portion overwhelms the endoplasmic reticulum retention system and proceeds to the *medial*-Golgi (43). BLAST searches indicated that the conserved 15-residue peptide encompassing the critical leucine is unique to GlcNAc-TV but has been conserved throughout metazoan radiation. Because mutations affect subcellular localization, it may be that the region is conserved because of a role in targeting to the *medial*-Golgi. If so, this mechanism is either GlcNAc-TV-specific or acts via its conformational properties, plausible since the peptide is bounded by two conserved cysteines. Conformational elements participate in the subcellular localization of lysosomal hydrolases where a common surface is recognized to initiate formation of the mannose 6-phosphate-targeting signal (44).

Our data are concordant with the dominant transcript being SL1 *trans*-spliced to the first splice acceptor upstream of the initiator codon and is typical of monocistronic *C. elegans* genes with a proximal promoter (34). yk126h8 contains an additional 383 nucleotides that occur in 4 non-coding exons 3994–4533 bp upstream and may represent a minor isoform from a distal upstream basal promoter. Distal promoters driving expression of this type of transcript at low levels are observed in *C. elegans*, for example *pkc-1* (45). The genomic fragment used for constructing the GFP reporter transgenes included both potential promoters. From these, GLY-2 expression can be crudely summarized as occurring in some of the structures that have valve properties, the vulva, the spermathecal valve, and the pharyngeal-intestinal valve. The other major locus of expression is neuronal, present in many but not all 302 neurons in the adult hermaphrodite (46). Curiously, mammalian brain is rich in GlcNAc-TV transcripts, but enzyme activity is barely detectable, and *Mgat-5*° mice are not obviously affected (4). However, failure to nurture pups is significantly more common in *Mgat-5*° mice in a 129/Sv background.[3]

The essentially complete sequence of the *C. elegans* genome (8) contains a single gene that is orthologous to mammalian Golgi GlcNAc-TV proteins at both the primary sequence and domain organization level. This is unusual for glycosylation-related genes in the nematode. The *C. elegans* genome contains many gene families, and glycosyltransferases are well represented (14, 47, 48). Multiple glycosyltransferase homologues, C-type and S-type lectin domains as well as nucleotide-sugar synthases, occur in a cluster (49). Core 2 GlcNAc-T-like sequences are the 167th largest gene family (23, 48); there are nine polypeptide GalNAc-T-like sequences (15), three homologues of GlcNAc-TI (16), and evidence for at least two α1,3 fucosyltransferases (17). There are two β4-galactosyltransferase homologues, of which mutations in one, *sqv-3*, affects epithelial morphogenesis, resulting in defects in vulval invagination as well as oocyte receptiveness to sperm (18, 19). Many mammalian glycosyltransferases are also present in multiple copies (50), but as in the worm, GlcNAc-TV has only one functional copy. Disruption of the *Mgat-5* locus in mice results in a

[3] M. Granovsky, J. Pawling, P. Cheung, and J. W. Dennis, unpublished observations.

complete loss of both enzyme activity and GlcNAcβ1,6-branched structures (4). Although structural studies have yet to observe complex *N*-glycans in *C. elegans*, GlcNAc-TV activity in wild-type animals is detectable, absent in animals with *gly-2* deleted, and restored by transgenes containing *gly-2* genomic DNA. From our present study, it appears that *Ce-gly-2* is orthologous to *Mgat-5*, structurally conserved at both genomic and polypeptide levels, and functionally interchangeable with mammalian GlcNAc-TV. Such "deep homology" is a feature of ancient and pivotal genes that occur in conserved pathways (41), but ablation of the *gly-2* gene in *C. elegans* is without visible defects despite resulting in an enzymatically null phenotype. This situation is not unusual; many genes with severely defective alleles are viable in *C. elegans* (*e.g.* 23, 54). It may be that the contributions are subtle under laboratory growth conditions. *Mgat-5*° mice are also without overt phenotype but display several phenotypes that are dependent on extrinsic conditions. Suppression of tumor growth and metastasis induced by the *Polyomavirus* middle T-antigen is observed (4)m and abnormalities in T-cell function, although significant, do not appear to compromise the animals greatly under laboratory conditions (3). The tractability of screens in *C. elegans* to uncover synthetic phenotypes enables this conundrum to be addressed and should mutate genes that interact genetically with *gly-2*. These would reveal GlcNAc-TV-dependent pathways and phenotypes, identifying the contributions to fitness made by β6-GlcNAc-branched *N*-glycans.

Acknowledgments—We thank Lynda Doughty for DNA sequencing, Giselle Knowles for FACS analyses, and John Hudson and Cindy Todoroff for critical readings of the manuscript.

REFERENCES

1. Dennis, J. W., Granovsky, M., and Warren, C. E. (1999) *Bioessays* **21,** 412–421
2. Granovsky, M., Fode, C., Warren, C. E., Campbell, R. M., Marth, J. D., Pierce, M., Fregien, N., and Dennis, J. W. (1995) *Glycobiology* **5,** 797–806
3. Demetriou, M., Granovsky, M., Quaggin, S., and Dennis J. W. (2001) *Nature* **409,** 733–739
4. Granovsky, M., Fata, J., Pawling, J., Muller, W. J., Khokha, R., and Dennis, J. W. (2000) *Nat. Med.* **6,** 306–312
5. Dennis, J. W., Laferte, S., Waghorne, C., Breitman, M. L., and Kerbel, R. S. (1987) *Science* **236,** 582–585
6. Riddle, D. L., Blumenthal, T., Meyer, B. J., and Priess J. R. (eds) (1997) *C. elegans II*, Cold Spring Harbor Laboratory Press, Cold Spring Harbor, NY
7. Wood, W. B. (ed.) (1988) *The Nematode Caenorhabditis elegans*, Cold Spring Harbor Laboratory Press, Cold Spring Harbor, NY
8. The *C. elegans* Sequencing Consortium (1998) *Science* **282,** 2012–2018
9. Sternberg, P. W., and Han, M. (1998) *Trends Genet.* **14,** 466–472
10. Metzstein, M. M., Stanfield, G. M., and Horvitz, H. R. (1998) *Trends Genet.* **14,** 410–416
11. Wodarz, A., and Nusse, R. (1998) *Annu. Rev. Cell Dev. Biol.* **14,** 59–88
12. Padgett, R. W., Das, P., and Krishna, S. (1998) *Bioessays* **20,** 382–390
13. Greenwald, I. (1998) *Genes Dev.* **12,** 1751–1762
14. Campbell, J. A., Davies, G. J., Bulone, V., and Henrissat, B. (1997) *Biochem. J.* **326,** 929–939
15. Hagen, F. K., and Nehrke, K. (1998) *J. Biol. Chem.* **273,** 8268–8277
16. Chen, S., Zhou, S., Sarkar, M., Spence, A. M., and Schachter, H. (1999) *J. Biol. Chem.* **274,** 288–297
17. DeBose-Boyd, R. A., Nyame, A. K., and Cummings, R. D. (1998) *Glycobiology* **8,** 905–917
18. Herman, T., and Horvitz, H. R. (1999) *Proc. Natl. Acad. Sci. U. S. A.* **96,** 974–979
19. Herman, T., Hartwieg, E., and Horvitz, H. R. (1999) *Proc. Natl. Acad. Sci. U. S. A.* **96,** 968–973
20. Bulik, D. A., Wei, G., Toyoda, H., Kinoshita-Toyoda, A., Waldrip, W. R., Esko, J. D., Robbins, P. W., and Selleck, S. B. (2000) *Proc. Natl. Acad. Sci. U. S. A.* **97,** 10838–10843
21. Berninsone, P., Hwang, H. Y., Zemtseva, I., Horvitz, H. R., and Hirschberg, C. B. (2001) *Proc. Natl. Acad. Sci. U. S. A.* **98,** 3738–3743
22. Guerardel, Y., Balanzino, L., Maes, E., Leroy, Y., Coddeville, B., Oriol, R., and Strecker, G. (2001) *Biochem. J.* **357,** 167–182
23. Warren, C. E., Krizus, A., and Dennis, J. W. (2001) *Glycobiology* **11,** 979–988
24. Warren, C. E., Krizus, A., Partridge, E. A., and Dennis, J. W. (2002) *Glycobiology* **12,** 8G
25. Brenner, S. (1974) *Genetics* **77,** 71–94
26. Epstein, H. F., and Shakes, D. C. (eds) (1995) *Caenorhabditis elegans:* Modern Biological Analysis of an Organism—Methods in Cell Biology, Vol. **48,** Academic Press, Inc., San Diego, CA
27. Ausubel, F. M., Brent, R., Kingston, R. E., Moore, D. D., Seidman, J. G., Smith, J. A., and Struhl, K. (1993) *Current Protocols in Molecular Biology*, John Wiley & Sons, Inc., New York, NY
28. Srivastava, O. P., Hindsgaul, O., Shoreibah, M., and Pierce, M. (1988) *Carbohydr. Res.* **179,** 137–161
29. Zhu, L., van den Heuvel, S., Helin, K., Fattaey, A., Ewen, M., Livingston, D., Dyson, N., and Harlow, E. (1993) *Genes Dev.* **7,** 1111–1125
30. Mello, C. C., Kramer, J. M., Stinchcomb, D., and Ambros, V. (1991) *EMBO J.* **10,** 3959–3970
31. Zwaal, R. R., Broeks, A., van Meurs, J., Groenen, J. T., and Plasterk, R. H. (1993) *Proc. Natl. Acad. Sci. U. S. A.* **90,** 7431–7435
32. Liu, L. X., Spoerke, J. M., Mulligan, E. L., Chen, J., Reardon, B., Westlund, B., Sun, L., Abel, K., Armstrong, B., Hardiman, G., King, J., McCague, L., Basson, M., Clover, R., and Johnson, C. D. (1999) *Genome Res.* **9,** 859–867
33. Waterston, R., Martin, C., Craxton, M., Huynh, C., Coulson, A., Hillier, L., Durbin, R., Green, P., Shownkeen, R., and Halloran, N. (1992) *Nat. Genet.* **1,** 114–123
34. Blumenthal, T., and Steward, K. (1997) in *C. elegans II* (Riddle, D. L., Blumenthal, T., Meyer, B. J., and Priess J. R., eds) pp. 117–145, Cold Spring Harbor Laboratory Press, Cold Spring Harbor, NY
35. Weinstein, J., Sundaram, S., Wang, X., Delgado, D., Basu, R., and Stanley, P. (1996) *J. Biol. Chem.* **271,** 27462–27469
36. Korczak, B., Le, T., Elowe, S., Datti, A., and Dennis, J. W. (2000) *Glycobiology* **10,** 595–599
37. Shoreibah, M. G., Hindsgaul, O., and Pierce, M. (1992) *J. Biol. Chem.* **267,** 2920–2927
38. Llopis, J., McCaffery, J. M., Miyawaki, A., Farquhar, M. G., and Tsien, R. Y. (1998) *Proc. Natl. Acad. Sci. U. S. A.* **95,** 6803–6808
39. de Souza, S. J., Long, M., Klein, R. J., Roy, S., Lin, S., and Gilbert, W. (1998) *Proc. Natl. Acad. Sci. U. S. A.* **95,** 5094–5099
40. Munro, S. (1995) *EMBO J.* **14,** 4695–4704
41. Fitch, D. H. A., and Thomas, W. K. (1997) in *C. elegans II* (Riddle, D. L., Blumenthal, T., Meyer, B. J., and Priess J. R., eds) pp. 815–850, Cold Spring Harbor Laboratory Press, Cold Spring Harbor, NY
42. Sacchetti, A., El Sewedy, T., Nasr A. F., and Alberti, S. (2001) *FEBS Lett.* **492,** 151–155
43. Fullekrug, J., Scheiffele, P., and Simons, K. (1999) *J. Cell Sci.* **112,** 2813–2821
44. Baranski, T. J., Cantor, A. B., and Kornfeld, S. (1992) *J. Biol. Chem.* **267,** 23342–23348
45. Land, M., Islas-Trejo, A., and Rubin, C. S. (1994) *J. Biol. Chem.* **269,** 14820–14827
46. Chalfie, M., and White, J. (1988) In Wood, W. B. (ed.) *The Nematode Caenorhabditis elegans*, pp. 337–391, Cold Spring Harbor Laboratory Press, Cold Spring Harbor, NY
47. Oriol, R., Mollicone, R., Cailleau, A., Balanzino, L., and Breton, C. (1999) *Glycobiology* **9,** 323–334
48. Apweiler, R., Attwood, T. K., Bairoch, A., Bateman, A., Birney, E., Biswas, M., Bucher, P., Cerutti, L., Corpet, F., Croning, M. D., Durbin, R., Falquet, L., Fleischmann, W., Gouzy, J., Hermjakob, H., Hulo, N., Jonassen, I., Kahn, D., Kanapin, A., Karavidopoulou, Y., Lopez, R., Marx, B., Mulder, N. J., Oinn, T. M., Pagni, M., and Servant, F. (2001) *Nucleic Acids Res.* **29,** 37–40
49. Jungmann, J., and Munro, S. (1998) *EMBO J.* **17,** 423–434
50. Lo, N. W., Shaper, J. H., Pevsner, J., and Shaper, N. L. (1998) *Glycobiology* **8,** 517–526
51. Kyte, J., and Doolittle, R. F. (1982) *J. Mol. Biol.* **157,** 105–132
52. Saito, H., Nishikawa, A., Gu, J., Ihara, Y., Soejima, H., Wada, Y., Sekiya, C., Niikawa, N., and Taniguchi, N. (1994) *Biochem. Biophys. Res. Commun.* **198,** 318–327
53. Saito, H., Gu, J., Nishikawa, A., Ihara, Y., Fujii, J., Kohgo, Y., and Taniguchi, N. (1995) *Eur. J. Biochem.* **233,** 18–26
54. Harfe, B. D., and Fire, A. (1998) *Development* **125,** 421–429